NASA CR 135274

IMPACT RESISTANT BORON/ALUMINUM COMPOSITES FOR LARGE FAN BLADES

by

T.L. Oller G.S. Doble
C.T. Salemme P. Melnyk
J.H. Bowden

GENERAL ELECTRIC COMPANY

Prepared For

National Aeronautics and Space Administration

NASA Lewis Research Center

NAS3-19729

1. Report No.	2. Government Accession No.	3. Recipient's Catalog No.
NASA CR 135274		

4. Title and Subtitle	5. Report Date
IMPACT RESISTANT BORON/ALUMINUM COMPOSITES FOR LARGE FAN BLADES	December 1977
	6. Performing Organization Code

7. Author(s)	8. Performing Organization Report No.
T.L. Oller, C.T. Salemme, J.H. Bowden, G.S. Doble, P. Melnyk	R77AEG667
	10. Work Unit No.

9. Performing Organization Name and Address	11. Contract or Grant No.
General Electric Company 1 Jimson Rd. Cincinnati, Ohio 45215	NAS3-19729
	13. Type of Report and Period Covered
12. Sponsoring Agency Name and Address	Contractor Report
National Aeronautics and Space Administration Washington, D.C. 20546	14. Sponsoring Agency Code

15. Supplementary Notes

Project Manager, David L. McDaniels
NASA-Lewis Research Center
Cleveland, Ohio 44135

16. Abstract

This report describes the results of a 14-month program beginning in October, 1975 designed to investigate the impact resistance of 0.02 cm (8 mil) boron/1100 aluminum and to demonstrate the fabrication technology required for a large boron/aluminum blade.

The technical program was comprised of three technical tasks. Task I encompassed the fabrication of blade-like specimens incorporating the boron/aluminum materials and process technology considered most appropriate from a FOD resistance viewpoint. Following fabrication, these blade-like specimens were subjected to static ballistic impact testing to determine their relative FOD impact resistance levels. It was determined that a ±30° or a ±15° layup exhibited good impact resistance.

Based on the FOD test results from Task I, the design of a large solid boron/aluminum fan blade was conducted in Task II. General Electric used the CF6 fan blade as a baseline for these design studies.

In Task III, the solid boron/aluminum fan blade design completed in Task II was used by TRW to fabricate two blades. This effort enabled the assessment of the scale up of existing blade manufacturing details for the fabrication of a large B/Al fan blade. Existing TRW CF6 fan blade tooling was modified for use in fabricating these blades.

17. Key Words (Suggested by Author(s))	18. Distribution Statement
Composite Blades Fan Blades Boron/Aluminum Composite Impact Testing Aluminum	

19. Security Classif. (of this report)	20. Security Classif. (of this page)	21. No. of Pages	22. Price*
Unclassified	Unclassified	121	

* For sale by the National Technical Information Service, Springfield, Virginia 22151

TABLE OF CONTENTS

LIST OF ILLUSTRATIONS

LIST OF ILLUSTRATIONS (Concluded)

LIST OF TABLES

1.0 SUMMARY

Resin and metal matrix composites are recognized as having significant potential as replacement materials for titanium fan and compressor blade applications. For example, substantial cost and weight reduction benefits on the order of 25% have been projected for the CF6 fan with the use of composite materials. Heretofore, the lack of foreign object damage (FOD) resistance such as large bird ingestion has been a major deterrent to the use of composites for large fan blade application. Recently, however, significant improvement in impact resistance of 0.02 cm (8 mil) boron/1100 aluminum composite materials has been achieved. Recognizing the significance of this recent development, NASA sponsored a program at General Electric in conjunction with TRW to evaluate the impact performance of boron/aluminum and fabricate large fan blades using the boron/aluminum material. This report presents the results of that program.

The technical program was comprised of three technical tasks. Task I encompassed the fabrication of blade-like specimens incorporating the boron/aluminum materials and process technology considered most appropriate from a FOD resistance viewpoint. Following fabrication, these blade-like specimens were subjected to static ballistic impact testing to determine their relative FOD impact resistance levels. It was determined that a ±30° or a ±15° layup exhibited good impact resistance.

Based on the FOD test results from Task I, the design of a large solid boron/aluminum fan blade was conducted in Task II. General Electric used the CF6 fan blade as a baseline for these design studies. The Task II design effort resulted in the identification of a preliminary boron/aluminum fan blade design that incorporated the results of Task I FOD testing while still considering other design requirements such as structural strength and frequency characteristics. Ply shape and layup angle definition were completed under this task.

In Task III, the solid boron/aluminum fan blade design completed in Task II was used by TRW to fabricate two blades. This effort enabled the assessment of the scale up of existing blade manufacturing details for the fabrication of a large B/Al fan blade. Existing TRW CF6 fan blade tooling was modified for use in fabricating these blades.

2.0 INTRODUCTION

Turbofan engines can be generally categorized in two broad classes: (1) high bypass fan with large fan blades for low temperature, subsonic engine applications, and (2) the low bypass fan with small blades for higher temperature supersonic engine application. Past efforts to develop composite materials as a replacement for titanium in fan blades have emphasized weight reductions. More recently, cost effectiveness has shifted the emphasis to lower fabrication cost, lower operating cost (improved specific fuel consumption resulting from weight reductions and aerodynamic improvements), and lower maintenance cost. The application of composites in large, subsonic fan blades has previously concentrated on the polymeric matrix materials. The metal matrix composites with higher operating temperature capability have been restricted to the smaller, supersonic fan blade applications. However, the lack of adequate foreign object damage (FOD) resistance has restricted the use of both types of composites for fan blade applications.

Recent developments in metal matrix composites caused a shift in emphasis of B/Al to the application of large fan blades. First, the development of large 0.02 cm (8.0 mil) diameter boron fibers has decreased the cost of boron and significantly increased the impact properties of boron/aluminum. This has made the boron/aluminum composite more weight and cost effective relative to the polymeric composites. The use of a ductile 1100 series aluminum matrix for the boron/aluminum has also dramatically increased the shear deformation capability and therefore the impact resistance, as measured by notched charpy impact tests. Also development of the rapid air bonding process allows reduced fabrication costs due to the reduced molding time at temperature.

The current program was undertaken, therefore, in order to further demonstrate FOD advances and to develop fabrication technology for a large fan blade such as the CF6.

To prove the FOD resistance improvements, ballistic impact tests were conducted on several boron/aluminum specimens. This testing demonstrated good impact resistance for both ±30° and ±15° boron/aluminum layups and for panels with titanium leading edge spars.

Two all-boron/aluminum CF6 blades were fabricated to demonstrate the capability of making a large complex blade shape from 0.02 cm (8 mil) boron/1100 aluminum using the rapid air bonding process.

3.0 BLADE-LIKE SPECIMEN STATIC IMPACT TESTING

The purpose of this task was to determine the relative local impact resistance of several all-boron/aluminum and boron/aluminum shell titanium spar design candidates. The designs that demonstrated the highest relative local impact resistance were selected for use in the design, production scale-up, and fabrication of full scale CF6 fan blades in the subsequent task.

The use of blade-like specimen static impact testing to evaluate material candidates is much more appropriate to assess local soft body impact resistance than the Charpy or Izod impact tests that have been used to evaluate the candidate material before this program. Although the Charpy and Izod test approaches are used in early materials selection because of their low cost, they do not simulate the conditions to which a blade is subjected during a soft body impact such as a bird impact. The impact strength level obtained in Charpy or Izod tests cannot, therefore, be used to assess the impact resistance of the material in blade applications. The use of static impact specimens did not completely simulate an actual blade situation, however, more realistic blade whirligig testing is very costly and would severely limit the amount of testing, thereby reducing the range of variables which could be considered.

3.1 TEST SPECIMEN GEOMETRY

Figure 1 defines the test specimen geometry. The specimens were 25.4 cm (10-inches) long and had a constant airfoil shape which simulated the leading edge portion of the CF6 fan blade at the 75% span height. The forward 3.81 cm (1.5-inch) of the actual blade was simulated. The airfoil shown is symmetrical to allow laying up the boron/aluminum plies as they would be in a real blade. Both all-boron/aluminum and spar/shell designs were evaluted by using this constant geometry. A wire mesh outer ply covering the entire skin of the panels and nickel plate leading edge protection was applied to all the boron/aluminum panels except one as shown in Figure 2. The leading edge spar panels did not include any wire mesh plies. Detail drawings of both leading edge, internal spars and the all-B/Al specimens are shown in Figures 3 through 7, respectively.

3.2 STATIC IMPACT TEST MATERIAL DESIGN CANDIDATES

A total of eight boron/aluminum design candidates were identified for evaluation. In addition, one polymeric design was tested for use as a comparison with the boron/aluminum and boron/aluminum shell-titanium spar design candidates. There were five all-boron/aluminum candidates and three spar/shell candidates.

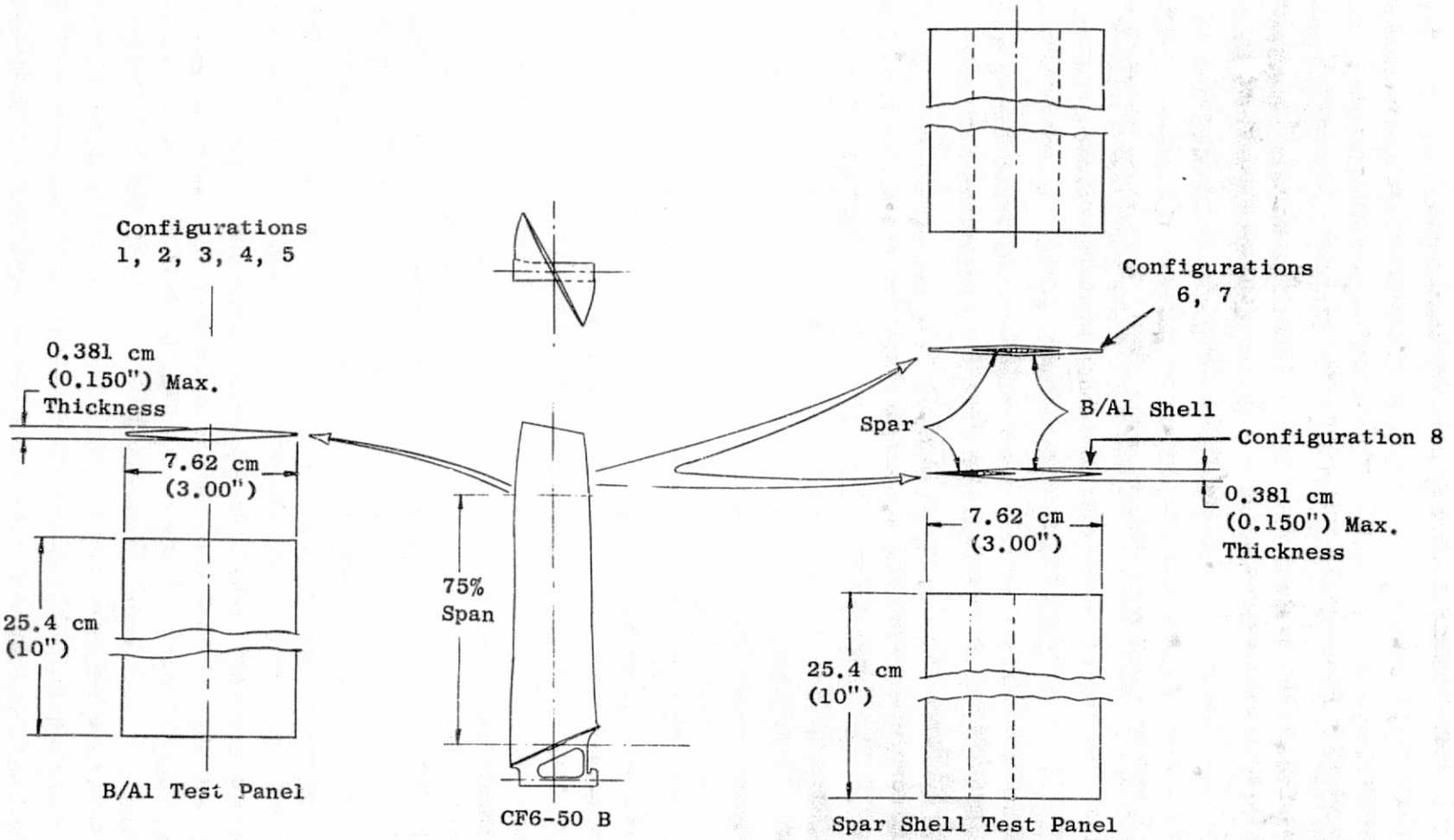

Figure 1. Blade Like Specimen Geometry Used for Static Impact Testing.

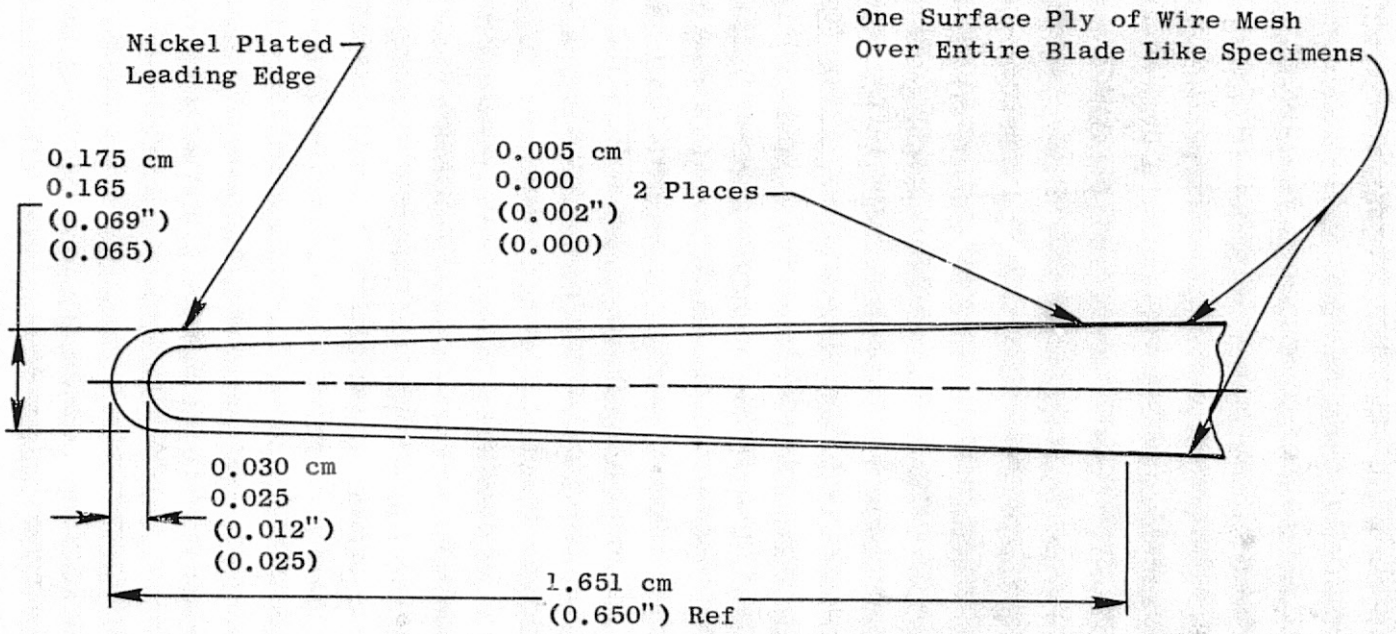

Figure 2. Nickel Plate Leading Edge Protection.

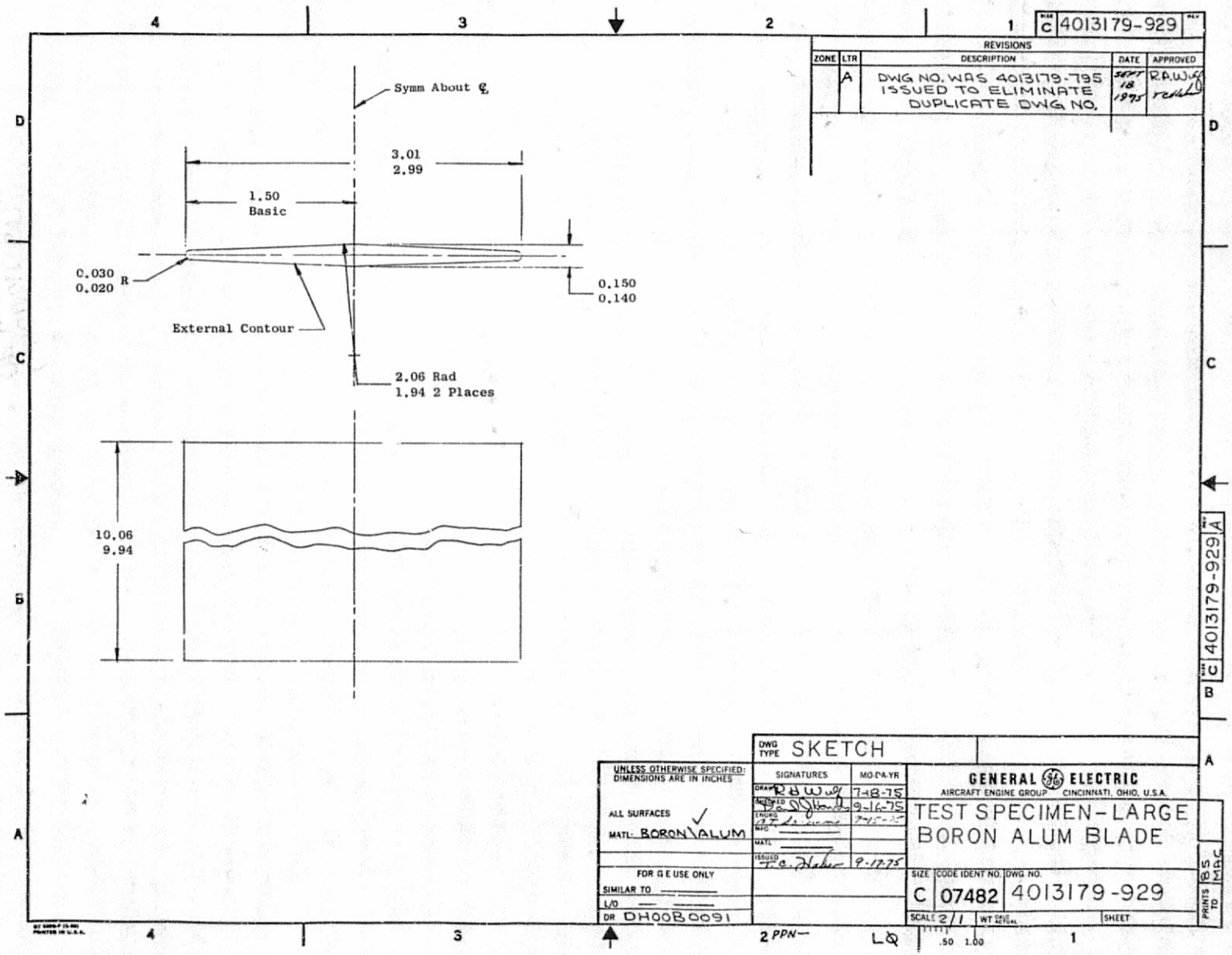

Figure 3. Large B/Al Blade Test Specimen.

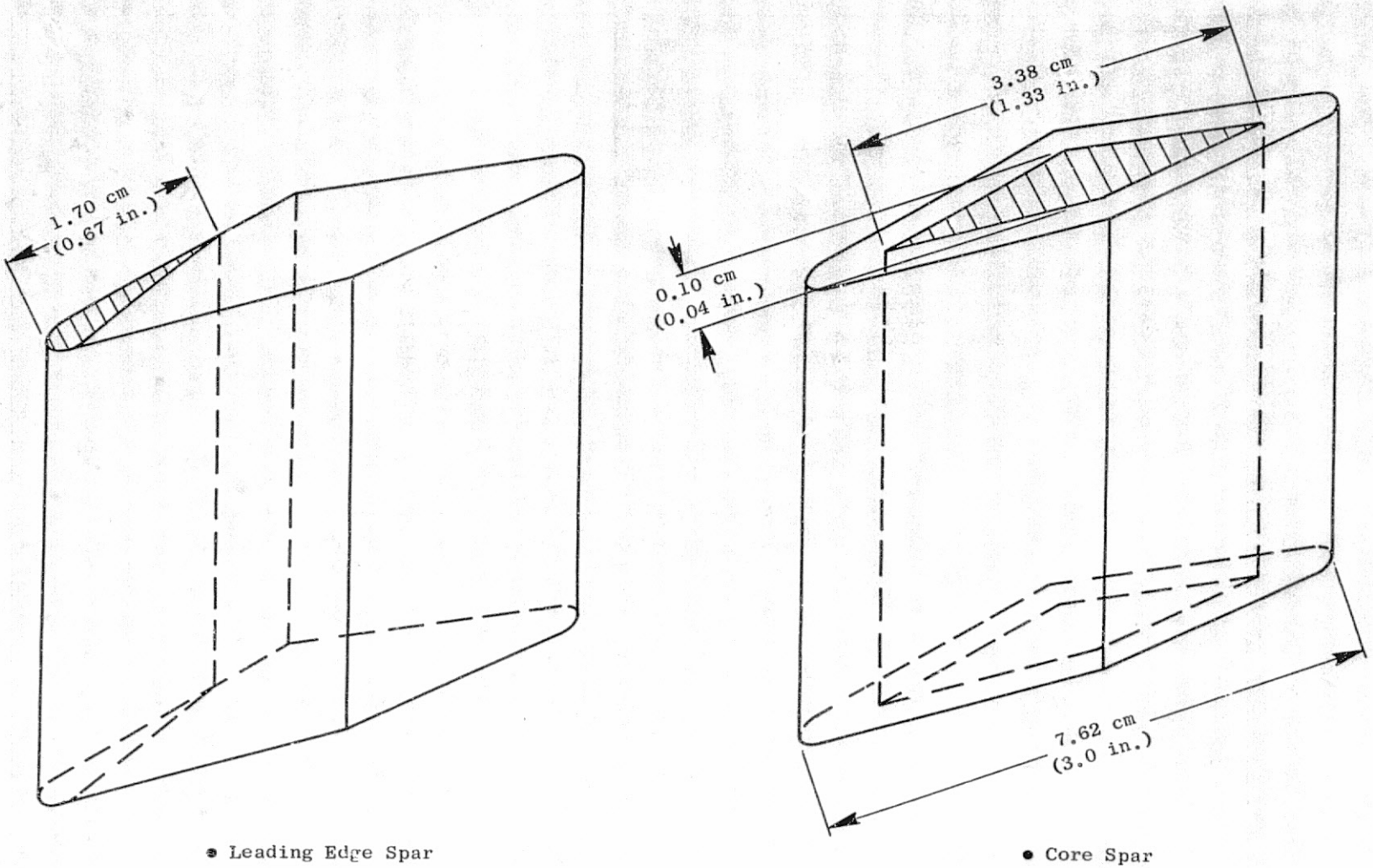

• Leading Edge Spar

• Core Spar

Figure 4. Titanium Spar Designs.

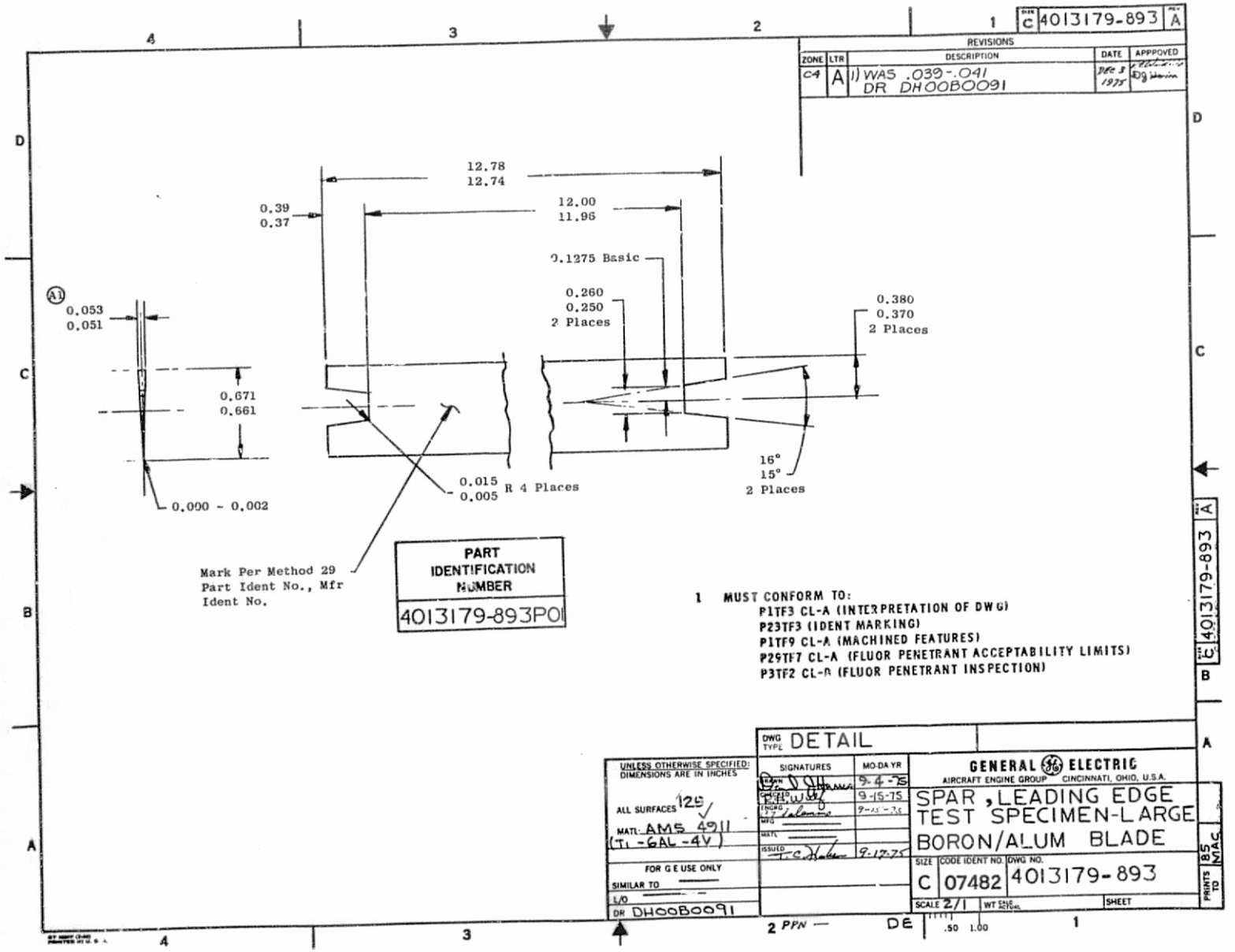

Figure 5. Spar, Leading Edge Test Specimen - Large B/Al Blade.

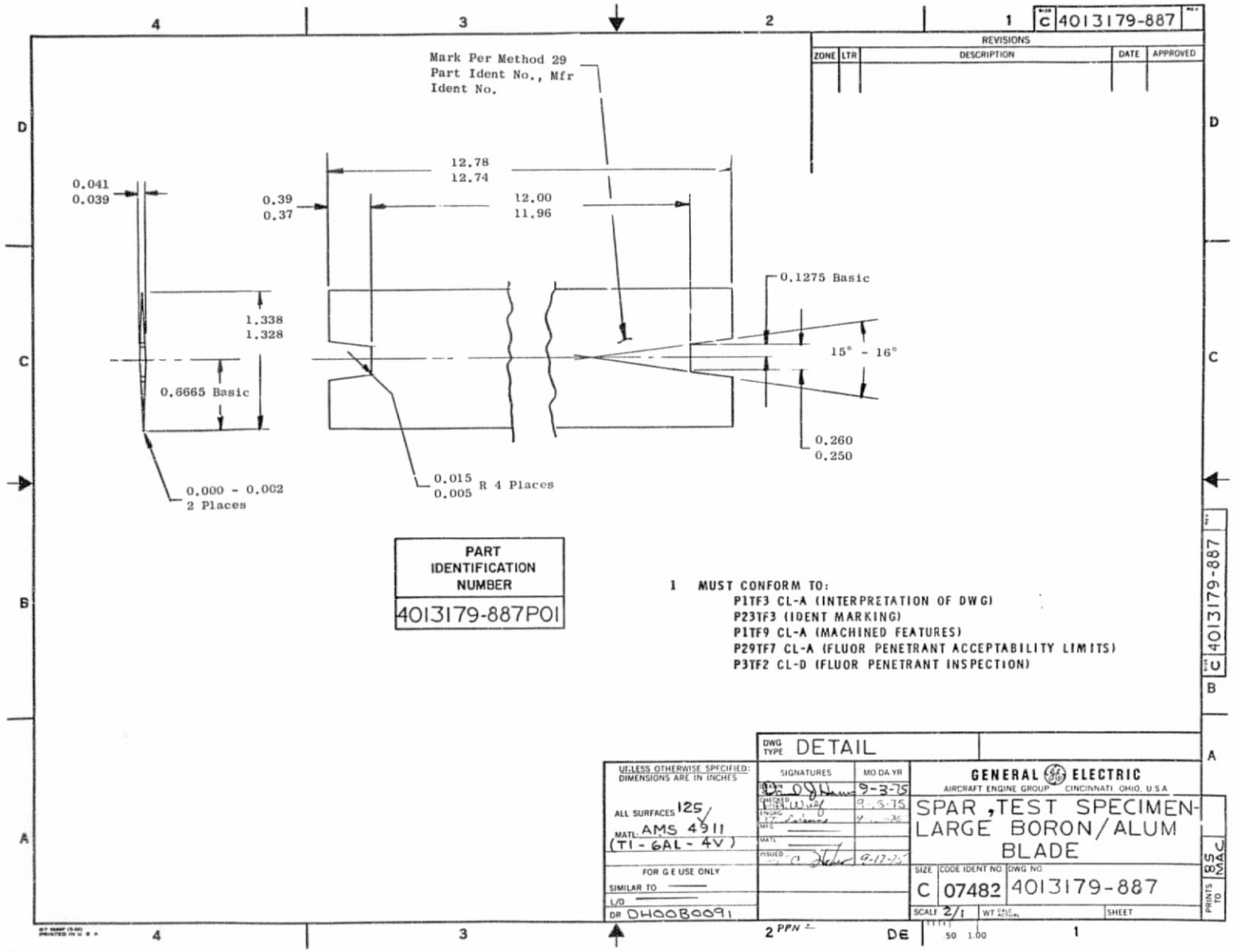

Figure 6. Flat Patterns Test Specimen, Standard Layup - Large B/Al Blade.

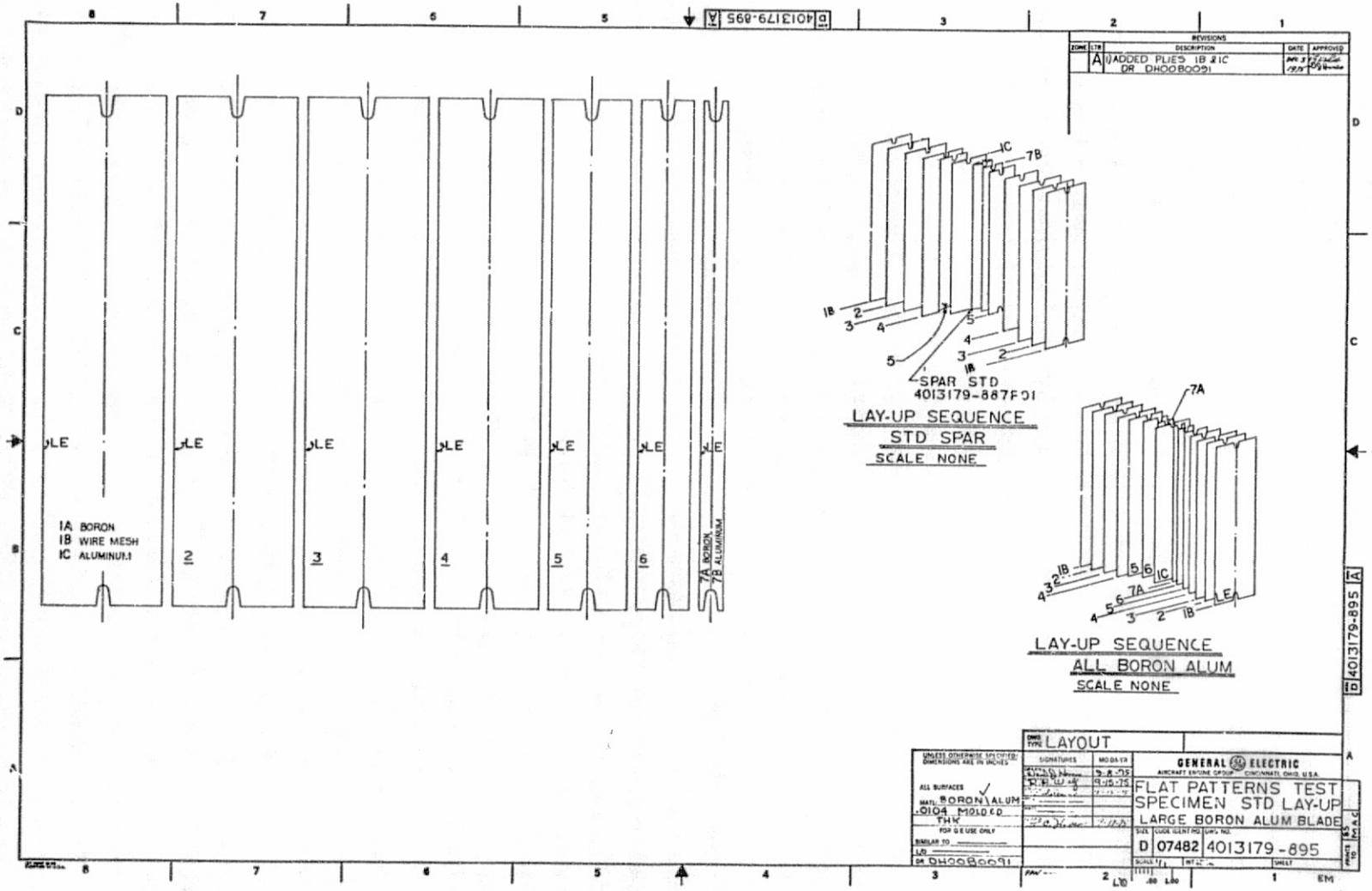

Figure 7. Spar, Test Specimen - Large B/Al Blade.

In all cases, 0.02 cm (8 mil) diameter boron filaments and 1100 aluminum matrix were used. Processing was accomplished by TRW using rapid air bonding. Wire mesh and leading edge nickel plate were applied to selected panels as fully described in Section 3.1.

Table I summarizes the material/process design candidates. Configurations 1 and 2 were fabricated from all-boron/aluminum material. The ±15° balanced layup design for Configuration 1 was chosen because it considers both the radial strength requirements for centrifugal load and fatigue life which tend to require longitudinal (radial) fibers, and impact strength which is enhanced by fibers in a more chordal direction. Configuration 2 represented a new design approach in that symmetry in the ply layup is not maintained. In fact, plies at +20° and 0° are used. This layup offered the potential for improved impact resistance because, under impact, stress waves are carried along the +20° plies to the root while no -20° plies are present to transmit stress to the tip. At the tip, stress waves might be reflected back reinforcing other oncoming stress waves. Charpy specimens using this layup had previously shown marked impact improvement relative to the ±15° layup. Configuration 3 was identical to Configuration 1 except that the outer stainless steel mesh plies were replaced by boron/aluminum plies and the leading edge was not nickel plated.

Configurations 4, 5, 6, and 7 represented an evaluation of standard spar/shell designs. B/Al shells were diffusion bonded to a titanium spar. Inclusion of the titanium spar greatly increases the radial strength of the blade, allowing the B/Al plies to be oriented at much higher angles (+30° and ±45°). Two design factors were evaluated. The first was the relative impact resistance of these high angle plies (Configurations 4 and 5, and secondly, the effect of the impact on the spar/shell interface at different ply angles (Configurations 6 and 7). In addition, comparison of the impact results of Configurations 1, 2, 4, and 5 were evaluated for an all-B/Al application.

Configuration 8 represented an unconventional spar/shell design approach in which the titanium spar was not buried, but rather was used as the leading edge protection. This design offered some potential benefits in terms of impact resistance and lower weight as the nickel plated leading edge protection was not needed.

3.3 MANUFACTURING PROCESS

Fabrication of blade-like specimens was performed using a single set of fabrication parameters and varying the orientations and titanium spar locations. The processing conditions employed for the fabrication of blade-like specimens were selected to give maximum impact resistance and to simulate the manufacturing process to be used for a CF6 boron-aluminum blade. The basic approach was to produce diffusion-bonded monotapes, cut the monotapes to the appropriate ply dimensions, surface treat the monotapes, and bond the blade-like specimens in air. Bonding conditions were selected on the basis of good impact resistance obtained on a previous program and included 454° C (850° F) primary fabrication and 468° C (875° F) secondary fabrication.

Table I. Material/Process Design Candidates.

Configuration	Design	Material Boron Dia. (mil)	No. of Specimens	Al Matrix.	Titanium Spar	Fiber Orientation	Nickel Leading Edge Plated Over SS Mesh
1	All B/Al	0.02 (8)	2	1100	No	±15°	Yes
2	All B/Al	0.02 (8)	2	1100	No	0/+20°	Yes
3	All B/Al	0.02 (8)	2	1100	No	±15°	No
4	All B/Al	0.02 (8)	2	1100	No	±30°	Yes
5	All B/Al	0.02 (8)	2	1100	No	±45°	Yes
6	Spar Shell	0.02 (8)	2	1100	Core	±30°	Yes
7	Spar Shell	0.02 (8)	2	1100	Core	±45°	Yes
8	Spar Shell	0.02 (8)	2	1100	Leading Edge	±30°	No
9	Polymeric*	-	2	-	No	±0 ±22	Yes

*PR288 Epoxy/80% As Graphite/20% S-Glass.

Monotapes were fabricated from 0.02 cm (8 mil) boron-1100 aluminum alloy in a 50 volume percent reinforcement. The filaments were wound to a 0.024 cm (9.6 mil) center-to-center spacing and the nominal thickness of the monotapes was 0.026 cm (10.4 mils). The 0.026 cm (10.4 mil) thickness was used for lofting the blade-like specimens and was also used for the CF6 blade. Monotapes were of good quality and metallographic examination indicated complete bonding.

A die to produce the required blade-like shape was designed and machined. A schematic of the die set is shown in Figure 8. The set consists of a die and punch combination of closed die construction. The leading and trailing edge radii were produced by hand blending on a diamond wheel.

Monotapes were cut to ply dimensions lofted to the required shape. After cutting, the monotapes were given a surface treatment to improve the secondary matrix-matrix bond. The plies were located with notched pins centered on the die and bonded in air using a 468° C (875° F) bonding temperature. Initial runs were well bonded as evidenced by the micrograph shown in Figure 9. A photograph of the specimen is shown in Figure 10 and the entire run of specimens is illustrated in Figure 11. The excellent filament distribution maintained by the monotape process is shown in the macrograph in Figure 12.

A total of 16 blade-like specmens were fabricated and delivered to General Electric for test. Quality evaluation of the blades was based upon ultrasonic C-scan measurements. C-scan indications of defects of varying degree were present on 12 of the 15 specimens. Initial C-scan results are compared to General Electric inspection results in Table II. The initial variation in C-scan inspection was due to differences in sensitivity, the TRW inspection being performed at a less sensitive setting. Because of the unbonded areas indicated in the GE C-scans, the panels were subsequently repressed at a higher temperature, 496° C (925° F) in an attempt to eliminate or reduce the C-scan indications (see Appendix A). Specimens were reinspected using one specimen as a calibration standard. The repressing produced some improvement although most of the moderate and severe defects were still present. Success on repressing depends upon a surface free of oxides. Two of the specimens had more severe defects after repressing. It is believed that the repressing operation improved the matrix-matrix shear strength even where ultrasonic indications were not completely eliminated.

3.4 STATIC IMPACT TEST CONDITIONS

The static impact program was conducted using cantilever-supported airfoil-shape test specimens whose geometry was representative of the CF6 airfoil forward portion as fully described in Section 3.1. The specimens were impacted with foamed RTV projectiles. These projectiles were fired from a gas gun at varying velocities relative to the specimen to simulate local impact forces and stresses that represent bird impacts. Damage to the specimens was identified by failure mode or type and amount of damage.

Figure 13 shows a schematic representative of the test set-up. The specimen orientation was adjusted relative to the mounted gas gun to obtain

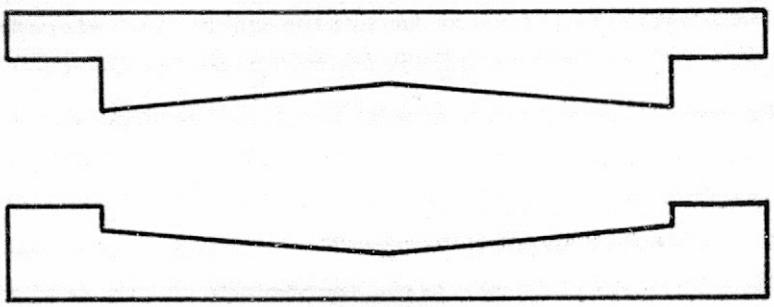

Figure 8. Schematic of Die Used for Fabrication of Blade-Like Specimens.

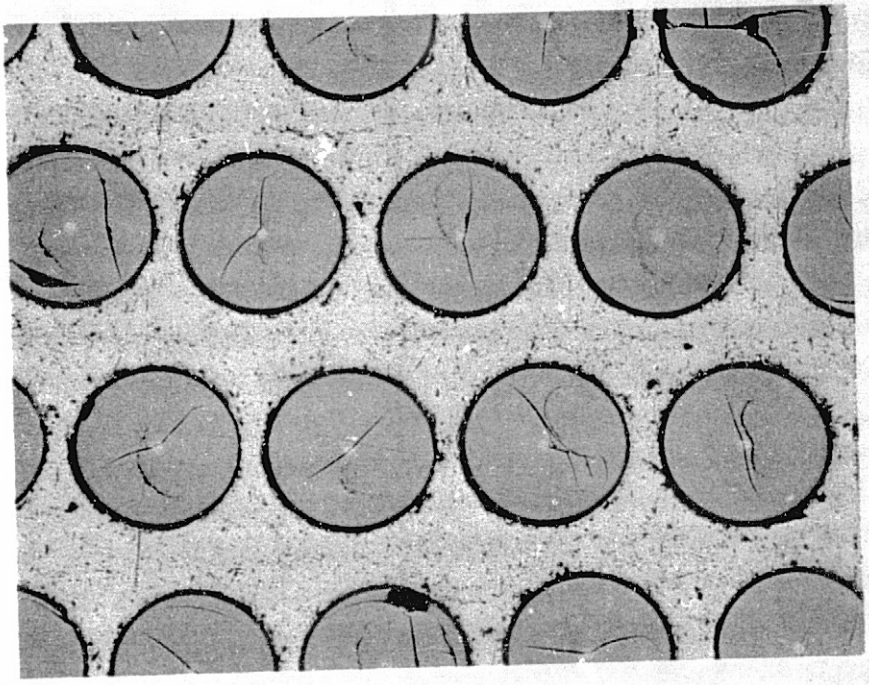

100X
Kellers Etch

Figure 9. Microstructure of First Blade-Like Specimens Bonded in Air.

Figure 10. Blade-Like Specimen.

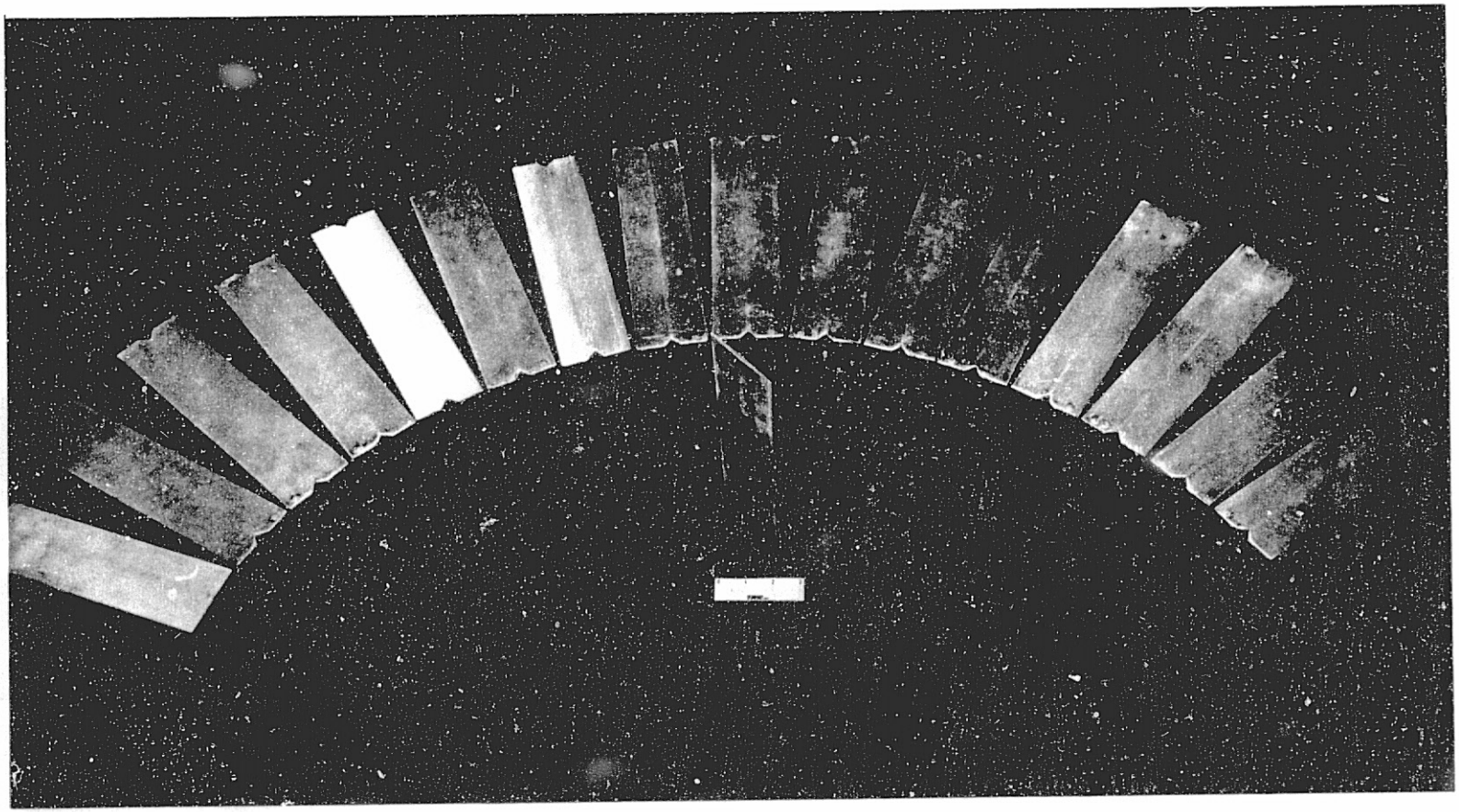

Figure 11. Blade-Like Specimens After Fabrication by Air Bonding.

Figure 12. Macrograph of Air-Bonded Blade-Like Specimen Illustrating Uniformity of Filament Distribution.

Table II. Task I Blade-Like Specimen Manufacturing Summary.

Configuration	Serial Number	Design	Fiber Orientation	Secondary Bonding Pressure MPa (ksi)	Remarks TRW	C-Scan Results TRW	C-Scan Results GE	Area of Indications-sq. cm (sq. in.) Slight	Mod	Severe	Percent	Specimen Weight Grams	Specimen Volume cm^3 (Cubic in.)	Remarks
3	16	.02 cm (8 Mil) Boron/A1100 Alum	±15°	69 (10)	No Wire Mesh	Slight Indication at Tip L.E. & Root	Slight Indications at Tip L.E.	0.161 (0.025)			0.1	140.0	54.6 (3.33)	OK for Test
	19	.02 cm (8 Mil) Boron/A1100 Alum	±15°	69 (10)	No Wire Mesh	None	None					138.5	54.1 (3.30)	OK for Test
1	25	.02 cm (8 Mil) Boron/A1100 Alum/316 SS Wire Mesh	±15°	69 (10)		None	None					136.0	50.0 (3.05)	OK for Test
	26	.02 cm (8 Mil) Boron/A1100 Alum/316 SS Wire Mesh	±15°	69 (10)		None	None					133.0	48.0 (2.93)	OK for Test
4	27	.02 cm (8 Mil) Boron/A1100 Alum/316 SS Wire Mesh	±30°	69 (10)		Slight Indications in Root T.E.	Slight Indications	7.74 (1.2)			4.0	133.0	48.5 (2.96)	OK for Test
	36	.02 cm (8 Mil) Boron/A1100 Alum/316 SS Wire Mesh	±30°	69 (10)	C-Scan Indications	Moderate Indications Along L.E. or 2.54 cm (1") Extending from Root to 60% Span	Moderate Indications		40.6 (6.3)		21.0	134.0	49.5 (3.02)	Consider Areas of Apparent Debond - May Give Misleading Test Data
5	34	.02 cm (8 Mil) Boron/A1100 Alum/316 SS Wire Mesh	±45°	69 (10)		None	Moderate & Slight Indications	11.6 (1.8)	7.10 (1.1)		9.7	140.0	52.1 (3.18)	Consider Areas of Apparent Debond - May Give Misleading Test Data
	35	.02 cm (8 Mil) Boron/A1100 Alum/316 SS Wire Mesh	±45°	69 (10)		Slight Indications Along Max. Thk. Line	Slight & Moderate Indications	15.5 (2.4)	7.10 (1.1)		11.7	136.5	50.1 (3.06)	Consider Areas of Apparent Debond - May Give Misleading Test Data
2	47	.02 cm (8 Mil) Boron/A1100 Alum/316 SS Wire Mesh	0 + 20°	69 (10)		None	None					135.5	50.1 (3.06)	OK for Test
	29-50	.02 cm (8 Mil) Boron/A1100 Alum/316 SS Wire Mesh	0 + 20°	69 (10)	Repressed	None	Moderate Indications		6.45 (1.0)		3.3	137.0	50.6 (3.09)	Marginal for Test
6	43	.02 cm (8 Mil) Boron/A1100 Alum/316 SS Wire Mesh Ti 6-4 Center Spar	±30°	83 (12)		None	Slight, Moderate, & Severe Indic.	18.7 (2.9)	8.39 (1.3)	18.7 (2.9)	23.7	157.0	54.1 (3.30)	Consider Areas of Apparent Debond - May Give Misleading Test Data
	37-49	.02 cm (8 Mil) Boron/A1100 Alum/316 SS Wire Mesh Ti 6-4 Center Spar	±30°	69-83 (10-12)	Repressed	Severe Indications	Severe Indications			7.74 (1.2)	4.0	145.0	50.1 (3.06)	Marginal for Test
7	39-48	.02 cm (8 Mil) Boron/A1100 Alum/316 SS Wire Mesh Ti 6-4 Center Spar	±45°	83 (12)	Repressed	None	Moderate & Severe Indications		12.2 (1.9)	3.87 (0.6)	8.3	147.0	51.1 (3.12)	Marginal for Test
	42	.02 cm (8 Mil) Boron/A1100 Alum/316 SS Wire Mesh/ Ti 6-4 Center Spar	±45°	83 (12)		Slight Indications	Severe & Slight Indications	27.7 (4.3)		3.23 (0.5)	16.0	142.0	48.0 (2.93)	Marginal for Test
8	44	.02 cm (8 Mil) Boron/A1100 Alum/Ti 6-4 Leading Edge Spar	±30°	69 (10)		None	Severe Indications in L.E. Spar Area	4.52 (0.7)		19.4 (3.0)	12.3	149.0	55.6 (3.39)	Metallic Leading Edge Appears to be Disbonded Over 50% of Surface of the Spars
	45	.02 cm (8 Mil) Boron/A1100 Alum/Ti 6-4 Leading Edge Spar	±30°	69 (10)		None	Severe Indications in L.E. Spar Area		5.81 (0.9)	22.6 (3.5)	14.7	150.5	56.0 (3.42)	Metallic Leading Edge Appears to be Disbonded Over 50% of Surface of the Spars

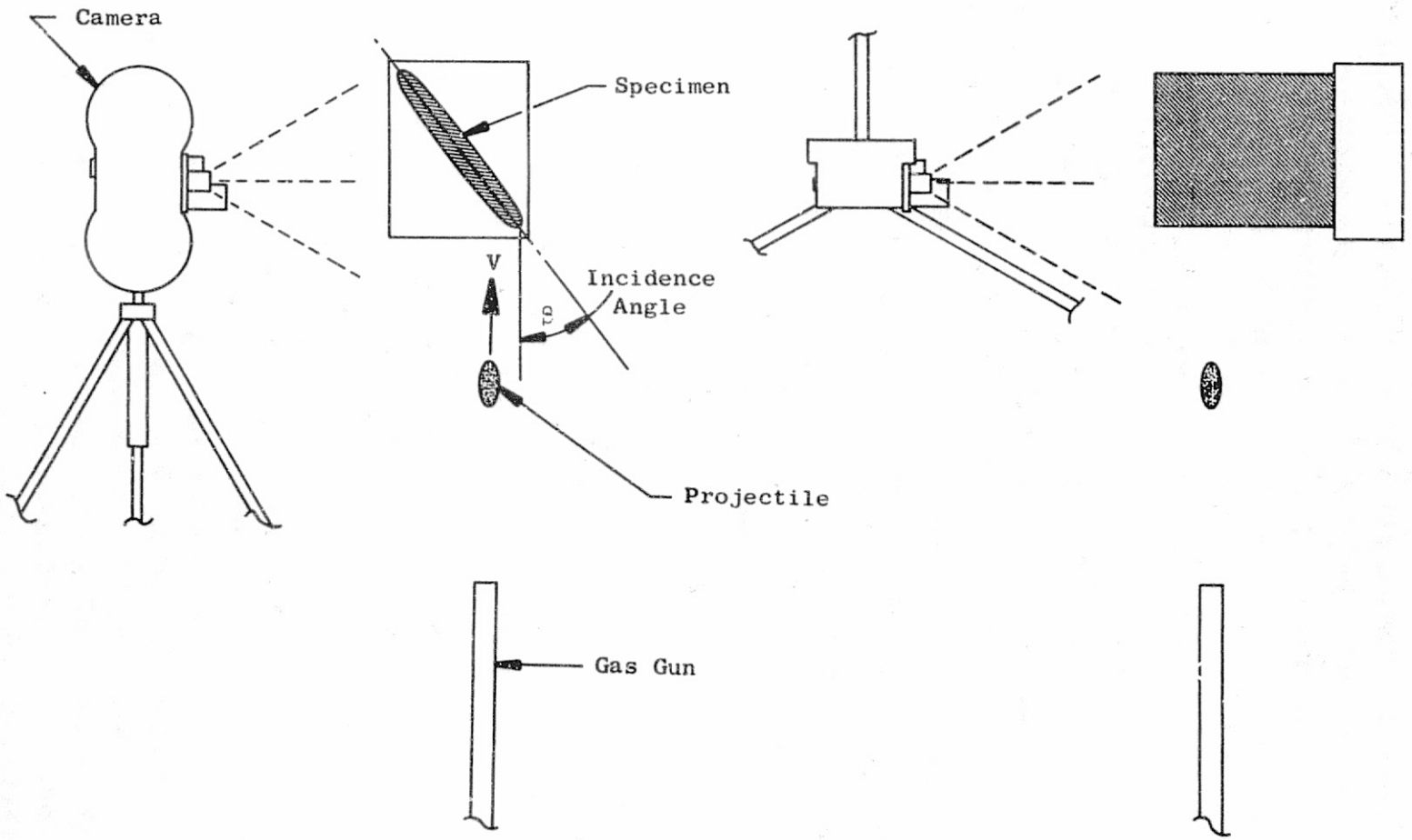

Figure 13. Static Impact Test Specimen.

the desired impact incidence angle between the specimen and the RTV projectile. Figure 14 presents a photograph of the test set-up showing the gas gun and specimen. High speed movies were used to record the specimen response to the impact and to measure the projectile velocity. Further, the movies played an important part in the evaluation of the test results.

3.5 TEST RESULTS AND DISCUSSION OF RESULTS

3.5.1 Design Modulus Versus Calculated Modulus

Prior to ballistic impact testing, natural frequencies were determined in a siren facility for all test specimens with the test specimen clamped over the lower 5 cm (2 inches) and free at the tip. The frequency and weight data for the 16 boron/aluminum specimens which were manufactured by TRW as well as two 80% AS/20% S-glass/PR288 epoxy specimens and an all 0° boron/aluminum specimens manufactured by General Electric are shown in Table III. A review of these data shows an unexpected variation in frequency which cannot be accounted for by change in layup angle. For example, specimen serial number 35 (±45° boron/aluminum) had a first flexural frequency of 67 Hz while specimen serial number 26 with a ±15° layup had a lower first flexural frequency (65 Hz). It would be expected that the lower angle layup (±15°) would exhibit a higher flexural frequency due to higher longitudinal modulus.

In order to help explain the measured frequencies, a simple load/deflection test was conducted on 10 of the specimens to obtain a modulus of elasticity for the specimens. This modulus was then used for comparison to the moduli calculated from the measured frequencies. The results of the load/deflection tests, the modulus and frequency calculations, and a comparison to measured values is shown in Table IV. Good agreement between dynamically measured and calculated moduli from the load/deflection test indicates that both the modulus values and the measured frequencies are correct. A comparison of the modulus for the all-boron/aluminum specimens to values obtained from Reference 1 is presented in Table V. This comparison shows the panel moduli in general, to, be lower than expected. It is felt this is due to the wire mesh outer covering applied to some specimens since the only panel tested (S/N 19) without wire mesh had a modulus comparable to Reference 1 values.

Because of the lower modulus of the stainless wire mesh ply, the effective moment of inertia (and therefore overall modulus) of the panel would be reduced to only 65% of the all B/Al panel value. This ratio is consistent with the observed modulus reduction.

Although the wire mesh caused a reduction in modulus in these small blade-like specimens, the wire mesh ply is a much smaller percent of the cross-sectional area in a large blade, and, thus, would have a much smaller effect on blade frequencies or modulus.

Figure 14. Test Series Number 1 Setup.

Table III. Blade-Like Shape Weights and Frequencies.

S/N	Description	Wt. (gms)		Frequency (Hz)			
		W/O Ni	With Ni	F_{1f}	F_{2f}*	F_{1t}*	F_{3f}
25	±15°	136	149	68	432	-	1192
26	±15°	133	146	65	381	429	1107
50	0°/+20°	137	149	68	452	-	1316
47	0°/+20°	135.5	148	68	435	405	1167
16	±15° No Ni and No Mesh	140	140	100	626	-	1732
19	±15° No Ni and No Mesh	138.5	138.5	96	618	552	1585
27	±30°	133	145	74	436	486	1232
36	±30°	134	148	68	379	480	1122
34	±45°	140	152	58	466	-	1034
35	±45°	136.5	149	67	418	470	1173
49	±30° Ti Core	145	157	64	442	-	1144
43	±30° Ti Core	157	169	68	411	444	1154
48	±45° Ti Core	147	158	62	346	452	956
42	±45° Ti Core	142	156	63	388	468	1100
44	±30° Ti LE	149	149	102	646	-	1722
45	±30° Ti LE	150.5	150.5	89	569	597	1526
17	0° ±35° Graphite	-	113	-	-	-	-
18	0° ±35° Graphite	-	114	57	375	286	1079
20	0°	-	146	69	388	464	1114

*Combination 2nd Flex and 1st Torsion.

Table IV. Measured Modulus and Frequencies.

Specimen S/N	Lay-up	Stiffness kN/m (lb/in.)	Modulus From Reference* MPa (psi)	Calculated MPa Modulus (psi) From Load Test	Calculated Flex Frequency (Hz) From Load Test	Measured Flex Frequency (Hz)	Modulus From Measured Frequency, MPa (psi)
19	±15° Ni/Mesh	11.42 (65.2)	0.200×10^6 (29.0×10^6)	0.190×10^6 (27.5×10^6)	103.9	96	0.162×10^6 (23.5×10^6)
21	0° ±35° G/E	4.45 (25.4)	---	0.070×10^6 (10.1×10^6)	71.6	Not Available	---
47	0°/+20°	4.73 (27.0)	0.203×10^6 (29.4×10^6)	0.121×10^6 (17.6×10^6)	75.8	68	0.098×10^6 (14.2×10^6)
26	±15°	5.78 (33.0)	0.200×10^6 (29.0×10^6)	0.113×10^6 (16.4×10^6)	72.0	65	0.092×10^6 (13.4×10^6)
42	±45° Ti Core	4.78 (27.3)	---	0.097×10^6 (14.0×10^6)	63.3	63	0.096×10^6 (13.9×10^6)
36	±30°	6.76 (38.6)	0.157×10^6 (22.8×10^6)	0.127×10^6 (18.4×10^6)	77.0	68	0.099×10^6 (14.4×10^6)
18	0° ±35° G/E	3.89 (22.2)	---	0.058×10^6 (8.4×10^6)	67.0	57	0.092×10^6 (13.3×10^6)
35	±45°	4.92 (25.8)	---	0.085×10^6 (12.4×10^6)	63.0	67	0.097×10^6 (14.0×10^6)
43	±30° Ti Core	6.79 (38.8)	---	0.103×10^6 (15.0×10^6)	72.6	68	0.091×10^6 (13.2×10^6)
45	±30° Ti LE No Mesh	9.54 (54.5)	---	0.137×10^6 (19.8×10^6)	91.2	89	0.130×10^6 (18.9×10^6)

*Values obtained from Figure 2 page 19, no wire mesh effects.

**Estimated based on ±10° data.

Table V. Estimated Modulus Compared to Measured Values.

Specimen	Modulus × 10^{-6} MPa (psi) Ref. 1	Dynamic*	Static**
19	0.200 (29.0)	0.162 (23.5)	0.190 (27.5)
47	0.203 (29.4)	0.98 (14.2)	0.121 (17.6)
26	0.200 (29.0)	0.92 (13.4)	0.113 (16.4)
42	--- ---	0.96 (13.9)	0.97 (14.0)
36	0.157 (22.8)	0.99 (14.4)	0.127 (18.4)
35	--- ---	0.97 (14.0)	0.85 (12.4)
43	--- ---	0.91 (13.2)	0.103 (15.0)
45	--- ---	0.130 (18.9)	0.137 (19.8)

*Calculated from test frequencies (equation).
**Calculated from static bend test (equation).

3.5.2 Initial Specimen C-Scans

Prior to any impact testing, the specimens were subjected to ultrasonic C-scan inspection to detect unbonded areas in the as-pressed specimens. These data identify specimen quality and serve as a baseline for comparison after the specimens were impacted. The pretest C-scans for all specimens are shown in Appendix A. Note that some of the specimens, as originally pressed, exhibited substantial delamination and were repressed in an effort to improve their quality.

The pretest C-scans further substantiate that the low specimen modulus values are chiefly due to the wire mesh. C-scans, which were run on specimen serial numbers 25 and 26 (±15° boron/aluminum) and specimen serial numbers 16 and 19 (±15° boron/aluminum without mesh or nickel), had essentially no indications of disbond and appeared to be of excellent quality. However, a comparison of the experimental modulus to the expected modulus showed that panels without wire mesh had a relatively high modulus while panels with wire mesh had a relatively low modulus. Since bonding was comparable, it appears that the wire mesh is responsible for the lower-than-expected modulus measured on the specimens with wire mesh.

3.5.3 Dimensional Variations

Due to unavoidable differences in the fabrication of each specimen, variations in the specimen dimensions are always present. Dimensional measurements made on each specimen prior to impact testing are shown in Table VI. From these data, it can be seen that the maximum variation in specimen width (B) is 1.7%, the variation in maximum thickness (A) is 10.6%, the variation in leading edge thickness (C) is 31.7%, and the variation in trailing edge thickness (D) is 23.3%. The question arises as to which variation has an effect on impact strength, which in turn requires knowledge of the failure mode. For the two test series which were run, there existed two primary failure modes. During the first series of tests, the majority of specimens experienced a root bending failure while for the second series of tests, a majority of the failures occurred at the leading edge in the region of the impact. Accordingly, for the first series the ratio Y/I_{min} (where Y = maximum distance from the I_{min} axis to the surface) would be a meaningful parameter, while for the second series, the leading edge thickness would have an effect. These parameters are shown in Table VII along with the ratio of each specimen to the average. For clarity, the specimens have been divided into two groups according to the test series they were tested in. In this comparison, it is assumed that a thicker leading edge or a lower Y/I_{min} value will produce better impact resistance.

Based on the results presented in Table VII, it is seen that dimensional variation has only a relatively small effect on specimen performance.

Table VI. Dimensional Measurements.

S/N	Layup	A cm (inches)	B cm (inches)	C cm (inches)	D cm (inches)	Cross Section Area cm^2 ($in.^2$)	$I_{min.}$ cm^2 ($in.^4$)
25	±15°	0.376 (0.148)	7.633 (3.005)	0.196 (0.077)	0.165 (0.065)	2.11 (0.327)	0.01523 (0.000366)
26	±15°	0.366 (0.144)	7.648 (3.011)	0.198 (0.078)	0.150 (0.059)	2.07 (0.321)	0.01428 (0.000343)
50	0°/+20"	0.376 (0.148)	7.643 (3.009)	0.201 (0.079)	0.168 (0.066)	2.14 (0.331)	0.01557 (0.000374)
47	0°/+20°	0.371 (0.146)	7.684 (3.025)	0.196 (0.077)	0.165 (0.065)	2.12 (0.328)	0.01503 (0.000361)
16	±15° No Mesh	0.396 (0.156)	7.620 (3.000)	0.191 (0.075)	0.191 (0.075)	2.23 (0.345)	0.01786 (0.000429)
19	±15° No Mesh	0.391 (0.154)	7.633 (3.005)	0.183 (0.072)	0.178 (0.070)	2.18 (0.338)	0.01686 (0.000405)
27	±30°	0.363 (0.143	7.671 (3.020)	0.180 (0.071)	0.155 (0.061)	2.02 (0.313)	0.01336 (0.000321)
36	±30°	0.373 (0.147)	7.666 (3.018)	0.198 (0.078)	0.157 (0.062)	2.10 (0.326)	0.01490 (0.000358)
34	±45°	0.384 (0.151)	7.663 (3.017)	0.211 (0.083)	0.168 (0.066)	2.18 (0.338)	0.01644 (0.000395)
35	±45°	0.373 (0.147)	7.656 (3.014)	0.191 (0.075)	0.170 (0.067)	2.10 (0.326)	0.01482 (0.000356)
49	±30° Ti Core	0.381 (0.150)	7.640 (3.008)	0.185 (0.073)	0.175 (0.069)	2.14 (0.331)	0.01573 (0.000378)
43	±30° Ti Core	0.394 (0.155)	7.668 (3.019)	0.221 (0.087)	0.180 (0.071)	2.27 (0.352)	0.01836 (0.000441)
48	±45° Ti Core	0.381 (0.150)	7.620 (3.000)	0.191 (0.075)	0.160 (0.063)	2.12 (0.328)	0.01557 (0.000374)
42	±45° Ti Core	0.366 (0.144)	7.706 (3.034)	0.188 (0.074)	0.150 (0.059)	2.06 (0.319)	0.01390 (0.000334)
44	±30° Ti LE	0.404 (0.159)	7.645 (3.010)	0.201 (0.079)	0.191 (0.075)	2.28 (0.354)	0.01898 (0.000456)
45	±30° Ti LE	0.406 (0.160)	7.630 (3.004)	0.201 (0.079)	0.196 (0.077)	2.30 (0.357)	0.01965 (0.000472)
17	0° ±35° G/E	0.378 (0.149)	7.752 (3.052)	0.249 (0.098)	0.178 (0.070)	2.27 (0.352)	0.01786 (0.000429)
18	0° ±35° G/E	0.381 (0.150)	7.747 (3.050)	0.264 (0.104)	0.170 (0.067)	2.31 (0.358)	0.01886 (0.000453)

Table VII. Geometry Parameters Affecting Impact Resistance.

Test Series Number 1

S/N	Layup	cm^{-3} ($in.^{-3}$)($Y/I_{min.}$)	$(Y/I_{min.})/(Y/I_{min.\ average})$
25	±15°	12.33 (202)	1.02
50	0°/+20°	12.08 (198)	1.01
16	±15° No Mesh	11.11 (182)	0.93
27	±30°	13.61 (223)	1.14
34	±45°	11.66 (191)	0.97
49	±30° Ti Core	12.08 (198)	1.01
44	±30° Ti LE	10.62 (174)	0.89

Test Series Number 2

S/N	Layup	Leading Edge Thickness cm (in.)	$t/t_{average}$
26	±15°	0.198 (0.078)	1.01
47	0°/+20°	0.196 (0.077)	0.99
19	±15° No Mesh	0.183 (0.072)	0.93
36	±30°	0.198 (0.078)	1.01
35	±45°	0.191 (0.075)	0.97
43	±30° Ti Core	0.221 (0.087)	1.12
42	±45° Ti Core	0.188 (0.074)	0.95
45	±30° Ti LE	0.201 (0.079)	1.02

3.5.4 Initial Impact Testing

In the first test series, the test setup described in Section 3.4 was used.

Static ballistic impact testing was performed on one of each type of specimen. The incidence angle was set at 25° and a 15 gm (0.528 oz.) RTV projectile 2.54 cm (1-inch) in diameter was used. The center of impact occurred at 75% span approximately 1.52 cm (0.6-inch) back of the leading edge. High speed movies were made during each impact and ultrasonic C-scans were made of the specimens following each impact. A test summary of this first series of tests is presented in Table VIII. Pictures of the specimens following testing along with the corresponding C-scans are included in Appendix B. Observations from the impact tests indicate the following:

- Final failure occurred at the root near the clamping attachment in bending on all specimens except the ±45° boron/aluminum with titanium core spar which suffered large permanent deformations.

- Very little local impact damage other than local yielding was observed on any of the specimens tested with the exception of serial number 50. This specimen was inadvertently tested with the +20° fibers going in the wrong direction.

Since local FOD damage resistance evaluation was the purpose of this testing, data from this first test phase is not entirely applicable since the specimens did not fail by local impact but instead had root bending failures, however, much useful information can still be obtained. Figure 15 presents the data for each specimen in terms of the normal kinetic energy, E_N, which is equal to:

$$E_N = \frac{W_S V_N^2}{2}$$

where:

W_S = RTV Projectile weight = 15 gms

V_N = velocity of impacting object relative to the specimen normal to the specimen

For each specimen, the horizontal ticks show the individual data points and the vertical line represents the region in which root failure occurred. This curve suggests that all the specimens failed at about the same level with the exception of the ±30° and ±30° with Ti leading edge specimens. The ±39° specimen showed a higher level of impact resistance [(about 75J (55 ft-lb) versus an average of 41-54J (30-40 ft-lb)] for the other specimens). The ±30° with Ti leading edge showed a substantial advantage with an average failure value of about 102J (75 ft-lb).

Table VIII. Blade-Like Shape Impact Test Results - Series Number One.

S/N	Layup	Impact No. 1		Impact No. 2		Impact No. 3		Impact No. 4		Impact No. 5	
		Velocity, m/sec (ft/sec)	Remarks	Velocity, m/sec (ft/sec)	Remarks	Velocity, m/sec (ft/sec)	Remarks	Velocity, m/sec (ft/sec)	Remarks	Velocity, m/sec (ft/sec)	Remarks
25	±15	106.7 (350)	10° Twist Tip-to-Root	156.1 (512)	Twist and 3/16" Bend	229.5 (753)	Fracture at Clamp	---	---	---	---
50	1/+20	112.8 (370)	5° Twist Local Bend	156.1 (512)	Twist and 7/16" Bend	228.6 (750)*	Fracture at Impact and Clamp	---	---	---	---
16	+15 No Ni	105.2 (345)	1/16" Bend at Impact	151.2 (496)	1/8" Bend at Impact	224.3 (736)	Fracture at Clamp	---	---	---	---
27	±30	59.7 (196)	No Damage	161.5 (530)	1/8" Bend Tip-to-Root	215.2 (706)	5/8" Bend Tip-to-Root	256.6 (842)	Fracture at Clamp	---	---
34	±45	93.6 (307)	5/8" Bend Tip-to-Root	154.8 (508)	1-1/8" Bend Tip-to-Root	227.1 (745)	Fracture at Clamp	---	---	---	---
49	±30 Ti Core	114.0 (374)	3/8" Bend Tip-to-Root	145.4 (477)	7/16" Bend Tip-to-Root	220.4 (723)	Fracture at Clamp	---	---	---	---
48	±45 Ti Core	98.8 (324)	9/16" Bend Tip-to-Root	162.8 (534)	1-3/16" Bend Tip-to-Root	221.6 (727)	2-5/8" Bend Tip-to-Root	---	---	---	---
44**	±30 Ti LE	89.3 (293)	-7/16" Bend Tip-to-Root	142.3 (467)	-5/16" Bend Tip-to-Root	224.0 (735)	-1/8" Bend Tip-to-Root	263.3 (864)	0.6 cm (1/4") Bend Tip-to-Root	285.0 (935)	Fracture at Clamp
17	0+35	106.7 (350)	No Damage	163.7 (537)	Fracture at Clamp	---	---	---	---	---	---
20	0	103.3 (339)	No Damage	161.8 (531)	10° Twist Tip-to-Root	226.2 (742)	15° Twist Tip-to-Root	---	---	---	---

*Estimated
**Bowed prior to test

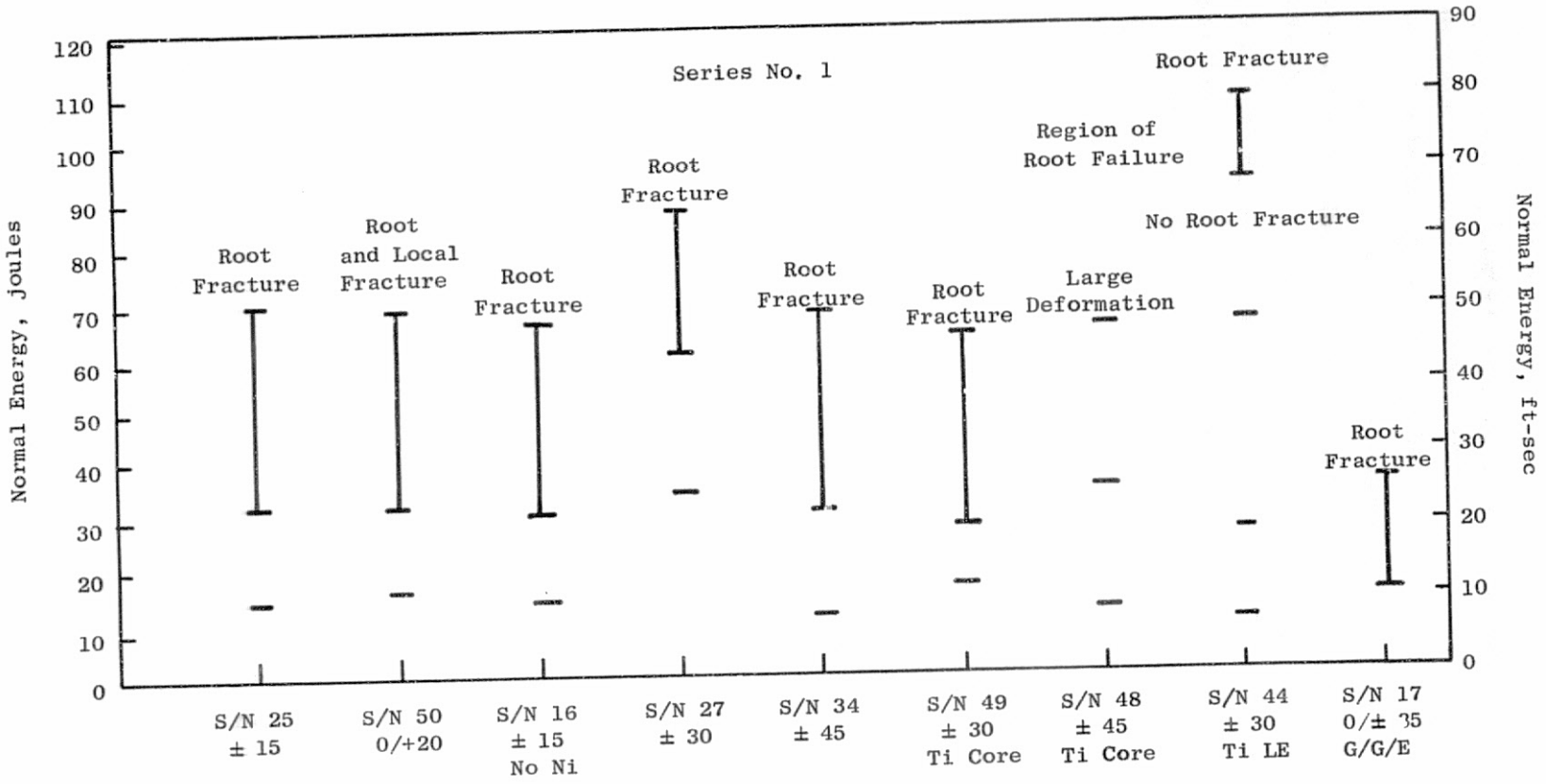

Figure 15. Normal Energy Range in Which Root Failure Occurred.

Several observations may be made from Figure 16 which shows "Percent C-Scan Indications Versus Total Normal Kinetic Energy". The total energy is defined as the sum of all the energies the specimens sustained. The first observation concerns the quality of the data obtained. Specifically, several of the specimens show a drop in percent C-scan indications with additional normal energy absorbed. This indicates a change in C-scan sensitivity or an error in measuring the area of C-scan indications. Assuming that the data presented is reasonably consistent relative to trends, an observation may be made relative to the propagation of C-scan indication versus specimen layup. For the higher angle layups (±30°, ±45°, etc.), the area of C-scan indications increase more rapidly than for the lower angle layups (±15°, 0°/+20°). The only exception to this trend is the ±30° with titanium leading edge.

3.5.5 Modified Impact Testing

As noted in Section 3.5.4, no real local failures were obtained in the first series of tests due to bending failures in the root of the cantilevered specimens. In an attempt to remedy this situation, seven of the specimens which had broken at the clamp were cut off just above the fracture and impacted one time each. Velocities ranged from 228 m/s (749 feet per second) for specimen No. 17 to 299 m/s (981 feet per second) for specimen No. 44. A 15 gm projectile was fired at a height of 8.9 cm (3.5-inches above) the clamp (versus the previous impacts which occurred 15.2 cm (6-inches) above the clamp). The same incidence angle of 25° was used for this testing.

The results of these retested specimens are shown below:

Shot No.	S/N	Layup	Velocity m/sec (ft/sec)	Normal K.E.J. (ft-lb)	Remarks
33	17	±0 ±35° Graphite	288 (749)	69.6 (51.3)	Fracture at clamp
34	44	±30° Ti LE	299 (981)	119 (88)	2.54 cm (1") of tip Le spar unbonded
35	16	±15° No Ni	259 (850)	90 (66)	Fracture at clamp - slight fracture at impact
36	27	±30°	285 (936)	109 (80)	Fracture at clamp - bend at impact
37	25	±15°	280 (918)	104 (77)	Fracture at clamp - gross delamination at impact

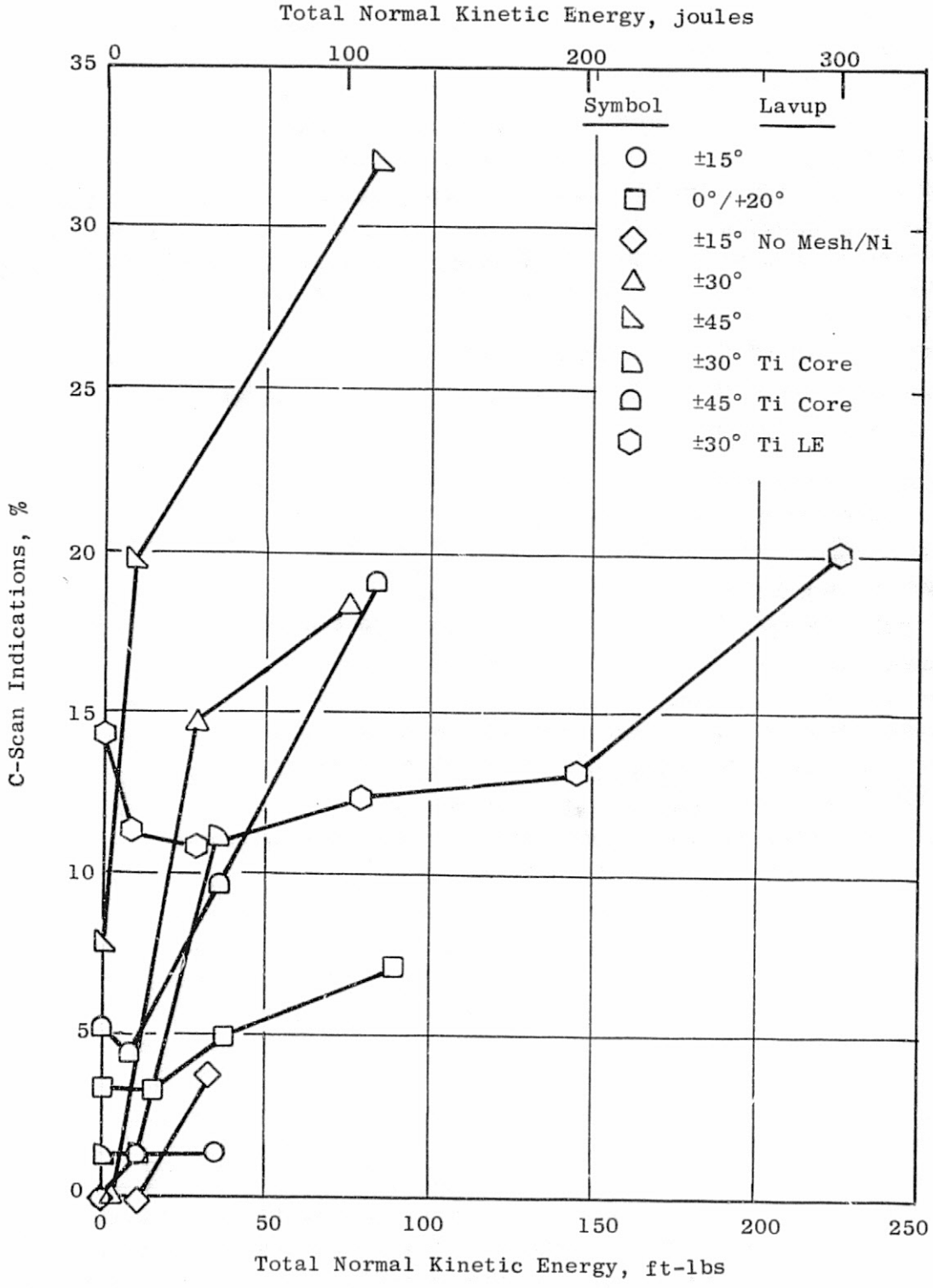

Figure 16. Percent C-Scan Indications Versus Total Kinetic Energy.

Shot No.	S/N	Layup	Velocity m/sec (ft/sec)	Normal K.E.J. (ft-lb)	Remarks
38	49	±30° Ti Core	277 (909)	103 (75.6)	Fracture at clamp - slight fracture at impact
39	34	±45°	281 (921)	105 (77.6)	Fracture at clamp - slight fracture at impact

From this series of tests, the following observations were made. (1) Even with the impact occurring closer to the clamp, all but one of the seven specimens fractured at the clamp; the one specimen which did not fracture at the root was the ±30° specimen with the Ti leading edge spar, and (2) five of the boron/aluminum specimens suffered some local damage of varying degrees with the ±30° titanium core spar specimen exhibiting the least local damage and the ±15° specimen suffering a gross delamination through the center ply.

These tests indicated that lowering the impact location provides some improvement but was not sufficient to insure a local failure prior to failure at the clamp. In addition, at the high velocities required for failure of the specimen, the velocity capability of the 2.54 cm (1-inch) gun had been reached. Therefore, a fixed-supported set-up was devised and a 5.1 cm (2-inch) gun with a 33 gm projectile 2.54 cm (1-inch) in diameter was used. The setup decided upon is shown schematically in Figure 17. The specimen was clamped in a vice with 0.63 cm (1/4-inch) pads of RTV on either side to soften the root clamp and thereby reduce the stress concentration. In addition, a 7.6 cm (3-inch) diameter by 5.1 cm (2-inch) long cylinder of RTV was attached to a bar parallel to the tip of the specimen leaving approximately a 3.8 cm (1.5 inch) gap between the specimen tip and the RTV. The 25° incidence angle was maintained. The theory behind this setup was that after the impact, the specimen would strike the RTV cylinder which would limit the bending strain energy in the root, therefore, preventing failure there. A series of trial shots were made with a scrap specimen. Review of the high speed film shots indicated that the increased volume of air coming from the 5.1 cm (2-inch) gun (versus the previous 2.54 cm (1-inch) gun) was causing the specimen to bend out of the path of the projectile with the resulting impact occurring on the trailing edge. In order to counteract this effect, a length of thin wire was tied to a part of the framework, run around the side of the specimen away from the impact, and tied back to the original point (see Figure 17). The wire was placed so that it would be cut by the projectile prior to specimen impact. Additional trial shots were made and high-speed movies showed this procedure to be successful in limiting the premature movement of the test specimen. A series of impacts were then run on the second set of specimens with the results shown in Table IX.

Appendix C presents photographs of the specimens after test and C-scan results after each impact.

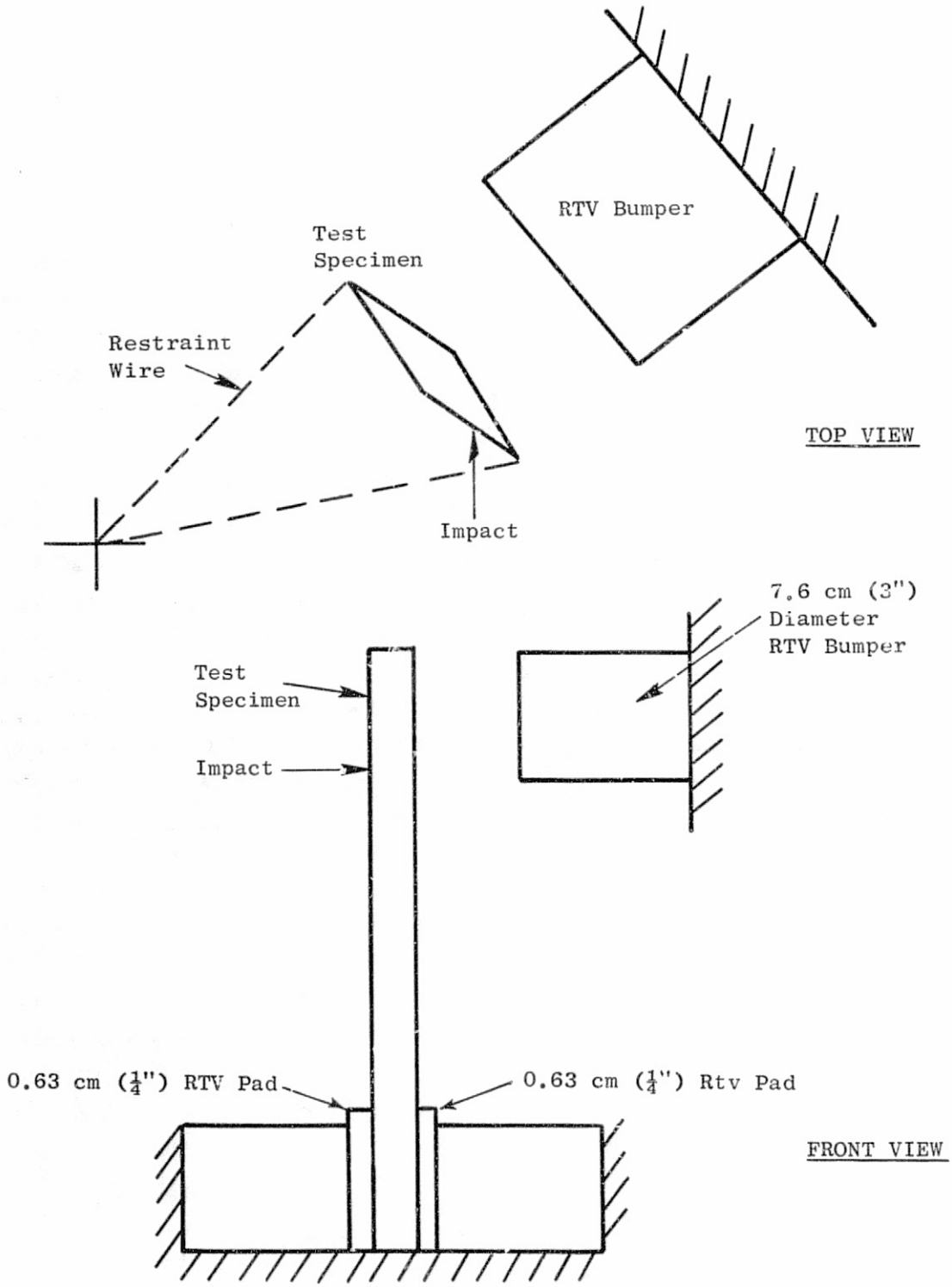

Figure 17. Test Setup Schematic.

Table IX. Blade-like Shape Impact Test Results - Series Number Two.

33 gm Projectile, 25° Incidence Angle									
		Impact No. 1		Impact No. 2		Impact No. 3		Impact No. 4	
S/N	Layup	Velocity, m/sec (ft/sec)	Remarks	Velocity, m/sec (ft/sec)	Remarks	Velocity, m/sec (ft/sec)	Remarks	Velocity, m/sec (ft/sec)	Remarks
18	0±35 Gr	201.2 (660)	No Damage	261.5 (858)	No Damage	323.1 (1060)	Fracture @ Impact & Clamp	---	---
47	0/+20	252.7 (829)	Crack @ Impact Nil E. Peeled Back	---	---	---	---	---	---
45	±30 Ti L.E.	199.9 (656)	L.E. Bend and Delamination Tip	19.2 (63)	More Unbond of Ti L.E. @ Tip	309.1 (1014)	Bend @ Impact, L.E. Tip Split	332.2 (1090)	Severe Local Damage
19	±15 No Ni No Mesh	199.3 (654)	Slight Crack @ Clamp	274.0 (899)	Additional Crack at Clamp	335.3 (1100)	Severe Crack @ Clamp - Deformation at Impact	---	---
26	±15	198.4 (651)	No Damage	280.7 (921)	Fract. @ Impact & at Clamp	---	---	---	---
36	±30	199.3 (654)	Slight Bend @ Impact	272.8 (895)	Add. Bend.	313.3 (1028)	Fracture @ Impact	---	---
43	±30 Ti Core	197.8 (649)	Slight Bend Tip-to-Root	270.4 (887)	Additional Bending	338.3 (1110)	Additional Bending	---	---
35	±45°	199.0 (653)	Severe Bend Tip-to-Root	---	---	---	---	---	---
42	±45° Ti Core	204.5 (671)	Bend Tip-to-Root, Ni Peeled Back	---	---	---	---	---	---

Figure 18 presents graphically the impact damage for each specimen as a function of the normal energy. Three specimens sustained similar maximum impact energies. These were S/N 45 (±30° with titanium leading edge), S/N 43 (±30° with titanium core spar), and S/N 19 (±15° without mesh or Ni). However, specimen S/N 43 did not sustain a fracture at the highest impact level and accordingly should be ranked higher than the other two specimens. In addition, specimen S/N 19 sustained a root fracture at the initial impact. In Figure 19, the "Percent C-Scan Indications Versus Total Normal Energy" for the specimens from test series No. 2 is presented. From these data, it appears that the ±15° without Ni/mesh specimens sustained the lowest increase in C-scan indications with increasing impact levels. The ±30° titanium core and ±30° titanium leading edge specimens were rated next as far as increase in C-scan indications. The remaining specimens either suffered a failure at a much lower energy level or had a large increase in percent C-scan indications.

Figure 20 presents a summary of the important impact parameters for all the panels tested in test series number 2. The figure shows the percent delamination and other parameters such as permanent deformation, fracture, and root cracks for each shot. Also indicated is the impact level where the utility of the panel was judged to be lost due to one or a combination of the above parameters.

3.5.6 Evaluation Summary

Based on the testing conducted, the following conclusions have been drawn:

- Addition of the wire mesh/leading edge protection adversely effected (lowered) panel modulus values.
- Some of the panels exhibited as-pressed delaminations which were not eliminated by the repressing attempts of TRW.
- In the initial test series, where root bending failures were experienced, the best impact resistance was exhibited by a panel with a titanium leading edge and ±30° boron/aluminum plies. An all-boron/aluminum panel with ±30° plies also exhibited good impact resistance.
- In the second test series, where local failures were predominant, both ±15° and ±30° layups exhibited excellent impact characteristics.
- In both test series, ±45° layups did not demonstrate good impact resistance relative to the ±15° or ±30° layups.
- In the second test series the ±15° layup without nickel plate and wire mesh out performed a ±15° layup with nickel plate and wire mesh suggesting the wire mesh lowered the soft body impact resistance as well as modulus.

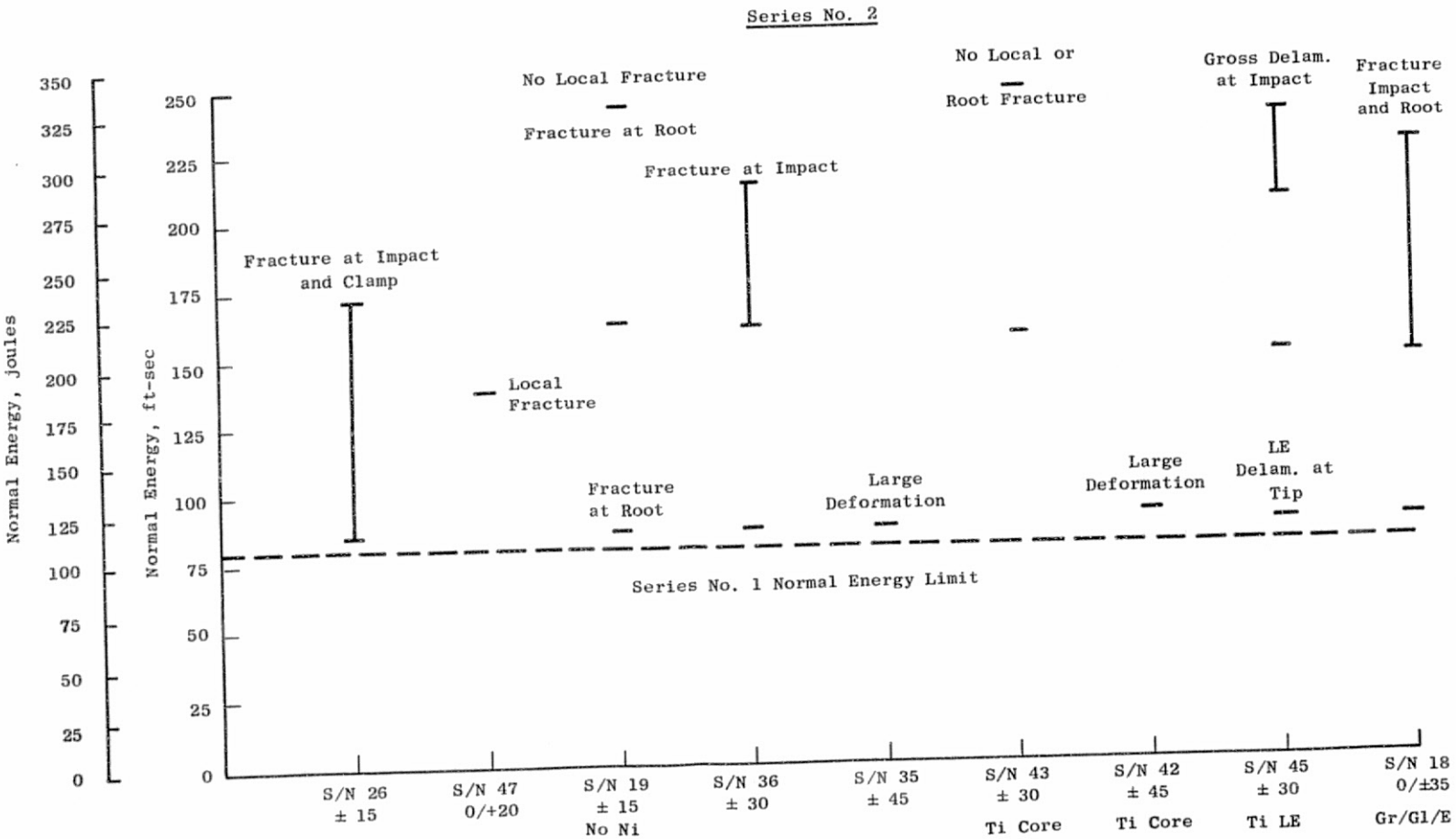

Figure 18. Normal Energy Range in Which Local Failure Occurred.

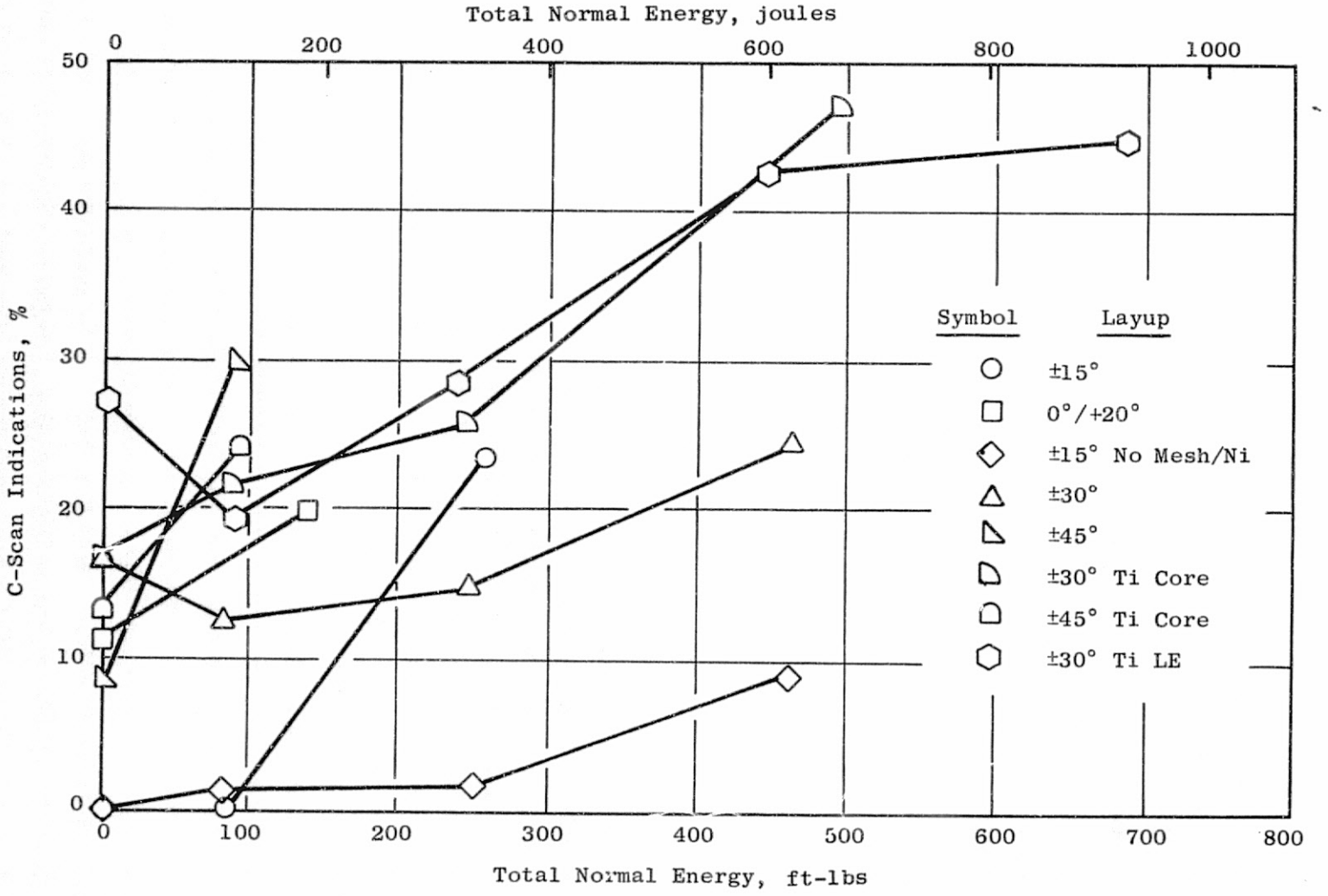

Figure 19. Percent C-Scan Indications Versus Total Normal Energy.

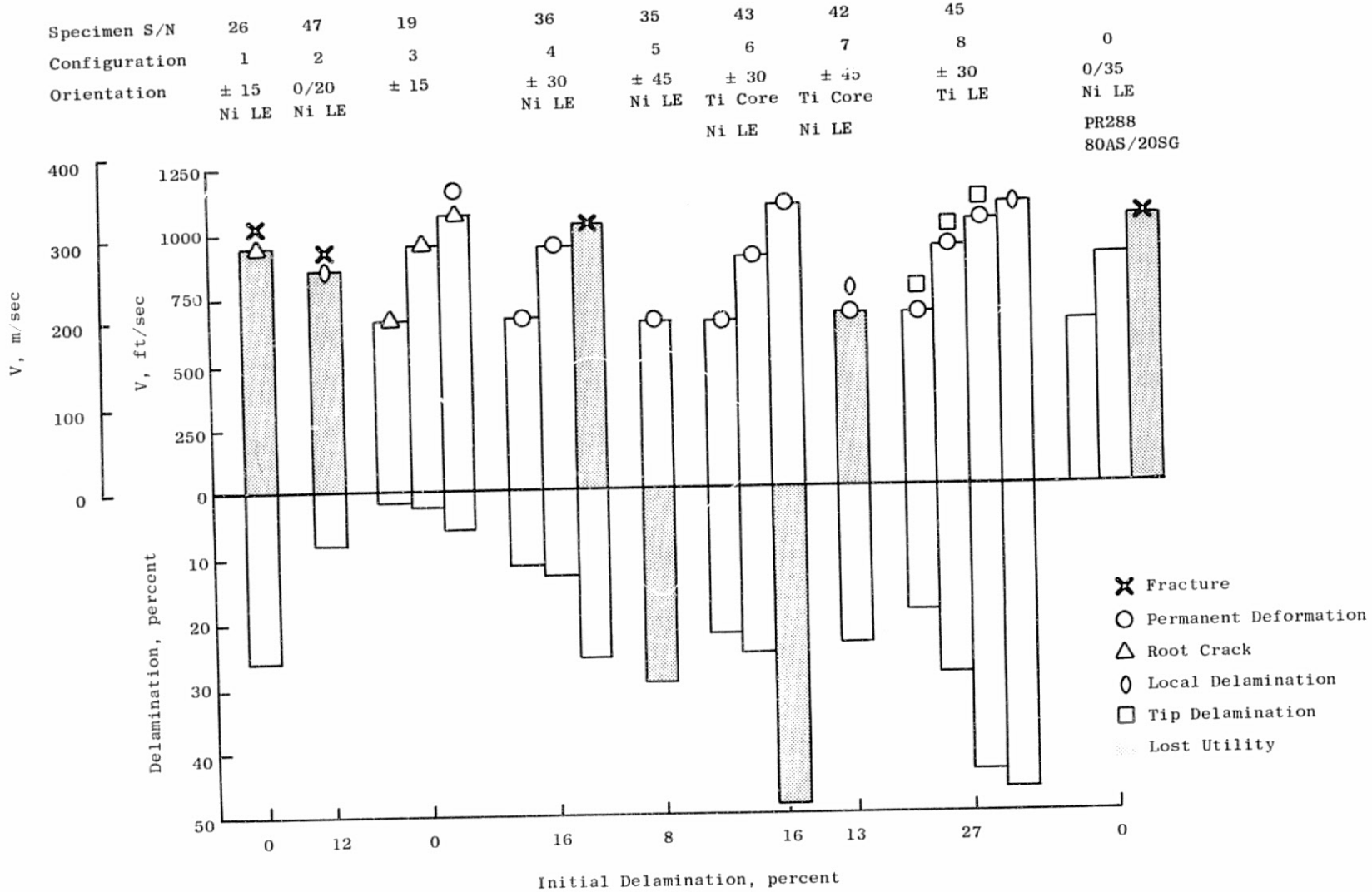

Figure 20. Test Series Number 2 Data Summary.

- In the first series of tests, the leading edge titanium spar was superior to the internal spar design and to all boron/aluminum panels indicating good bending strength at the root. In the second series of tests, both the leading edge and internal spar designs exhibited good resistance to local fracture and tearing but delaminations due to unbonding between the spar and boron/aluminum were experienced.

4.0 FAN BLADE DESIGN

The objective of the fan blade design phase was to perform preliminary design studies of a solid boron/aluminum blade using the results of Task I testing as a basis to select the material layup.

The as-designed CF6 titanium blade geometry, excluding the midspan shroud, was utilized to perform design studies on an airfoil material direct substitution basis to predict the frequencies, stresses, and weight of a 38-blade-design, solid boron/aluminum blade for comparison with the solid titanium design.

4.1 BLADE GEOMETRY

The CF6 forged titanium blade aero design definition used for the B/Al blade is presented in Table X, and the detailed geometry as a function of radial blade height is presented in Figure 21.

Ply patterns were generated from a titanium CF6 blade which had the midspan shroud removed. This was accomplished by generating thickness contours on the unshrouded CF6 blade using a set of pinpoint micrometers. The contours were made in 0.026 cm (10.4 mil) increments which represents the B/Al ply thickness. These contours were then lifted off the blade and used to loft flat patterns. The plies were extended into the root to form a constant thickness section from leading edge to trailing edge. Figure 22 presents the flat patterns used.

4.1.1 FOD Resistance

Based upon the static impact results presented in Section 3.5.6, there were two candidates for the solid boron/aluminum fan blade design in terms of FOD resistance. One candidate is a ±30° layup angle with 0.02 cm (8 mil) boron and 1100 aluminum. From the data presented in Section 3.5.5, it can be seen that this configuration was ranked highest in test series number one and second in test series number two. A second possible candidate was the ±15° 0.02 cm (8 mil) boron/1100 aluminum without mesh or Ni which was ranked best from test series number two. There were several factors which were taken into consideration before a decision was made:

- The specimen with the ±15° layup did not have an outer layer of mesh and the ±30° specimen did. In place of the mesh layer was an additional layer of boron/aluminum. In a real blade design, mesh is required for erosion and hard body FOD enhancement. This suggests the ±30° layup may be somewhat superior to the ±15° layup from an impact standpoint.

Table X. CF6-50 Forged Titanium Blade Aero Design.

Airfoil Definition	
Aero Design Point rpm	4080
Tip Speed	457 m/sec (1500 ft/sec)
Radius Ratio	0.412
Number of Blades	38
Aspect Ratio	3.85
Tip Chord	24.9 cm (9.8 in.)
Root Chord	16.3 cm (6.4 in.)
Blade Length	76.5 cm (30.1 in.)
Root Chamber, degree	82.1
Total Twist, degree	58°
Solidity, Tip	1.39
Solidity, Root	2.2
Root Tm/c	9%
Blade Weight	4.76 kg (10.5 lb)

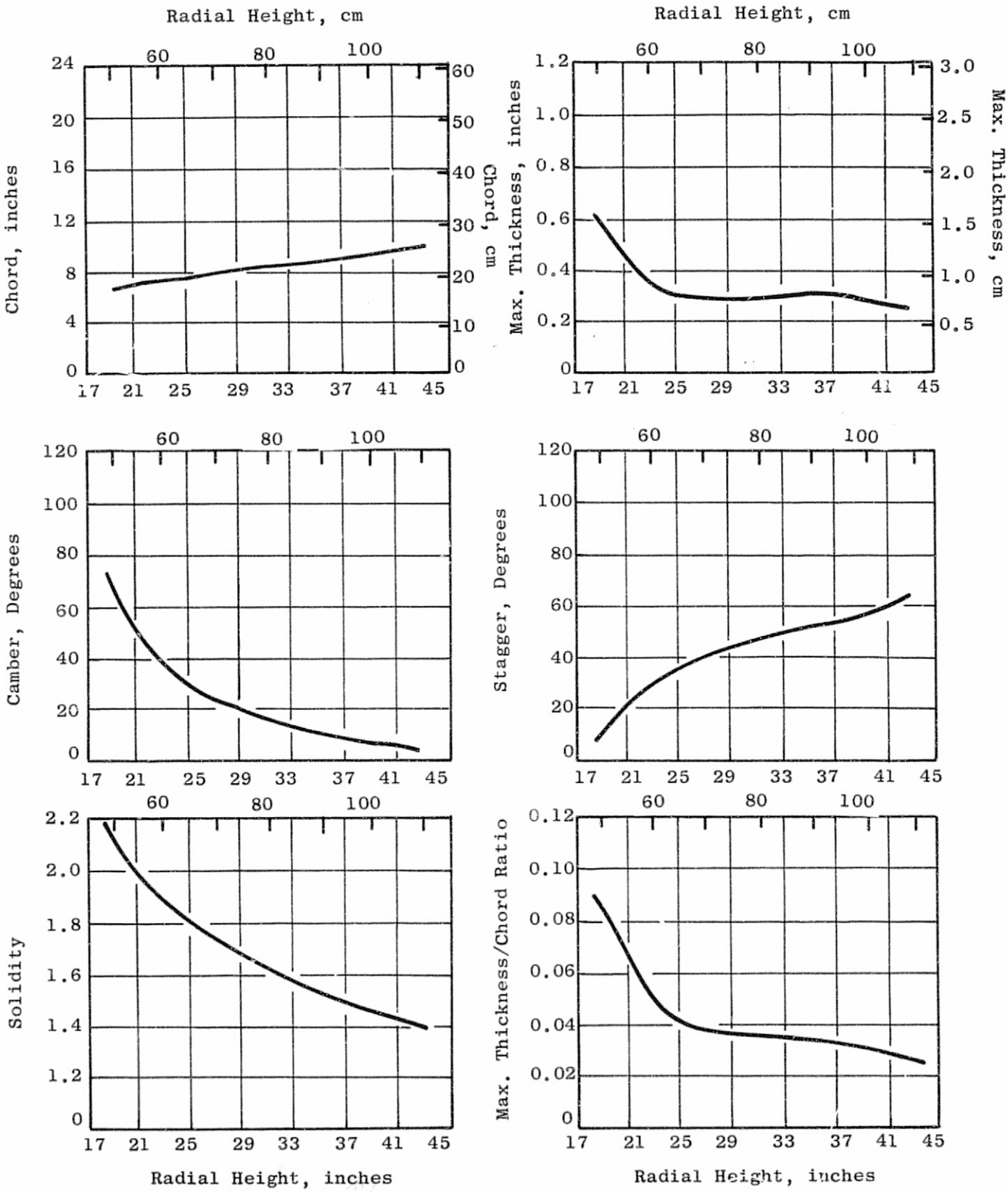

Figure 21. CF6-50 Titanium Blade Geometry.

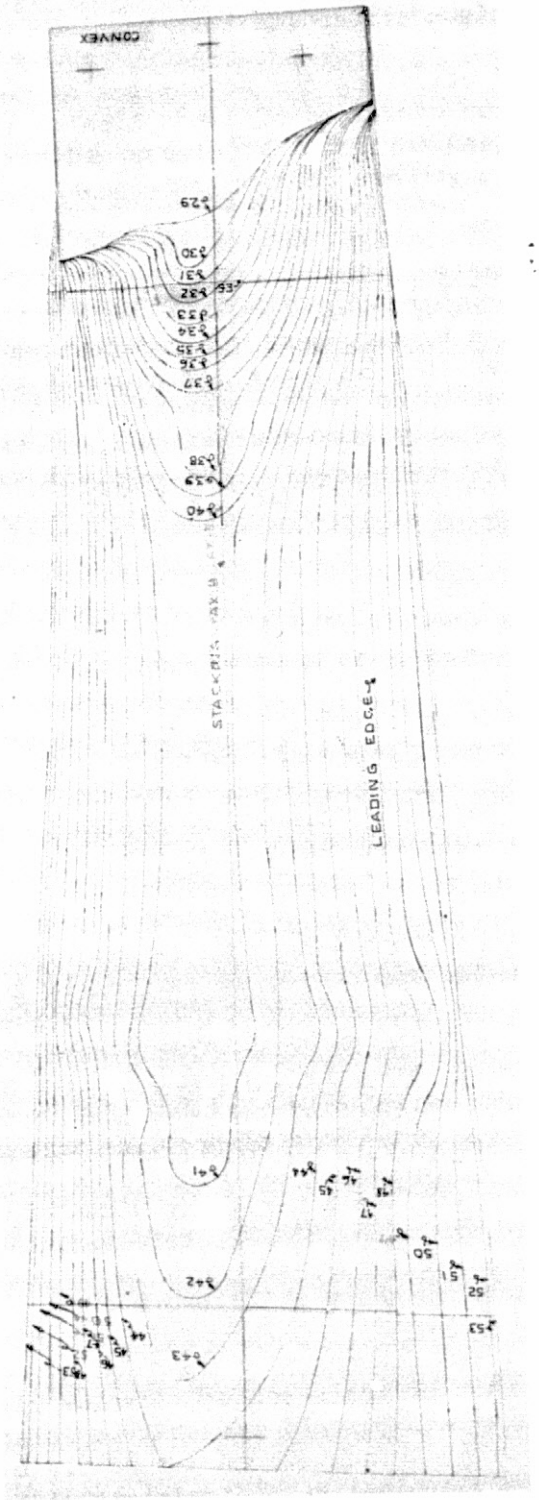

Figure 22. B/Al Blade Flat Patterns.

- The ±15° layup is a proven blade layup with excellent strength and fatigue properties while the ±30° layup may not have adequate strength and fatigue properties for the blade under consideration.

With the objective of utilizing the advantages of both layups, it was decided to use a blade layup comprised of ±30° plies on the outside of the blade for impact strength and torsional stiffness and a ±15° ply layup in the core to provide radial strength and bending stiffness.

4.1.2 Frequency Characteristics

The design of composite blading must avoid undesirable aerodynamically-induced excitations, whether they be forced or resonant vibrations. A Campbell diagram is constructed to predict potential vibration problems. It shows the blade natural frequency characteristics and potential forcing frequencies in the engine operational range. The Campbell diagram for the selected B/Al blade design showing the estimated frequency characteristics is shown in Figure 23.

The first flexural resonant mode of the blade is of primary concern. As indicated in Figure 23, the CF6 titanium blade is a "High Flex" design, i.e., the blade first flexural frequency is greater than the 2 per rev excitation line. This relatively high first flexural frequency of the titanium blade is achieved by the use of a part span shroud. This part span shroud causes undesirable aerodynamic losses. However, removal of the shroud would reduce the first flexural frequency and cause it to cross the 2 per rev excitation within the engine operating speed (a "Low Flex" design). For a titanium blade, the high flexural is required due to its high stress response and high notch sensitivity.

Most first-stage titanium fan blades require part span shrouds to obtain the required frequency response and to avoid limit cycle induced stresses. The part span shroud design is not readily adaptable to the boron/aluminum composite blades. However, good internal damping of the composite materials can have the effect of reducing the vibratory stress levels to acceptable levels. The very high modulus-to-density ratio of the composites results in frequency responses comparable with those of metallic midspan-shrouded blades.

Since the boron/aluminum composite design is a cantilevered blade (no part span shrouds), the resulting "Low Flex" boron/aluminum blade is designed to position the first flexural frequency to cross the 2 per rev excitation in a safe engine operational zone as shown in Figure 23.

The first torsional natural frequency of the B/Al CF6 cantilevered blade is considerably lower than that of the shrouded titanium blade and the resulting aeroelastic reduced velocity would probably be in an unacceptable range (see Figure 24). In order to achieve an acceptable blade from an engine installation and aeromechanical stability standpoint, the basic design (i.e., number of blades, chord, root thickness) must be modified for a boron/aluminum blade. For the CF6 application on the order of 30-34 boron/aluminum

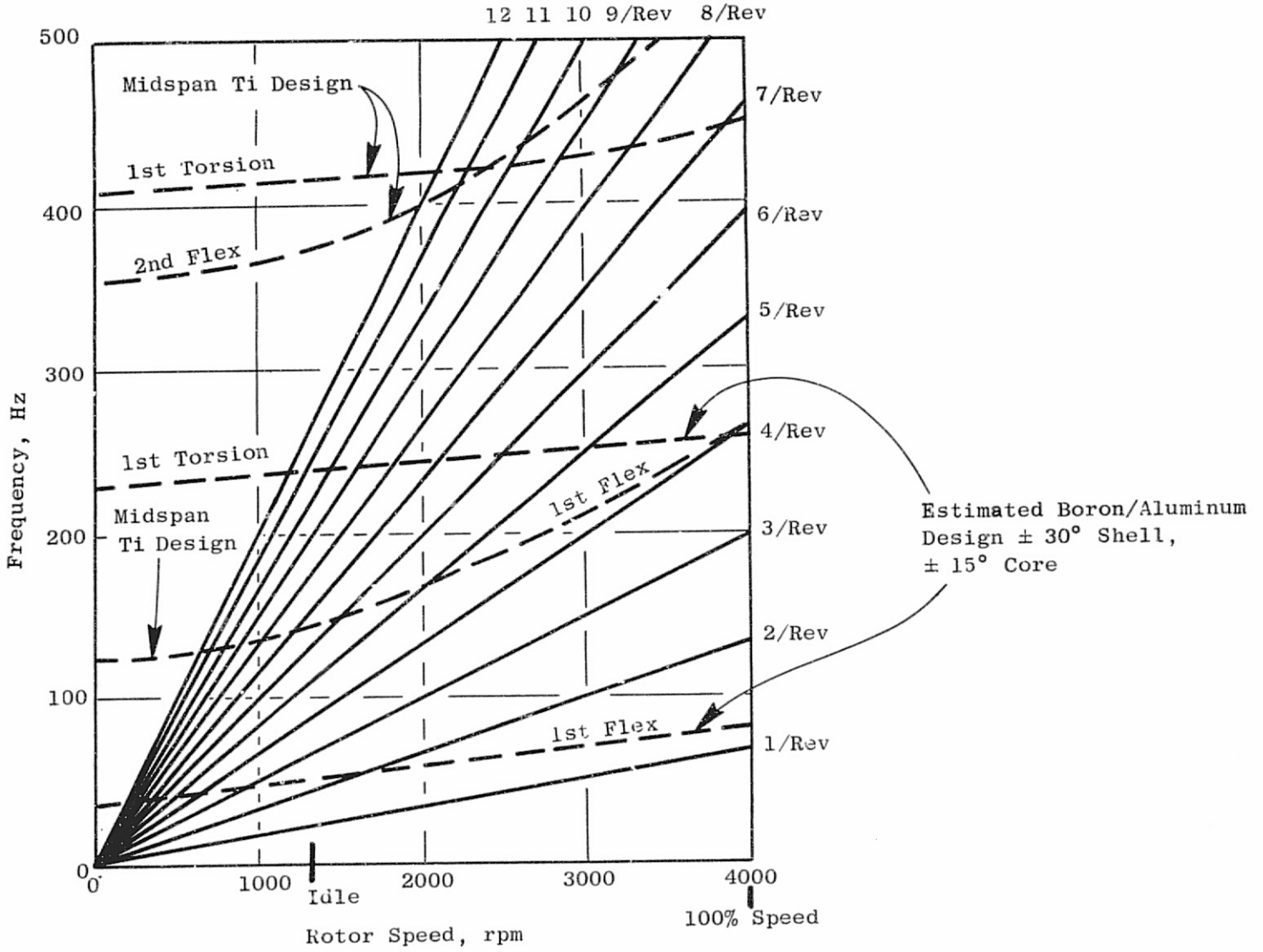

Figure 23. Campbell Diagram for the B/Al and Titanium Fan Blade.

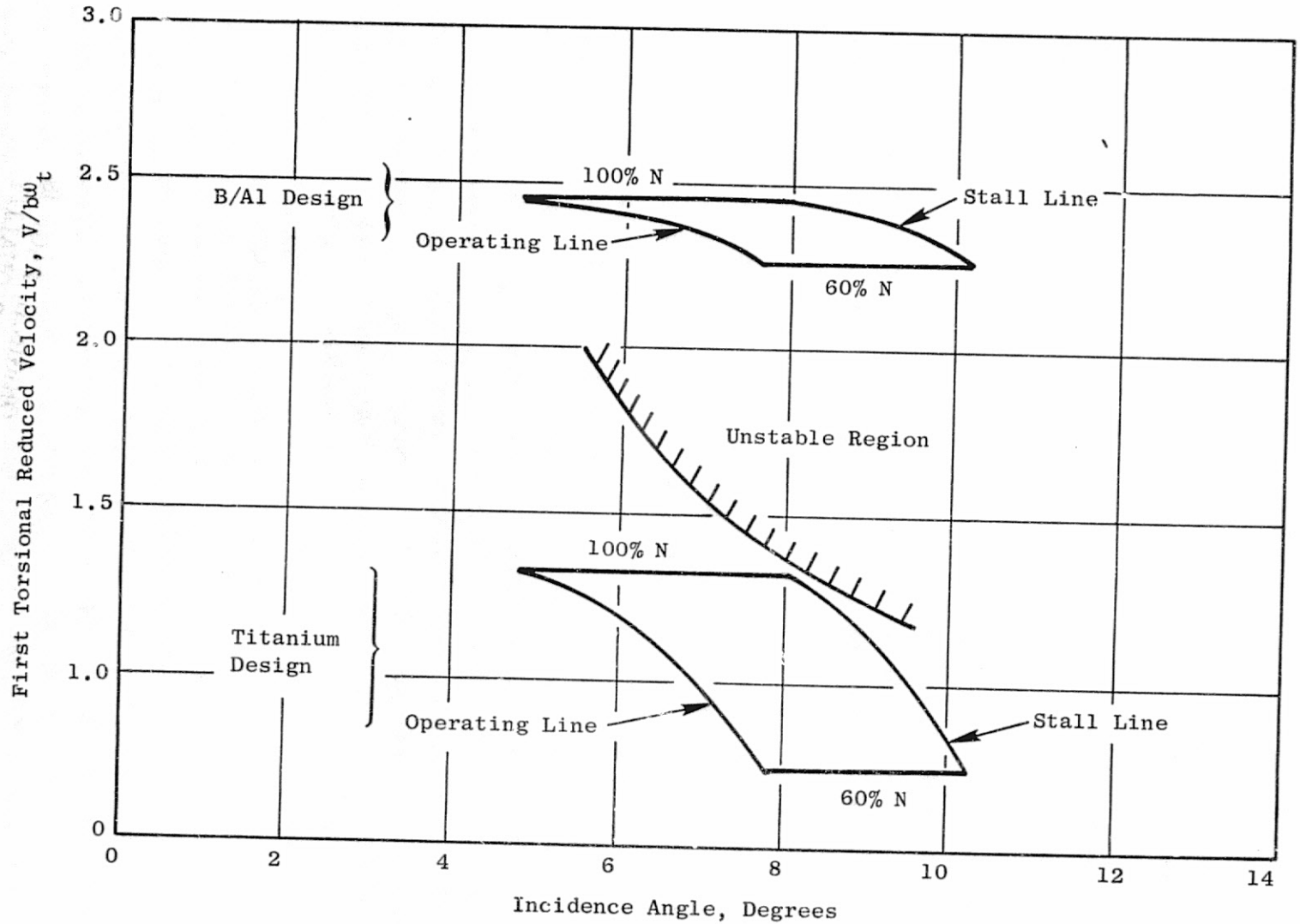

Figure 24. Blade Stability Map.

blades would be required versus 38 blades for the existing design. For the the current program where only impact resistance and manufacturing feasibility were of prime concern, the as-designed blade is adequate.

4.1.3 Steady State Stresses

The frequency response and aeromechanical stability of a blade are directed toward minimizing the induced stresses in the various operating environments. With complete consideration of these design aspects, the blade does experience stresses, generally categorized as steady state and vibratory. The steady state stresses are primarily the result of centrifugal loads, untwisting, and gas bending.

The "centrifugal" stresses vary from zero at the tip to a maximum at, or near, the blade root. These stresses are proportional to the material density and, thereby are lower in a composite blade than in a titanium blade. This stress usually constitutes about half of the total steady state stress.

For the B/Al blade as-designed, the average centrifugal stress was calculated to be 28.5 ksi at the root of the blade at 100% engine speed. This value is consistent with previous blade designs and would result in acceptable blade strength margins.

5.0 BLADE FABRICATION PROCESS DEVELOPMENT

Two CF6 first stage fan blades were fabricated to demonstrate the feasibility of large boron/aluminum fan blade fabrication by air bonding. Blades were made in existing tooling. Tooling and pressing procedures, primary monotape fabrication, and bonding of two blades will be described in the following sections.

5.1 BORON/ALUMINUM FABRICATION PROCESS

The TRW rapid air bonding process was employed during the program for fabrication of specimens and fan blades. Significant features of the process are the use of fully dense monotapes with a wrought structure as a starting material, the surface treatment given these monotapes to enhance secondary bonding, hot insertion into the die, and bonding in air. The advantages of air-bonding are a low cost in production, the use of existing hot die technology and facilities, and the production of properties equivalent to vacuum bonding. The rapid air-bonding process was established under internal research funding at TRW and was further developed under Air Force sponsorship.

The rapid air-bonding process employs monotapes, which are advantageous for fabrication of a complex blade shape because of the improved properties which result from the uniform filament distribution and alignment. The use of a wrought matrix, that is, using monotapes diffusion bonded from foil starting material, provides three additional advantages. First, the monotapes are highly formable, which is a requirement in the production of blades with a high degree of twist or section change. Second, the ductile matrix offers superior impact resistance. Finally, the use of foil provides very uniform thickness. The use of a fully dense starting material is of considerable benefit by eliminating debulking in the bonding of a blade which has taper and section thickness differences.

FOD resistance is a primary consideration in the fabrication of boron/aluminum for fan blades. While affected by filament, matrix composition, and filament orientation, the fabrication parameters have an over-riding influence on the final impact resistance. The rapid air-bonding process is well suited to providing high impact resistance through the use of a wrought ductile energy-absorbing matrix, the employment of a low fabrication temperature, and the use of a minimum cycle time. The versatility of rapid heating and cooling afforded by hot insertion during air-bonding is an important element in maintaining FOD resistance.

The fully dense monotape starting material has a smooth surface finish which, in certain alloy systems, may be difficult to bond. To promote bonding, an inexpensive chemical surface treatment has been developed. The tenacious oxide on the surface of aluminum is an impediment to bonding. The surface treatment both removes initial oxide and roughens the surface, promoting an intimate metal-to-metal interface. Both mechanical and chemical

treatments have been investigated but the latter is most effective in providing an appropriate surface topography. The important features of this process are the improved bondability of difficult-to-bond systems, the ability to bond at low temperatures, and the employment of an air atmosphere. The process also may be used in primary fabrication to provide adjustment in interfacial filament-matrix bond strength.

5.2 BLADE FABRICATION METHODS

Boron/aluminum CF6 first stage fan blades were made in a die used for production hot-straightening of titanium blades. The dies are tool steel with provision for Calrod Heating. The airfoil cavity in the die blocks is machined to the final dimensions of the blade while the root cavity and mid-span shroud are considerably relieved. The mid-span cavity was removed from the dies and tool steel plugs were machined to fill the mid-span cavity of the die. The plugs were welded into place in the preheated die block and the weld area subsequently tempered. The plug and weld areas were benched into airfoil form using a straight line blending into the airfoil die contour. Although the plug filled the mid-span on visual inspection, results of blade bonding indicated some discontinuity of airfoil form.

The design of the current titanium blade is not optimum for a boron/aluminum blade in terms of the transition between dovetail and airfoil. A plaster cast was made of the root area, including a section of the airfoil, to define the root cavity and airfoil transition. Preliminary examination indicated that extension of the boron/aluminum ply from the airfoil into the current root shape would require very sharp bends of the boron/aluminum monotape. The shape of the root die pocket is relatively complicated, conforming to the general shape of the machined blade. After an examination of the die and preliminary layouts, it was decided that the highest quality blade would result from a two-step fabrication process. The airfoil was bonded in one operation with the plies extending into the root cavity. The plies in the root were bonded together with root blocks in a second operation.

It was initially planned to use the dies, fixtures, cooling plates, and presses used in the hot-straightening operation for fabrication of a boron/aluminum CF6 blade. However, the hot-straightening operation uses lower loads than required for boron/aluminum and the die nest and fixturing are not massive enough to prevent lateral die movement. While existing fixtures and clamps could have been used, the probability of a successful boron/aluminum blade pressing was low. A new fixture was designed to provide initial alignment, prevent movement between die and platen, and minimize die rotation and movement due to relative platen shift, but available program funds did not allow this fixture to be constructed. The approach finally used was to rework and key massive retainer blocks to the press bed to restrict the lateral die movement due to reaction forces from the pressing load. While some elastic side movement occurred, the die block lateral position repeated within 0.025 cm (10 mils) under pressing load at temperature. A 1360-Mg (1500-ton) hydraulic press was used for the blade fabrication. Figure 25 illustrates the press while the die blocks, insulation, and restraining blocks are shown in Figure 26.

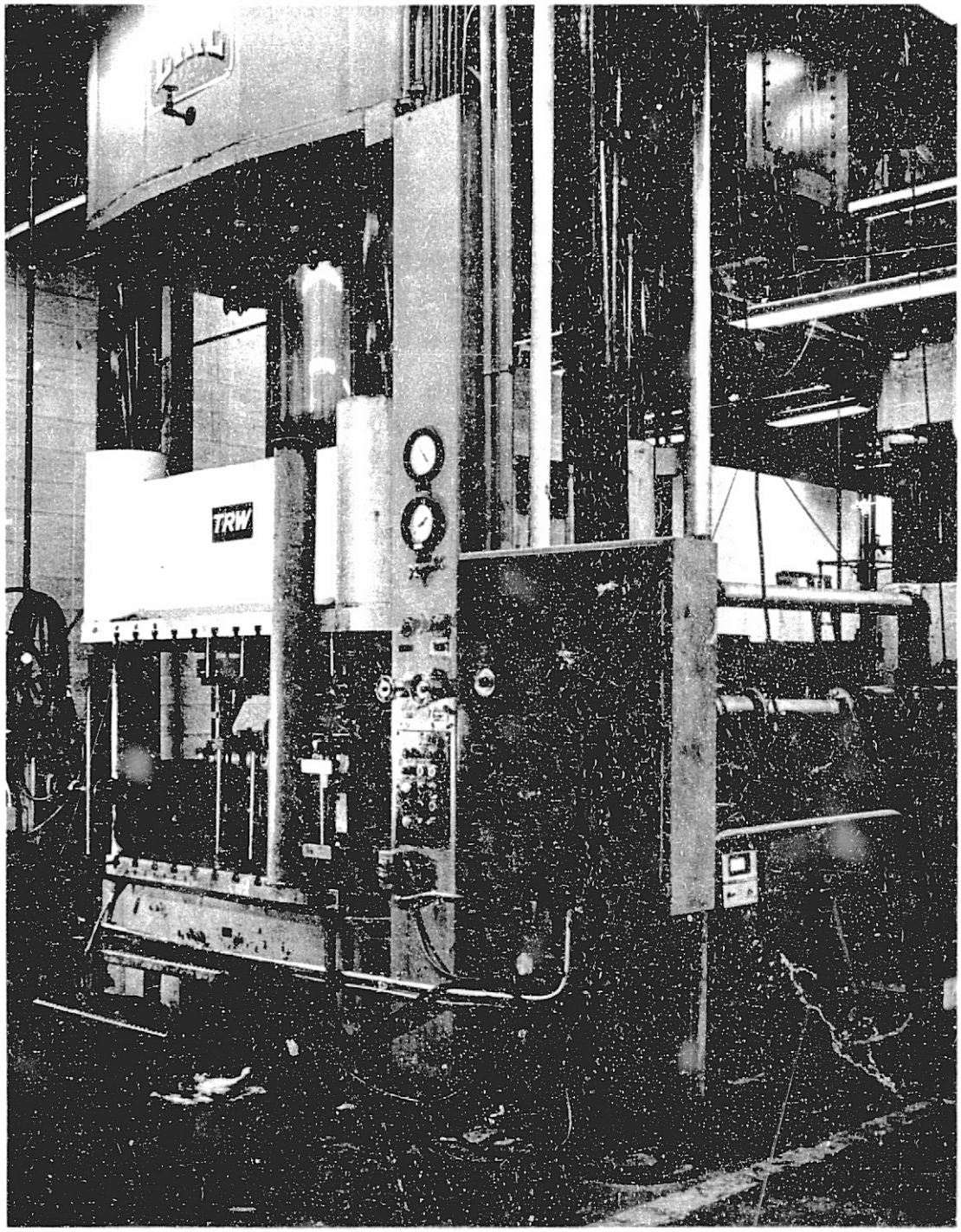

Figure 25. TRW Materials Technology 1360 Mg (1500-Ton) Hydraulic Press for Composite Manufacture.

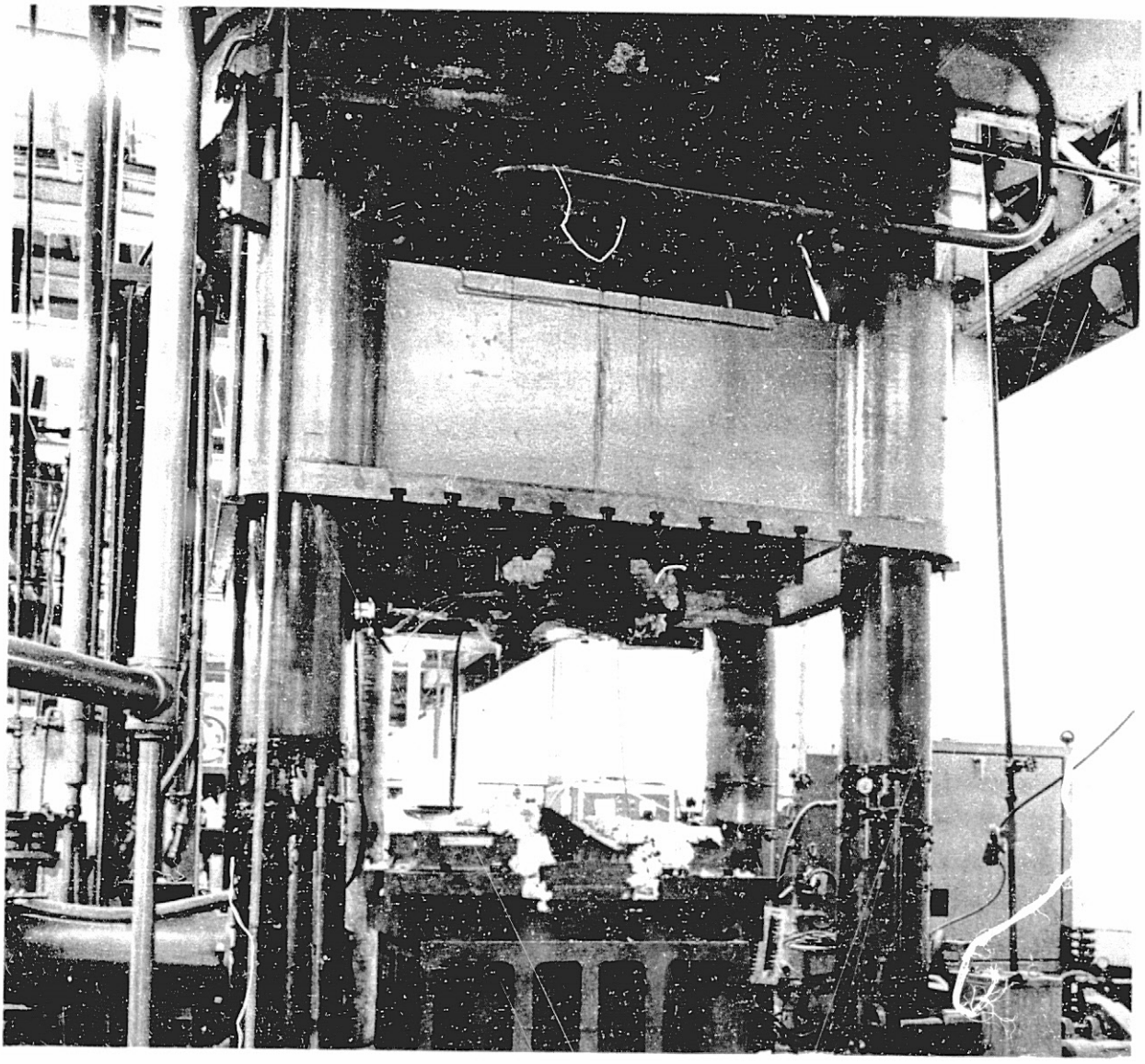

Figure 26. 1360 Mg (1500-Ton) Hydraulic Press.

Monotapes were made of 0.02 cm (8 mil) boron with an 1100 aluminum matrix using a 15° or 30° filament orientation. Winding was performed using a 4.5 m (15-foot) circumferential drum, Figure 27. Rectangular filament mats were cut at either 15° or 30° from the drum wound mat and assembled between sheets of 1100 aluminum foil. Nominal monotape size was 26.5 cm (10.5-inches) wide by 76 cm (30-inches) long. Monotapes were stacked up with graphite coated stainless separators between each monotape and inserted into an evacuated can similar to the one illustrated in Figure 28. Monotapes were step press bonded using parameters of 493° C (925° F), 70 MPa (10 ksi), 15 minutes at each of the three steps. As for the blade-specimens, monotapes contained 50 volume-percent reinforcement, a 0.024 cm (9.6 mil) center-to-center filament spacing, and were sized to a nominal thickness of 0.026 cm (10.4 mils). Monotapes appeared well consolidated and metallographic examination indicated completed bonding, Figure 29.

Ply lofting is a critical step in the successful fabrication of a boron/aluminum blade. The objective is to match the volume of the blade at each location in the bonding die. Insufficient volume will produce insufficient bonding while excess volume will produce filament breakage and may prevent complete die closure. Because the monotapes are fully dense, very little debulking occurs upon pressing. The fibers also restrain movement of the matrix so that very little material redistribution occurs upon pressing. The common method of boron/aluminum blade fabrication is to attempt to loft the plies as closely as possible to the blade and then to make further ply adjustments during subsequent blade pressings. The ply modifications are made on a cut-and-try basis and the more accurate the initial ply lofting, the fewer modifications are required. Ply lofting was performed by General Electric using blade models supplied by TRW (Section 4.1).

Initially, the lofting for the CF6 blade was to be performed from a glass-resin cast made of the actual die cavity. Holders and clamps to position the die were designed and casting material procured. However, under side loads, the relative movement between die and punch became apparent. It was decided that a more meaningful approach would result if the plies were lofted to the die at temperature and under pressing load to combine the effects of die contour and shifting. An aluminum isothermal forging of the CF6 airfoil was prepared using a pressing temperature of 425° C (800° F) and loads of 820 Mg (900 tons). Considerable deflection occurred upon loading although the use of a large initial offset brought the dies into registry at load. The requirement for this initial offset was eliminated in the later boron/aluminum blade pressing runs by the keying of restrainer blocks described in the tooling section. The resulting isothermal forging reproduced the die contour but the blade was over/print thickness. The blade was finally lofted using an unshrouded CF6 titanium blade and generating thickness contours at 0.026 cm (10.4 mil) intervals. Ply patterns were drafted to these contour maps including the definition of locating holes. Airfoil plies were extended into the root cavity to form a constant thickness section from leading edge to trailing edge.

After fabrication, the monotapes were sized to thickness and given a surface treatment to promote bonding. Plies were cut by hand for the two

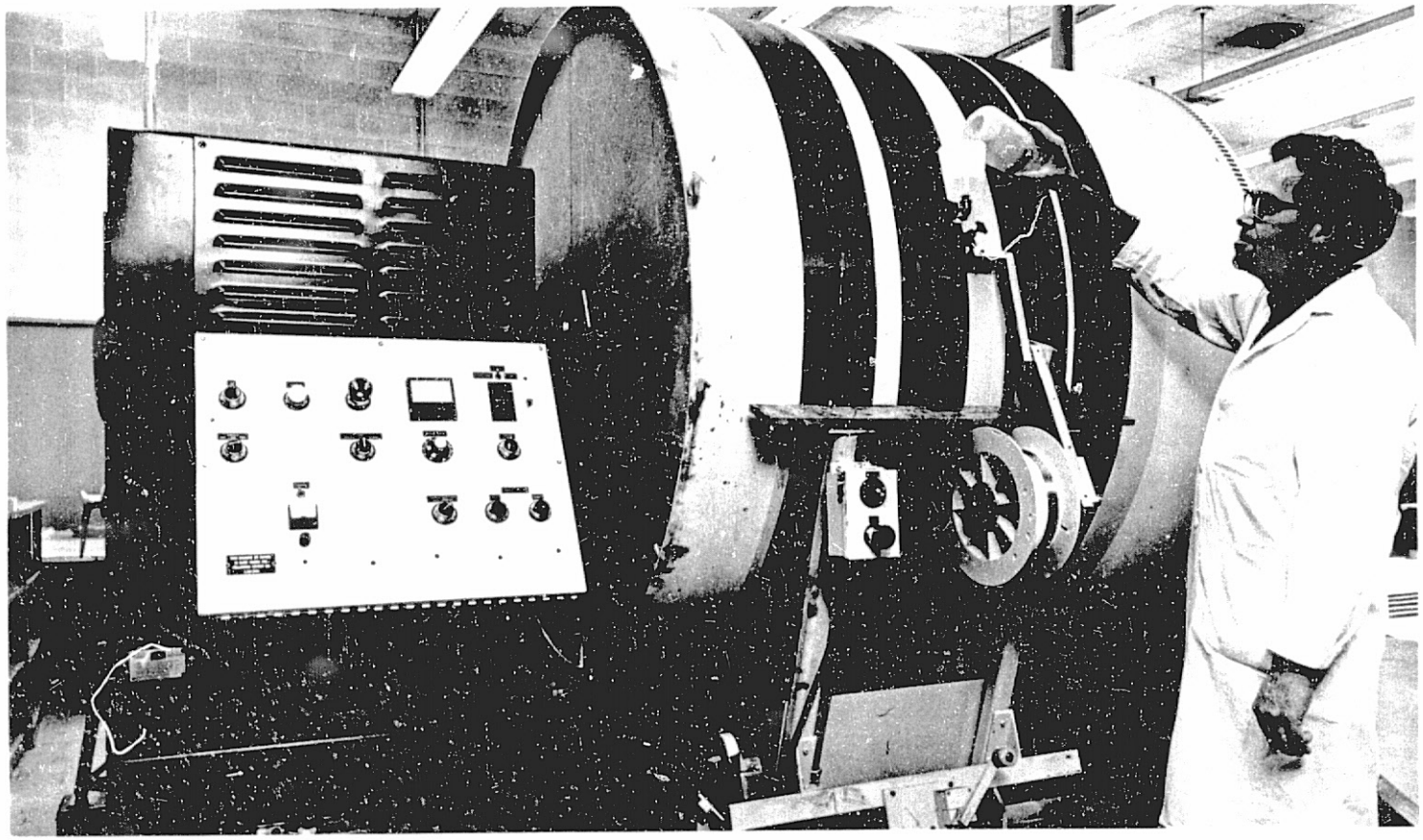

Figure 27. Filament Winding Machine for 4.5m (15 ft) Lengths.

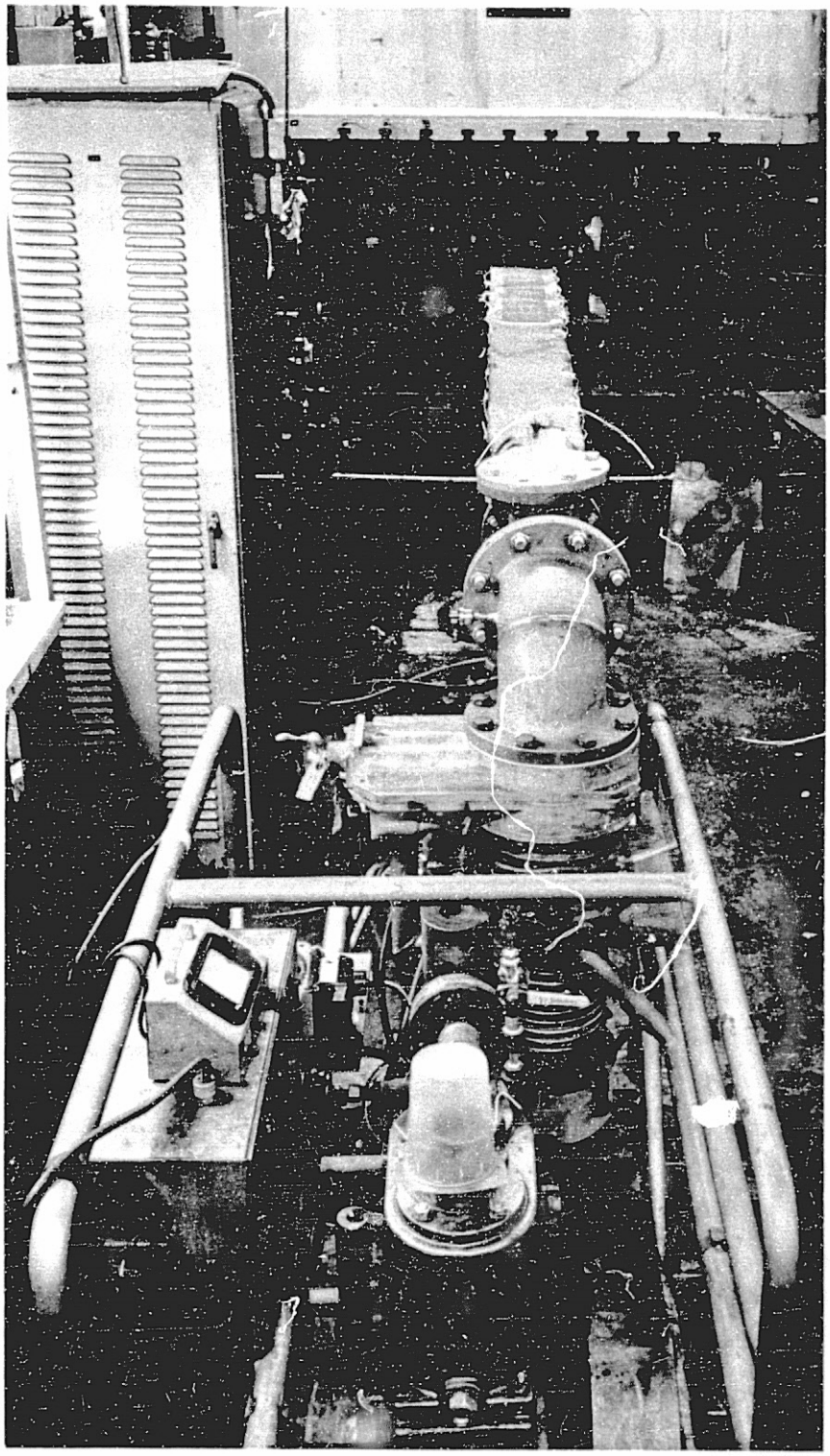

Figure 28. Vacuum System, 4.5 m (15 ft) Encapsulated Monotapes and 1360 Mg (1500-Ton) Press Used for for Vacuum Step Diffusion Bonding.

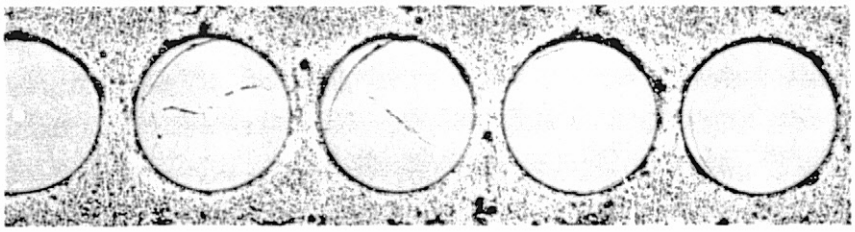

Figure 29. Monotape Microstructure, 100X.

blades and a typical set of cut plies for one-half of a blade is shown in Figure 30. Plies were located at root and tip as shown in Figure 31. Partial length plies were maintained in location by the sides of the root cavity. The use of pin locators was selected as the most convenient method for location in existing dies. The dies were inspected and locating holes drilled corresponding to a projection of the stacking axis.

5.3 BLADE FABRICATION

The ply orientation for the boron/aluminum CF6 blade was a ±15° core with ±30° surface plies. The layup is illustrated in Figure 32. The plies were assembled with the short plies in the center and full width plies on the surface. The center ply was a 0.025 cm (10 mil) thick piece of 2024 aluminum as a buffer ply. The surface plies included a 0.013 cm (5 mil) piece of aluminum and a monotape consisting of 150-mesh stainless steel wire cloth surrounded by aluminum. The mesh was at a 45° angle to the blade axis. Boron/aluminum blades can be made using either flat plies or plies formed to the airfoil contour, the choice depending upon the complexity of the airfoil. For the CF6 blade, flat plies were used. The plies are shown inserted into the die in Figure 31. The punch also has a hole corresponding to the pin and served as a positive ply location.

5.3.1 Blade No. 1

Blade No. 1 was laid up as shown in Figure 32. The center buffer ply and surface aluminum plies were 2024 aluminum. Blade No. 1 was placed into the cold die, the die closed, and a clamping load of 135 Mg (150 tons) [about 10.5 Mpa (1.5 ksi)] was applied. Cold insertion was used to insure accurate alignment. The dies were heated to 510° C (950° F) at the center with the tip of the blade maintained at approximately 490° C (910° F). Heating time was approximately 4 hours. The bonding cycle was performed at a load of 820 Mg (900 tons) [about (8.7 ksi)] for one-half hour. Blade No. 1 is shown in Figure 33 and a C-scan of the blade is shown in Figure 34. The blade was unbonded on both leading and trailing edges, particularly in the leading edge tip. Unbonded areas are shown as dark areas on the C-scan. Some surface wrinkles were found in the mesh ply but these are the result of the cold insertion process. Maximum pitch thickness measurements indicated that the blade was from 0.06 - 0.1 cm (25 to 40 mils) oversize. Pressure markings from the die revealed that the unbonding was due to lack of pressure on the unbonded areas.

Blade No. 1 was repressed three times with various thicknesses of aluminum added to the unbonded areas. The objective was to match the volume of the blade to the die as indicated by a uniform pressure pattern. For each repressing, the blade was inserted into the heated die. The C-scan shown in Figure 34 was taken after the third repressing and corresponds closely to the visual appearance of the pressure marks after the initial pressing. This observation would indicate that oxidation from the initial run prevented bonding during repressing even though the surfaces and blade were etched before each repressing. After the final run, all surfaces of the blade appeared to be in good contact with the die.

Figure 30. Cutup Plies for Half of Blade.

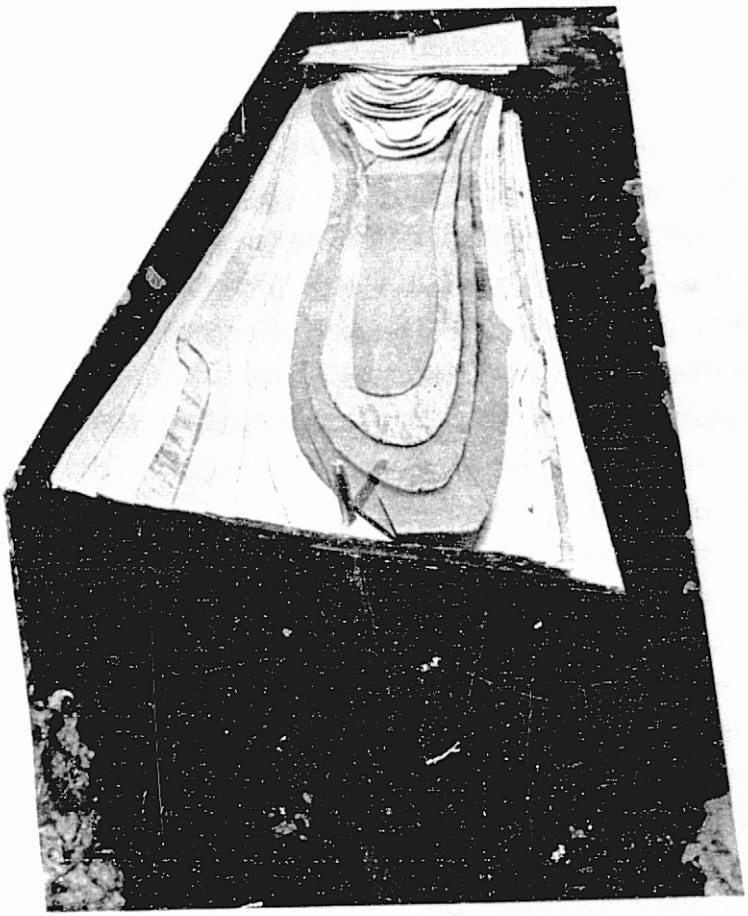

Figure 31. Plies Laid Up in Position.

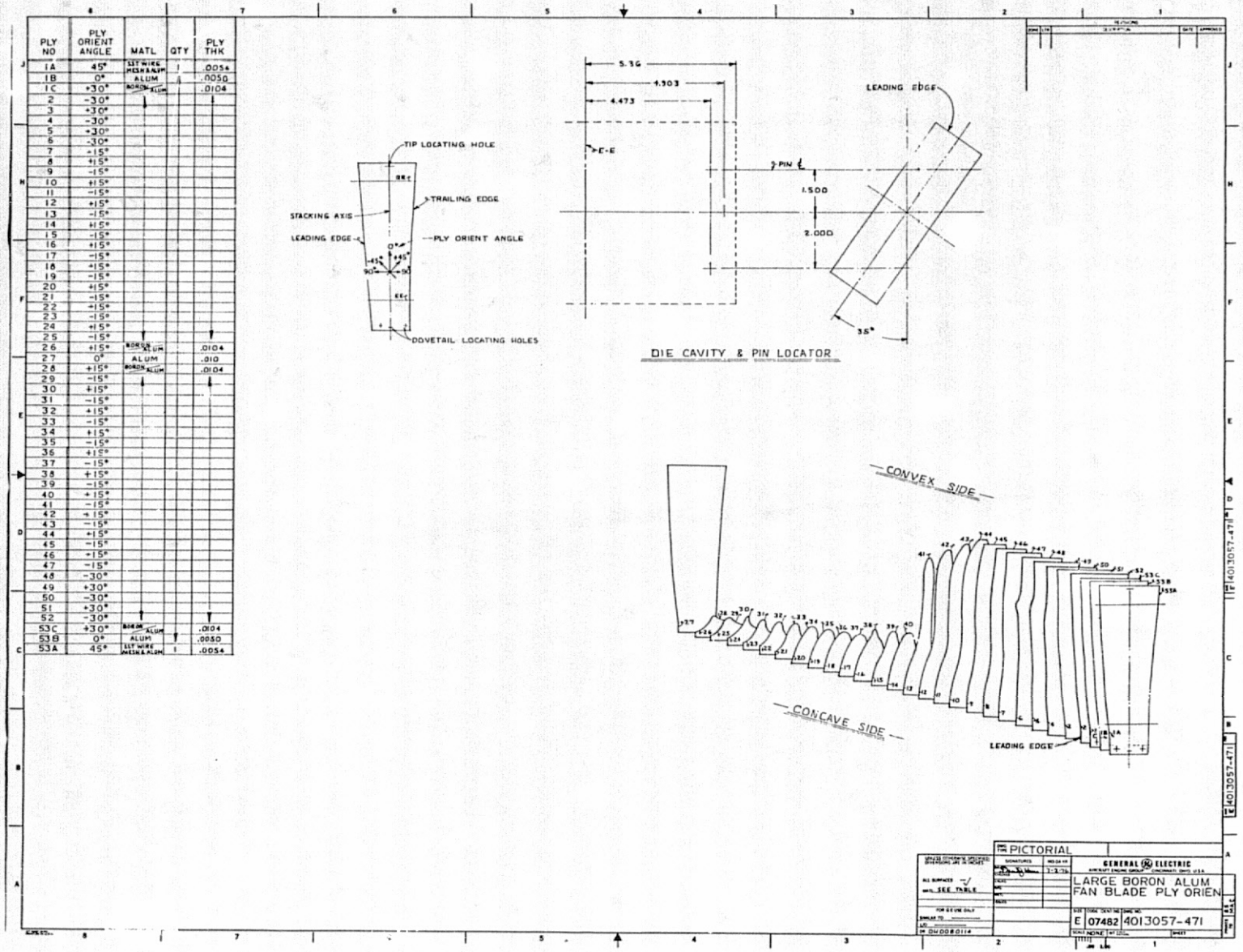

Figure 32. Blade Ply Orientation.

Figure 33. Blade No. 1.

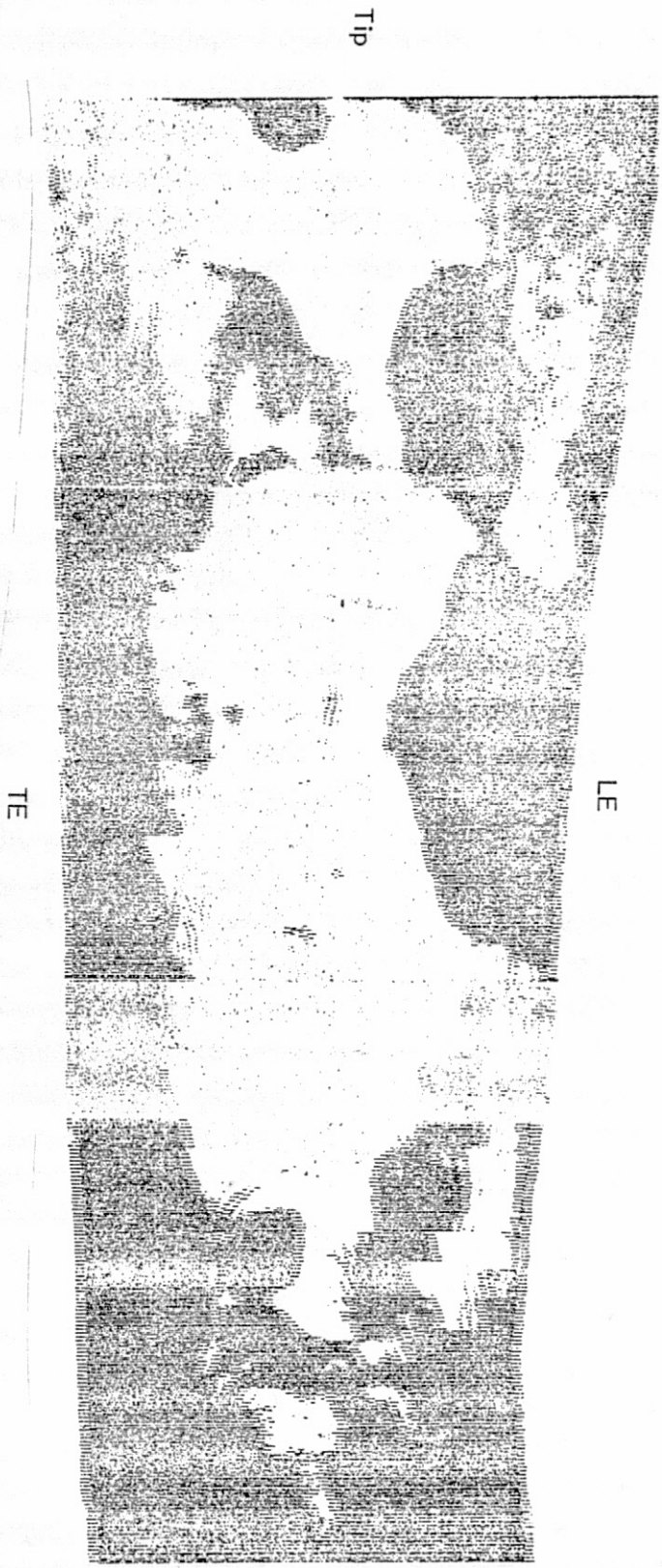

Figure 34. Blade No. 1 C-Scan.

5.3.2 Blade No. 2

Blade No. 2 used essentially the same construction as Blade No. 1 with the following exceptions. The mesh monotape was replaced with an equivalent thickness of 1100 aluminum. The center buffer ply and surface aluminum plies were replaced with equivalent thickness of 1100 aluminum, and plies 41 and 43 were removed to reduce the blade thickness in the region which was overbonded. The orientation of ply 42 was changed from +15° to -15° to maintain a balanced construction. Substitution for the 2024 alloy with 1100 was made because the temperature at the center of the die for Blade No. 1, 510° C (950° F), was above the solidus temperature of 2024. The 510° C (950° F) bonding temperature was necessary because of the temperature gradient in the die. Some additional aluminum pieces were also added to areas previously unbonded, based upon Blade No. 1 experience. Finally, some material was removed from the mid-span area.

Blade No. 2 was assembled and placed into the die which was at the bonding temperature. The bonding temperature at the center of Blade No. 2 was 524° C (975° F) and the load 910 Mg (1000 tons) [about 66 MPa (9.6 ksi)] for a 30-minute bonding cycle. Because of some surface imperfections, particularly at the mid-span area, some very small patch inserts were cut and the blade repressed one time. The repressed blade C-scan is illustrated in Figure 35. In general, the ply adjustments overcompensated as indicated by the shift in the unbonded area from the leading and trailing edges to the center. Both blades were tip cut and the leading and trailing edges blended. A microsection and microstruction of Blade No. 2 are shown in Figures 36 and 37. The blade was well bonded in this region and the filament distribution very uniform. Although not obvious from the C-scan, the degree of bonding was much better than Blade No. 1. This was especially apparent from the sound of ringing in the blade.

Since the purpose of these blades was to demonstrate feasibility of bonding the airfoil only, and because of the difficulty in diffusion bonding during repressing, adhesive bonding was employed for bonding the root plies and attaching root blocks. The shear strength of the adhesive was adequate to allow the blade to be held for frequency testing. The plies in the root were soaked with an 828 epoxy and bonded together under moderate pressure at 4 hours and 149° C (300° F). This system was selected for low viscosity, long pot life, and high shear strength. Root blocks were produced by isothermal forging in the die cavity. An assembly of plates was forged with stop-off used at the center line to allow the blocks to be split in half. A rectangular cavity was machined and the blade bonded to the blocks with an aluminum-filled casting resin. The blades are illustrated in Figures 38 and 39 after root bonding and tip cut, and before edge blending.

The measured and predicted bench frequencies for Blade No. 2, along with bench frequencies for a CF6 titanium blade, are shown in Table XI. The titanium blade is shown for both cantilevered and mid-span supported conditions. Frequencies for the boron/aluminum blade are about as-predicted but on the low side. These lower test values are probably due to nonoptimum pressing conditions. Note that the frequencies of the B/Al blade are higher

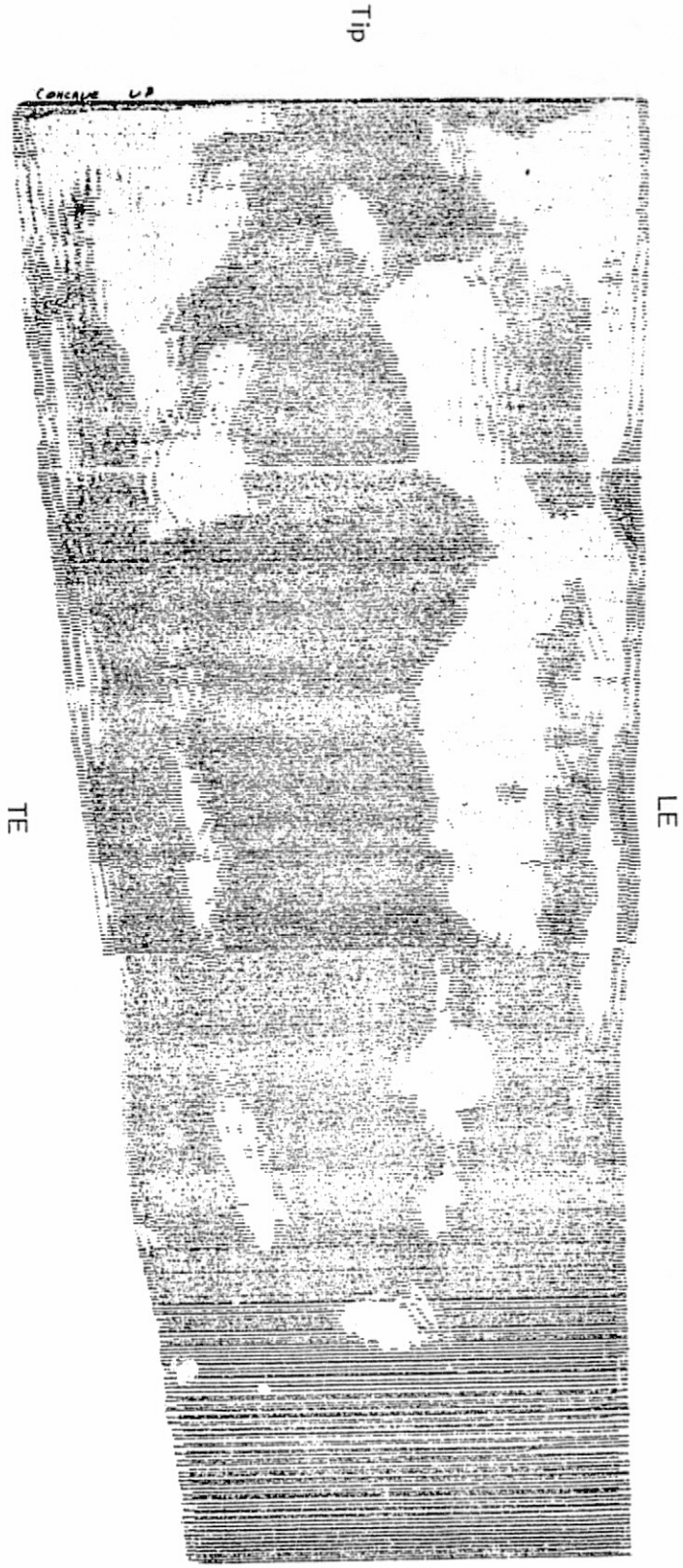

Figure 35. Blade No. 2 C-Scan.

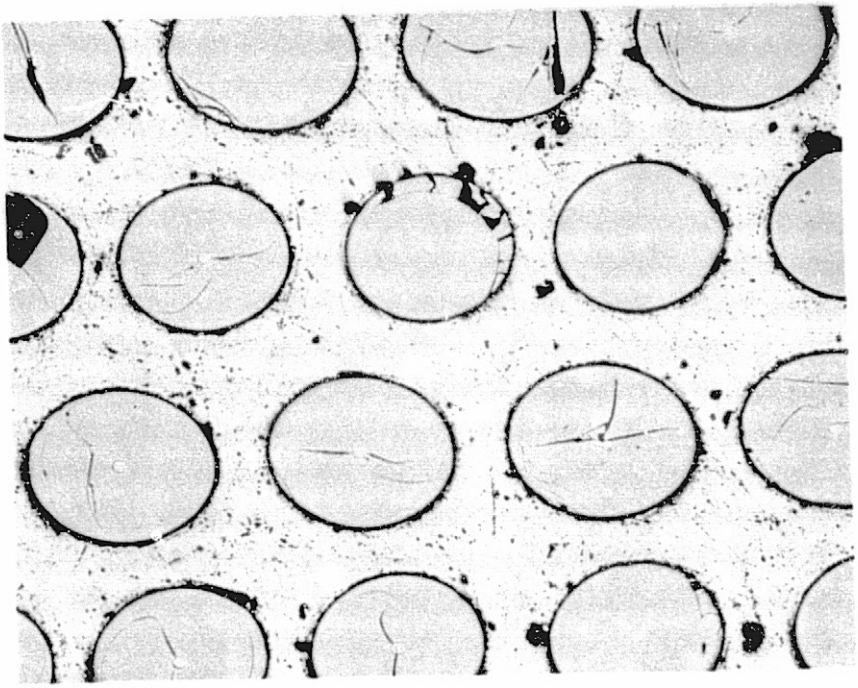

Figure 36. Microsection of Blade No. 2.

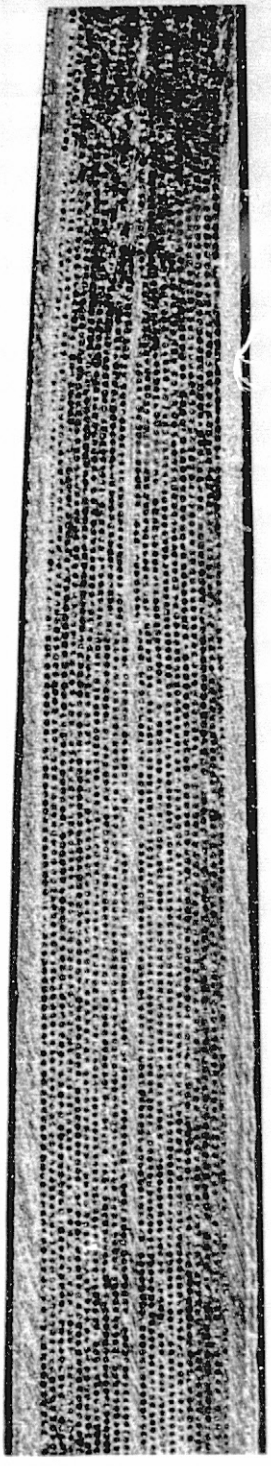

Figure 37. Microstructure of Blade No. 2.

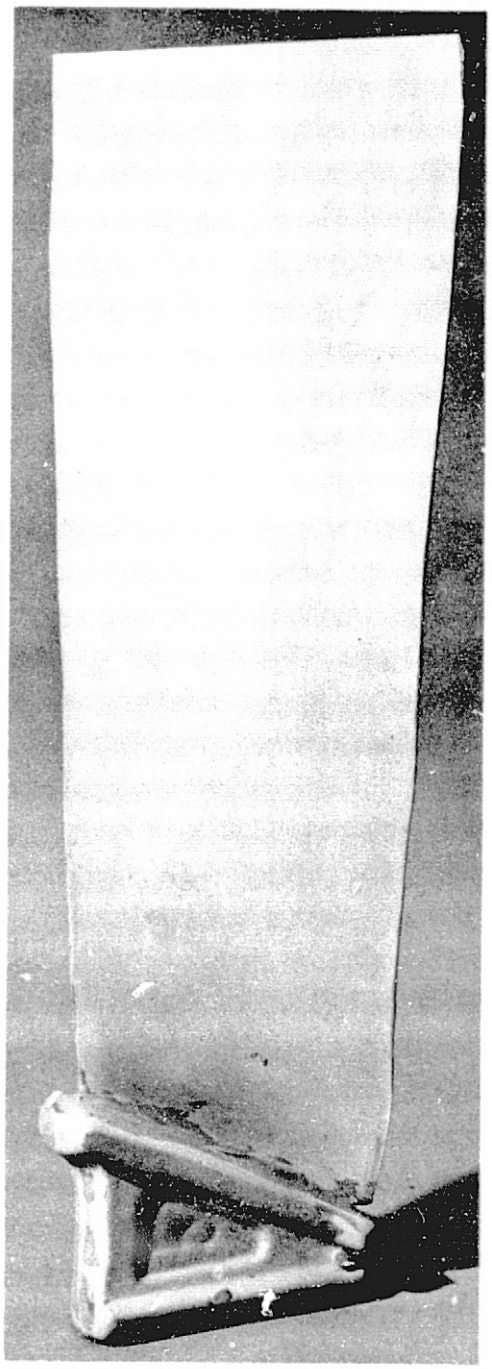

Figure 38. Blade No. 1.

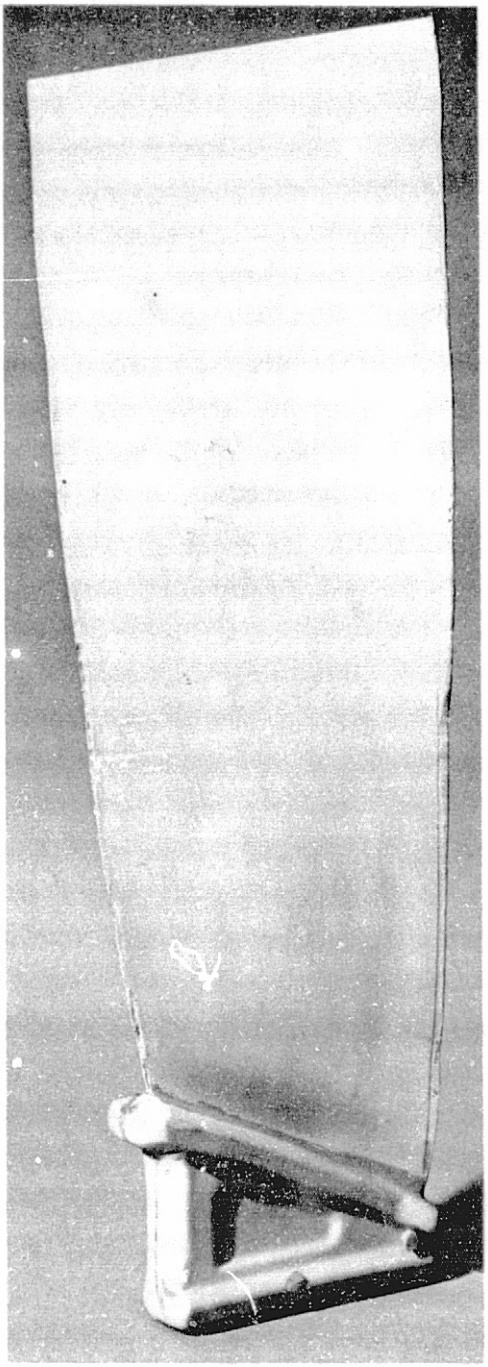

Figure 39. Blade No. 2.

Table XI. Bench Frequencies of B/Al and Titanium CF6 Blades.

Blade	Support	Frequency, Hz		
		1st Flex	2nd Flex	1st Torsion
CF6 Titanium	Mid-Span	176	382	458
CF6 Titanium	Cantilevered	20	70	148
CF6 B/Al	Cantilevered	31	112	220
CF6 B/Al Predicted	Cantilevered	36	---	235

than for the cantilevered titanium blade but much lower than the mid-span supported titanium blade. Due to its low first torsional frequency, the B/Al blade would not be aeromechanically acceptable since its reduced velocity (Vr) is 2.62, compared to a goal of less than 1.4.

5.4 SUMMARY

The feasibility of fabrication of a large impact resistant boron/aluminum fan blade has been demonstrated by the production of two CF6 first stage fan blades. Results indicate that the rapid air-bonding process can be used for the fabrication of large fan blades but considerable development efforts remain before it is a consistent reproducible process capable of producing high quality boron-aluminum fan blades. Primary fabrication of monotapes, scale-up of monotape surface treatment procedures, use of flat plies, and air bonding of a large blade have been successfully demonstrated. The two blades produced had two general problems, the diffusion bonding of the root plies after airfoil bonding, and lack of bonding in the airfoil. The difficulty in bonding the root plies would be eliminated through use of a die which would allow bonding of airfoil and dovetail in a single operation. The lack of bonding in the airfoil was caused by local mismatch in volume between monotape plies and die cavity as evidenced by the shift in well bonded areas with ply adjustments. Lofting of the blade more closely to the die cavity and elimination of die shifting would improve the bonding although a certain amount of ply adjustment is typical of metal matrix blade fabrication.

6.0 CONCLUSIONS

Heretofore, the lack of foreign object damage (FOD) resistance, such as large bird ingestion, has been a major deterrent to the use of composites for large fan blade application. However, recently significant improvement in impact resistance of 0.02 cm (8 mil) boron/1100 aluminum composite materials has been achieved. Recognizing the significance of this recent development, NASA sponsored a program at General Electric in conjunction with TRW to evaluate the impact performance of boron/aluminum and to fabricate large fan blades using the boron/aluminum material. Based on the program results, the following conclusions have been drawn:

- In the initial test series, where root bending failures were experienced, the best impact resistance was exhibited by a panel with a titanium leading edge and ±30° boron/aluminum plies. An all-boron/aluminum panel with ±30° plies also exhibited good impact resistance.

- In the second test series, with a modified test setup, where local failures were predominant, all-boron/aluminum with both ±15° and ±30° layups exhibited excellent impact characteristics.

- In both test series, ±45° layups did not demonstrate good impact resistance relative to the ±15° or ±30° layups.

- The ±15° layup without nickel plate and wire mesh out-performed a ±15° layup with nickel plate and wire mesh suggesting the wire mesh lowered impact resistance. The wire mesh also lowered modulus values.

- In the first series of tests, the leading edge titanium spar was superior to the internal spar design and to all-boron/aluminum panels indicating good bending strength. In the second series of tests, both the leading edge and internal spar designs exhibited good resistance to local fracture and tearing but delamination due to unbonding between the spar and boron/aluminum were experienced.

- The feasibility of fabrication of a large impact resistant boron/aluminum fan blade has been demonstrated by the production of two CF6-type first stage fan blades. Results indicate that the rapid air bonding process can be used for the fabrication of large fan blades. The two blades produced had two general problems; the diffusion bonding of the root plies after airfoil bonding, and the lack of bonding in the airfoil. The difficulty in bonding the root plies would be eliminated through use of a die which would allow bonding of airfoil and dovetail in a single operation. The lack of bonding in the airfoil was caused by local mismatch in volume between monotape plies and die cavity as evidenced by the shift in well-bonded areas with ply adjustments.

7.0 REFERENCES

1. David L. McDanels and Robert A Signorelli; "Effect of Angle Plying and Matrix Enhancement on Impact-Resistant Boron/Aluminum Composites," NASA TN D-8205.

APPENDIX A

GENERAL ELECTRIC NDT RESULTS BEFORE AND AFTER REPRESSING

PRECEDING PAGE BLANK NOT FILMED

PT. NAME B/A SPAR S/N 25
GAIN 7X1 INDEX .020 RANGE 62-90%
T. T. SPEED _____ STYLUS RATIO _____
MODE Pwj FREQ 5MHZ
INT. CKB DATE 12/1/75 COMMENTS UM721/10N

Ultrasonic Scan S/N 25

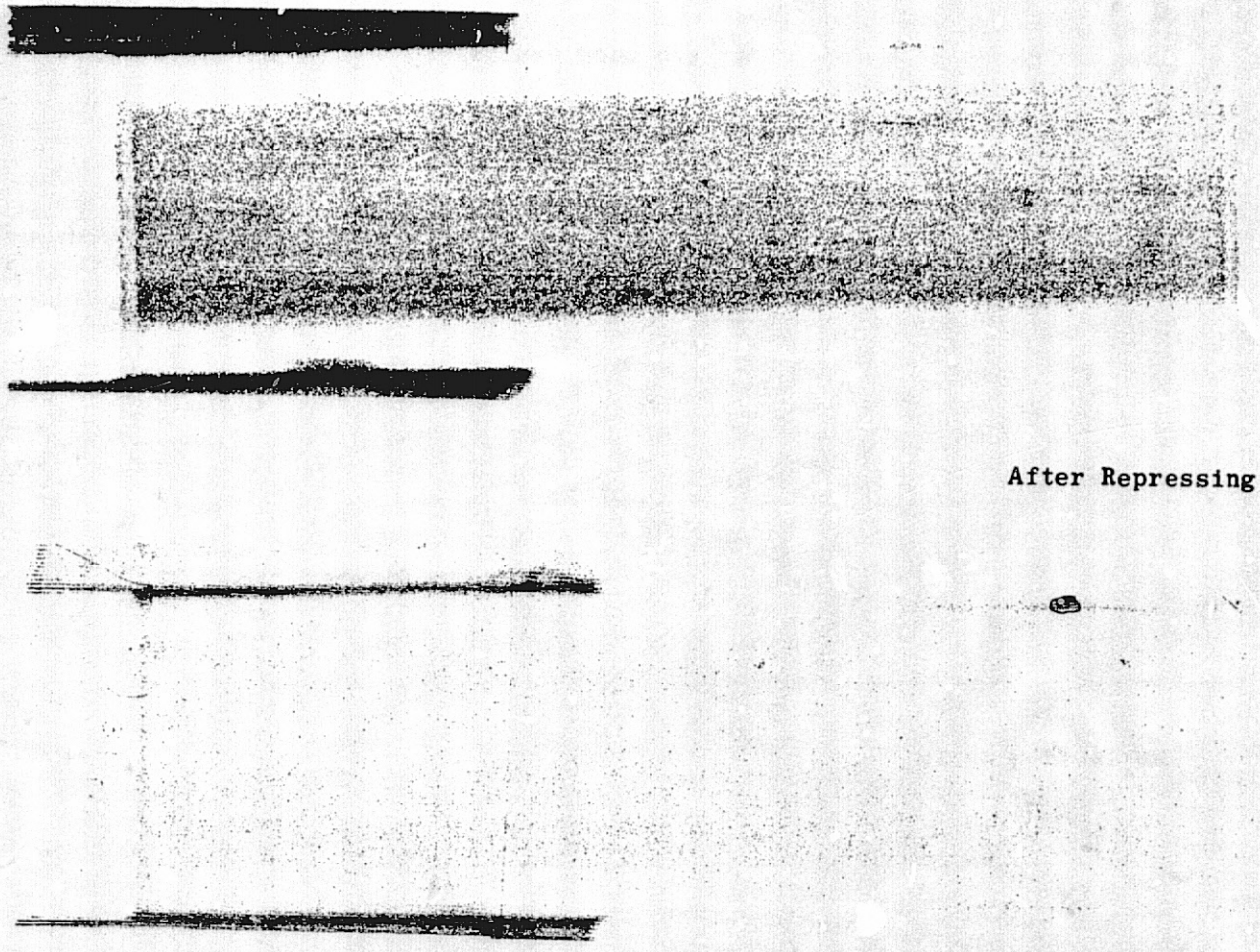

Ultrasonic Scan S/N 16

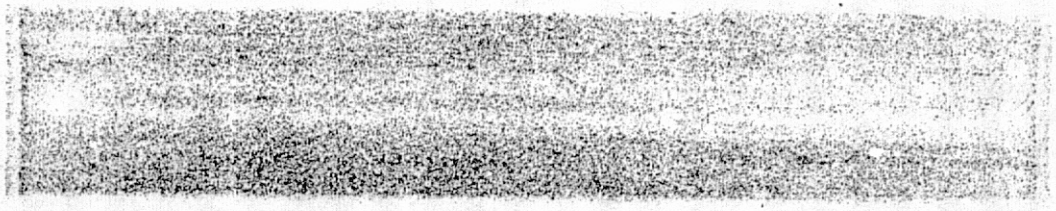

After Repressing

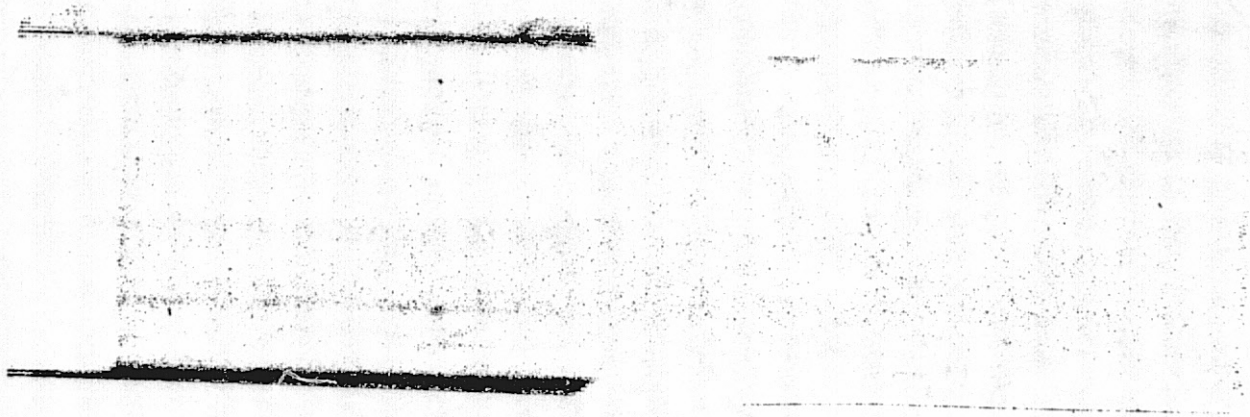

Before Repressing

Ultrasonic Scan S/N 19

Ultrasonic Scan S/N 26

After Repressing

Before Repressing

Ultrasonic Scan S/N 27

After Repressing

Before Repressing

Ultrasonic Scan S/N 50

After Repressing

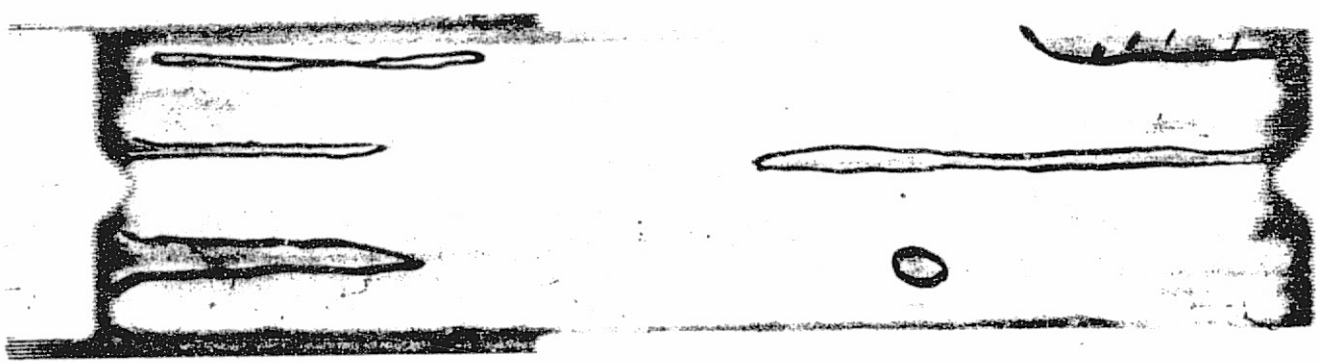

Before Repressing

Ultrasonic Scan S/N 34

After Repressing

Before Repressing

Ultrasonic Scan S/N 35

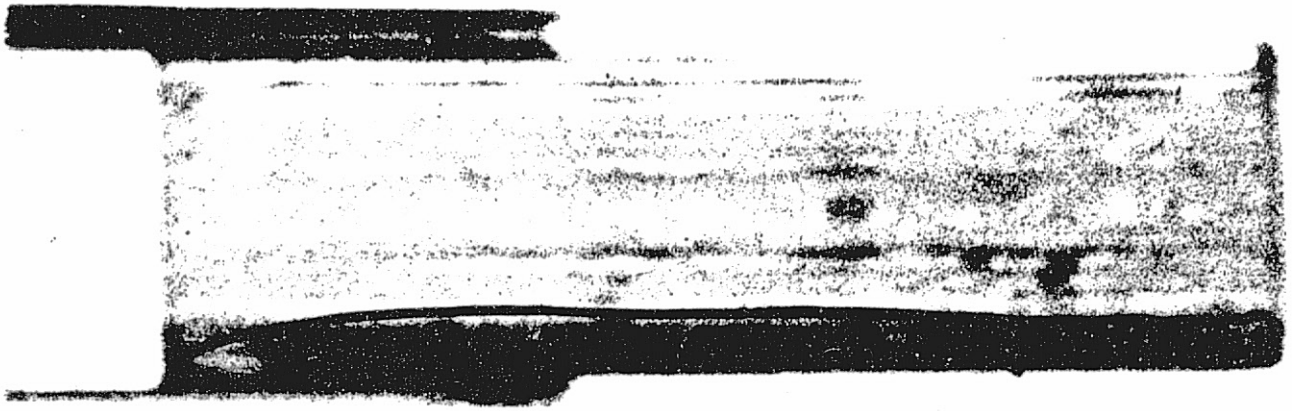

After Repressing

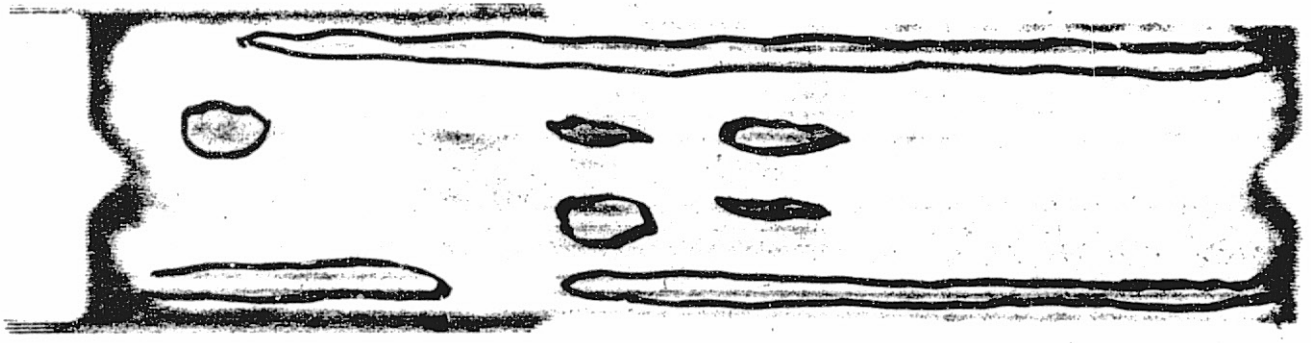

Before Repressing

Ultrasonic Scan S/N 36

After Repressing

Before Repressing

Ultrasonic Scan S/N 49

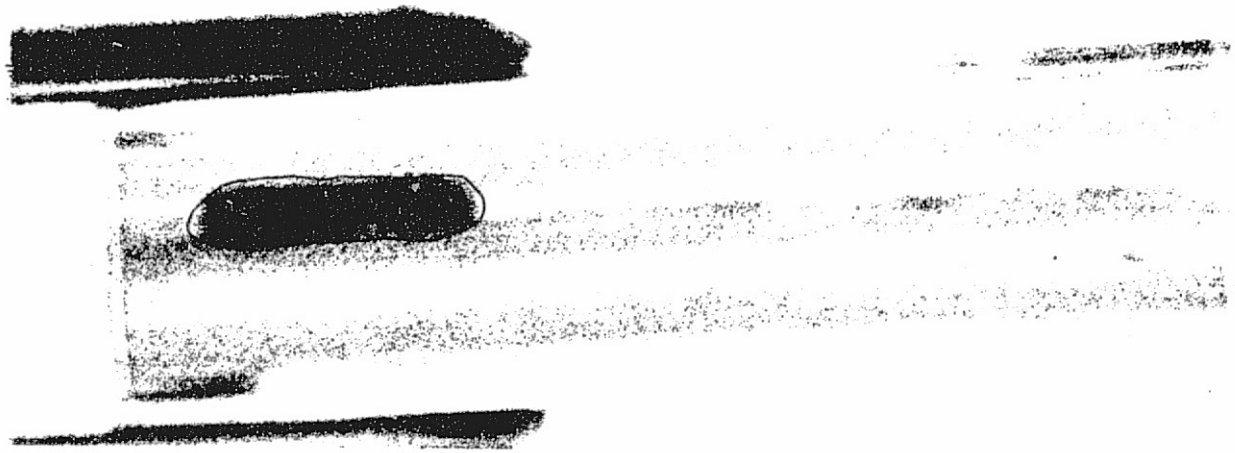

After Repressing

Before Repressing

BIAL Scan S/N 39-48
2X1 .020 67→90%
5MHz
CXB DATE 12/1/25 COMMENTS WM 721/10N

Ultrasonic Scan S/N 48

After Repressing

Before Repressing

Ultrasonic Scan S/N 42

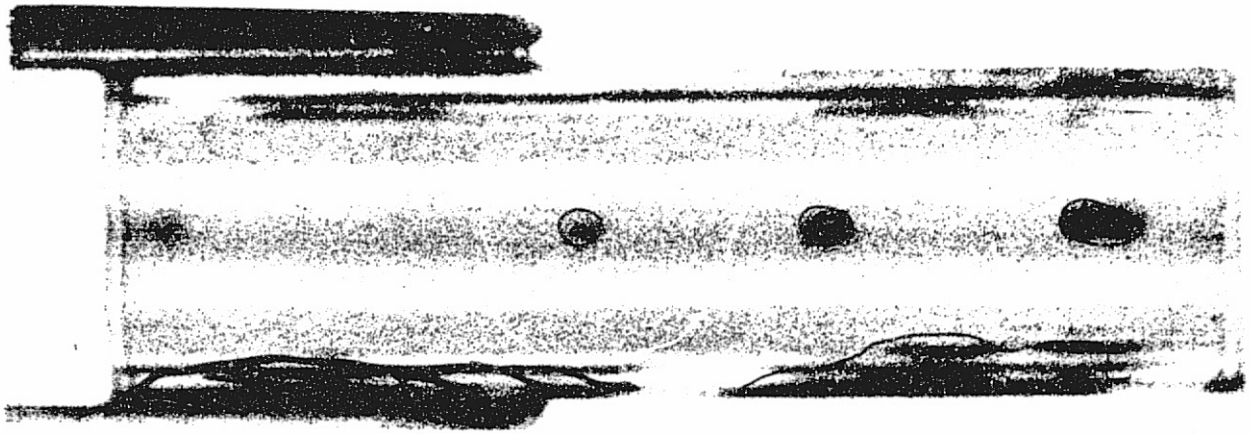

After Repressing

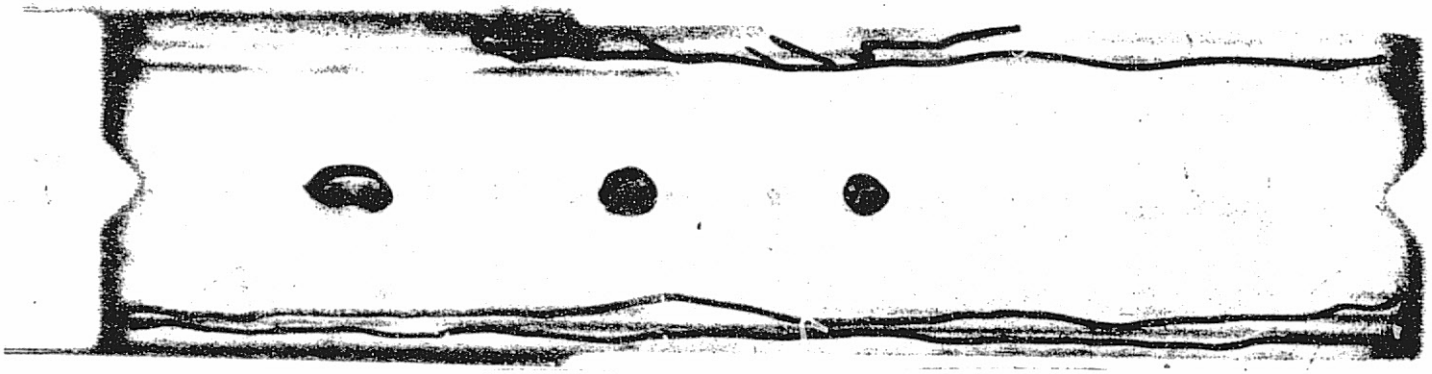

Before Repressing

Ultrasonic Scan S/N 43

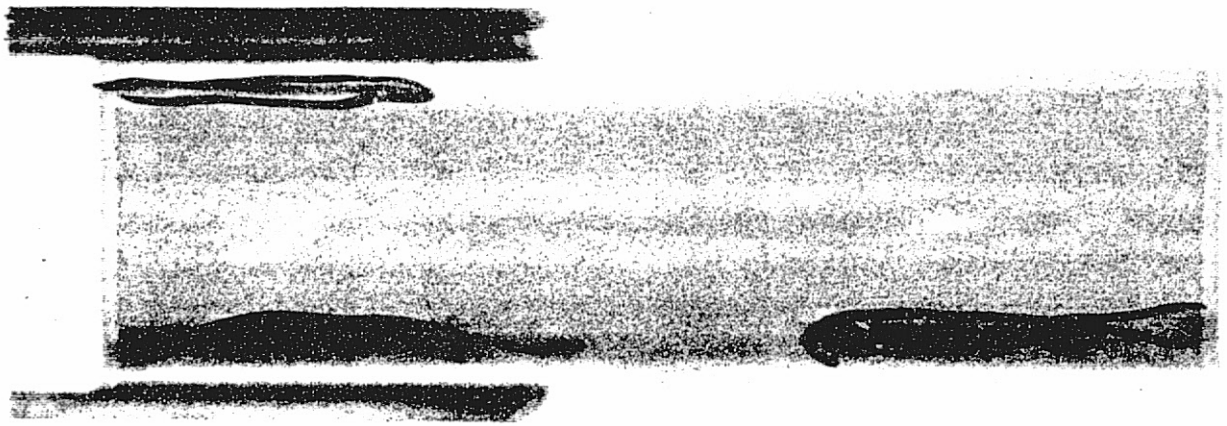

After Repressing

Before Repressing

Ultrasonic Scan S/N 44

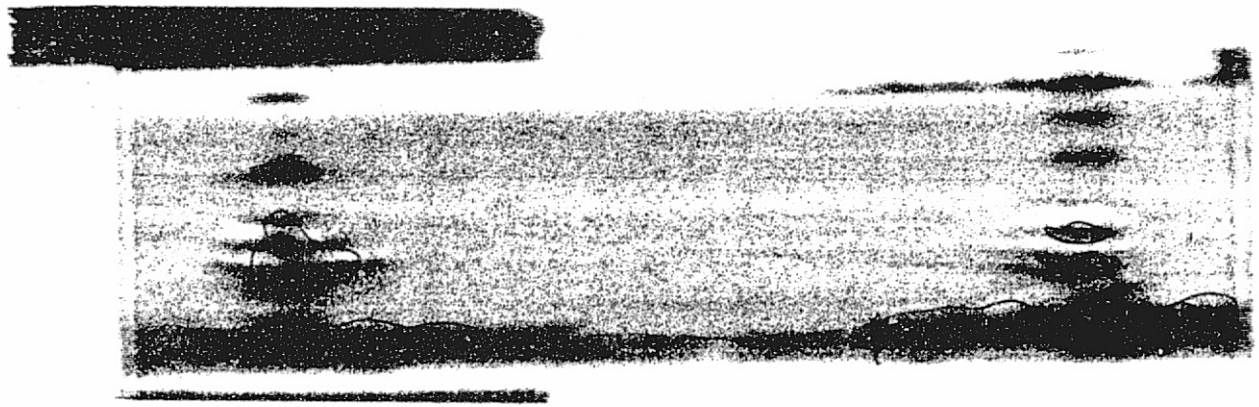

After Repressing

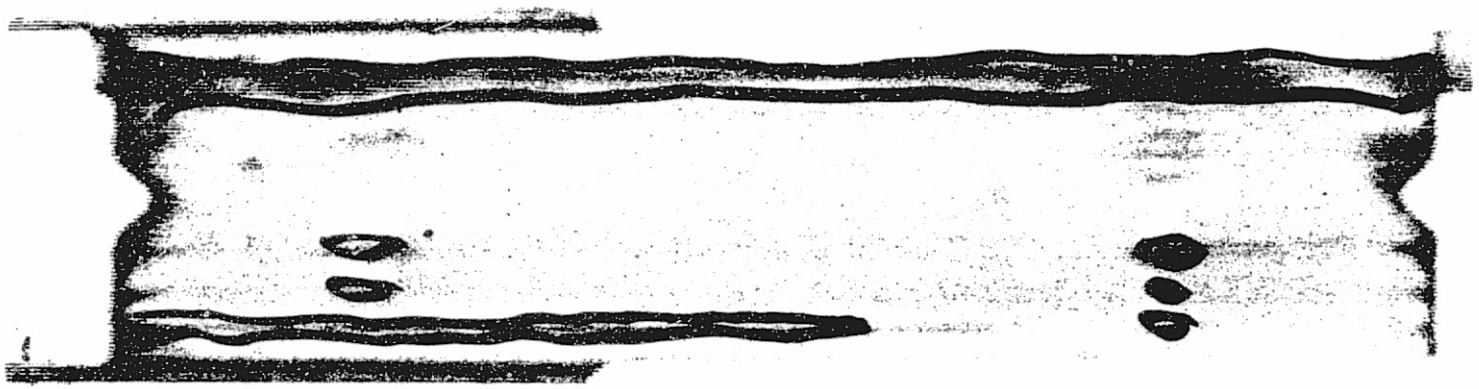

Before Repressing

Ultrasonic Scan S/N 45

After Repressing

Before Repressing

Ultrasonic Scan S/N 47

ORIGINAL PAGE IS
OF POOR QUALITY

ORIGINAL PAGE IS
OF POOR QUALITY

APPENDIX B

- Test Specimens after Test Series Number One and NDT Results Following Impacts

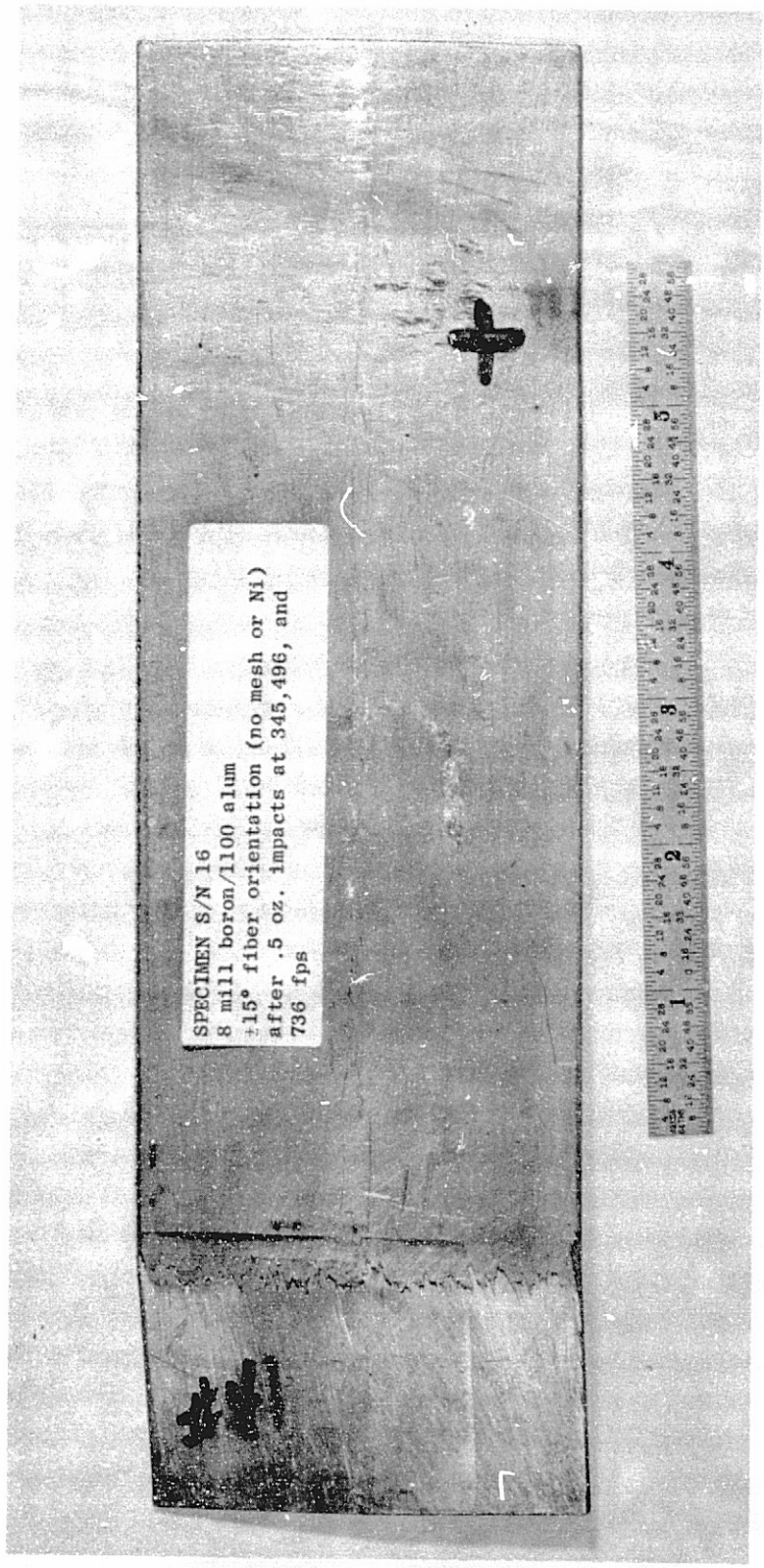

C-2

ORIGINAL PAGE IS
OF POOR QUALITY

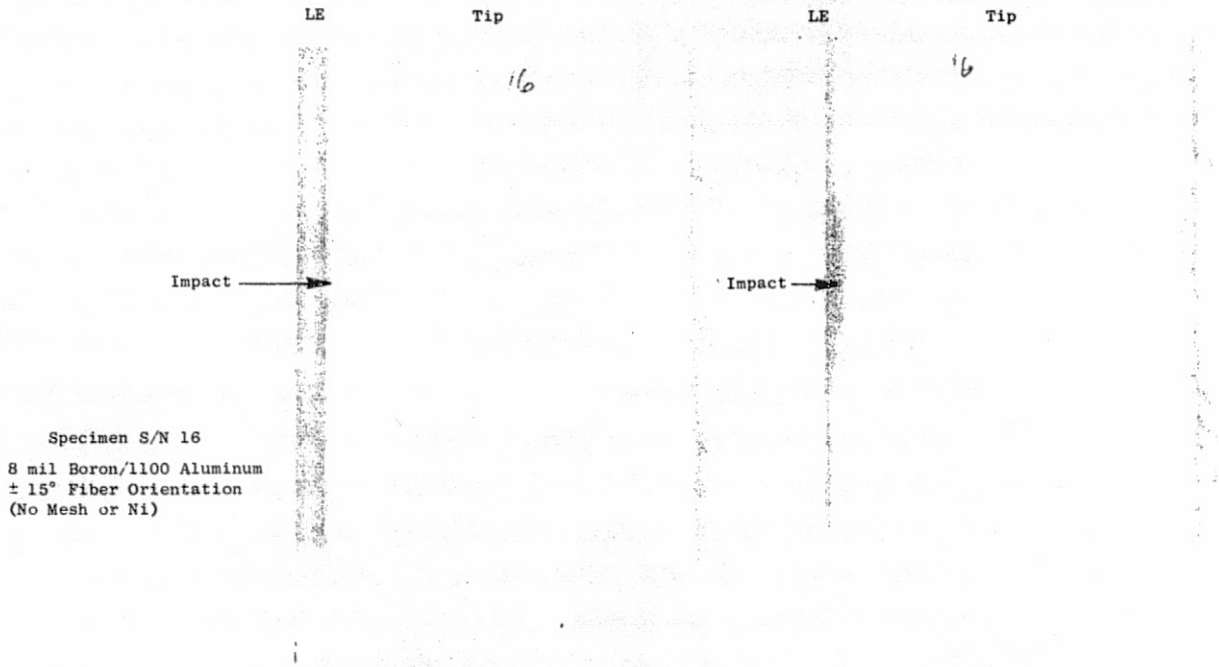

Specimen S/N 16

8 mil Boron/1100 Aluminum
± 15° Fiber Orientation
(No Mesh or Ni)

After Impact At 345 fps

After Impact At 496 fps

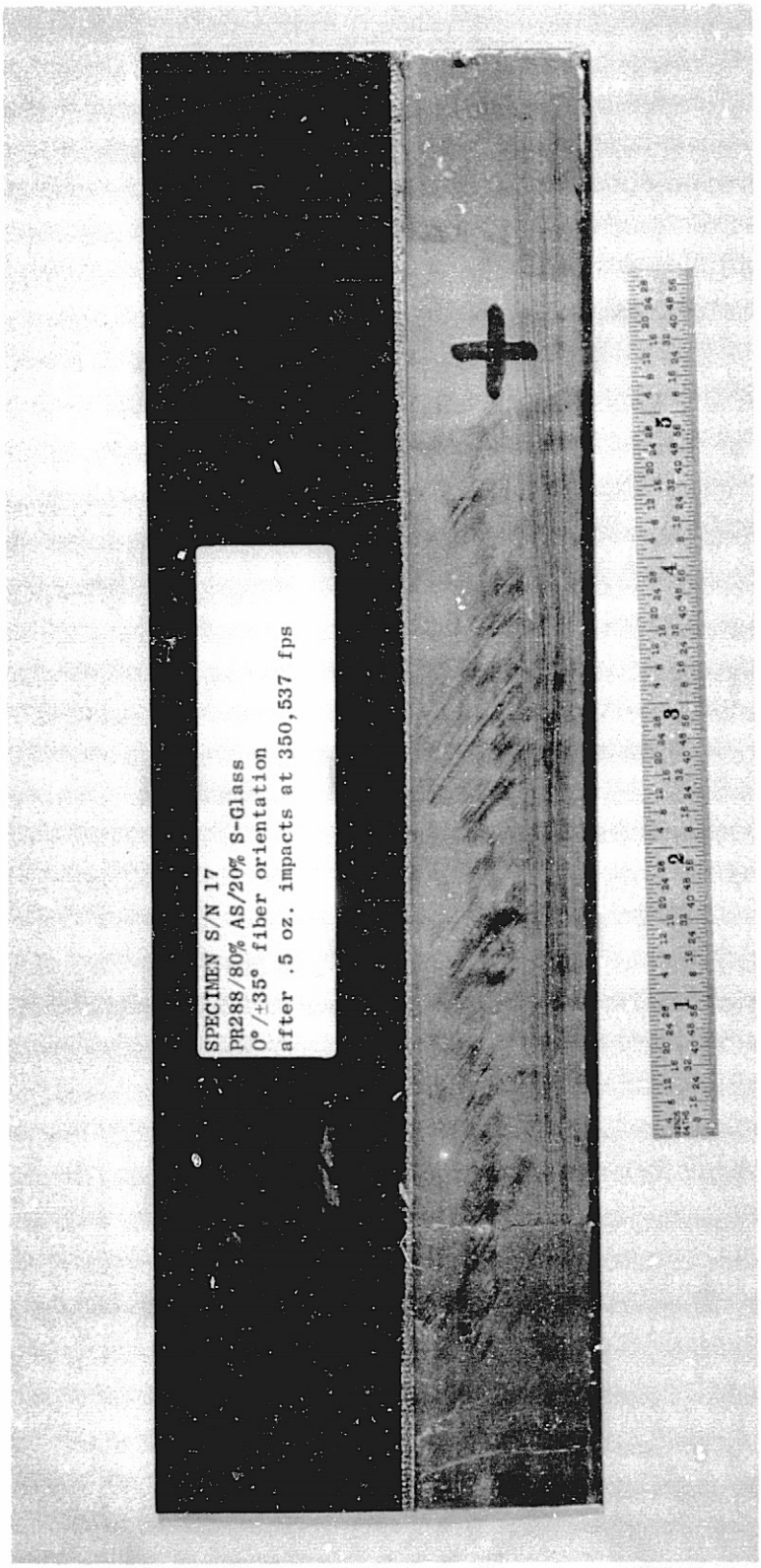

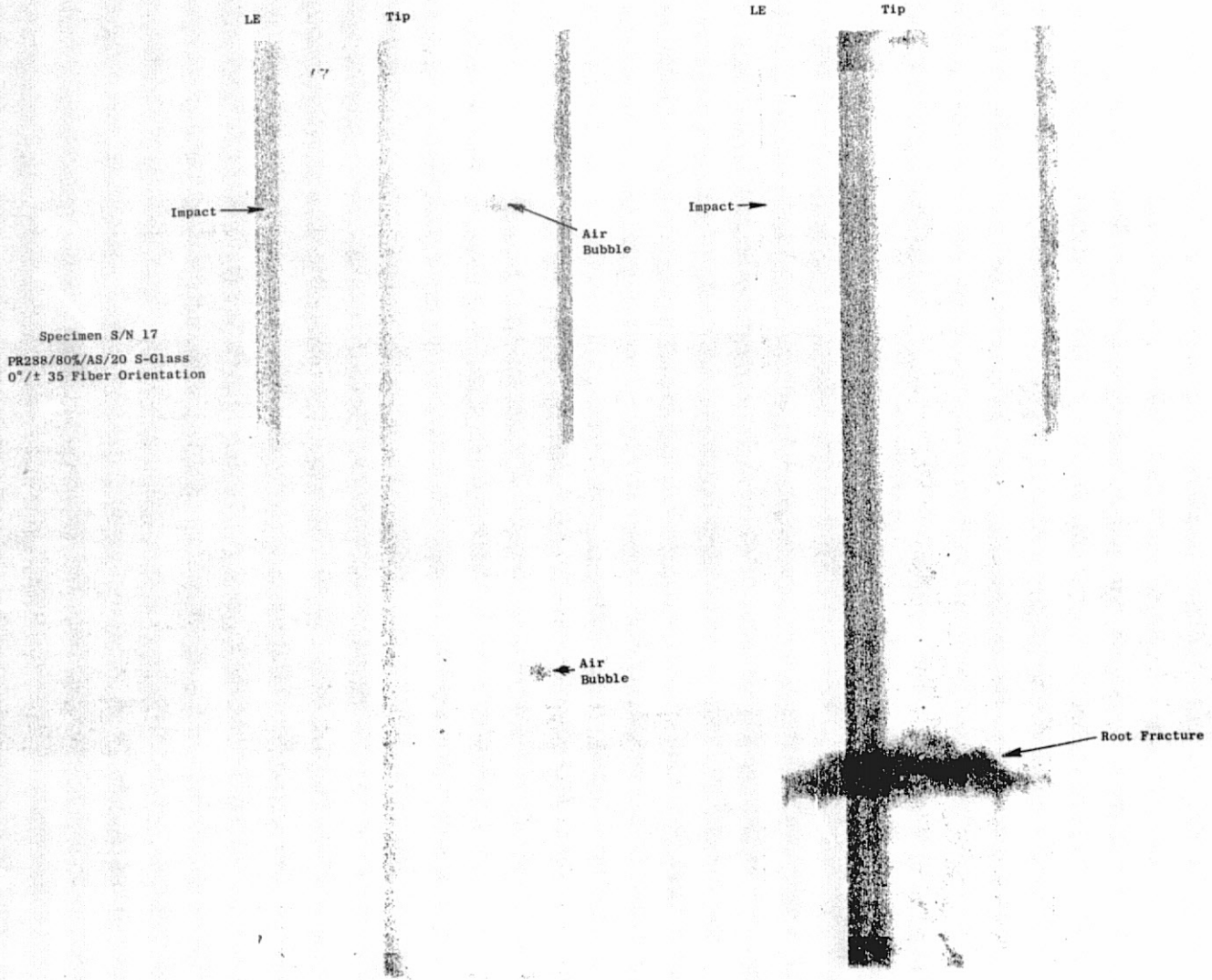

After Impact At 350 fps

After Impact At 537 fps

ORIGINAL PAGE IS
OF POOR QUALITY

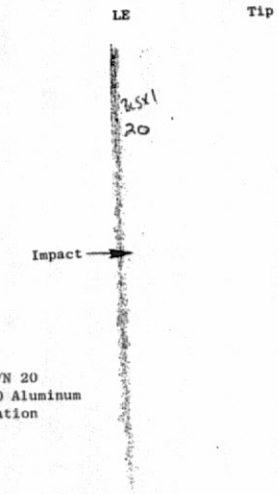

Specimen S/N 20
8 mil Boron/1100 Aluminum
0° Fiber Orientation

After Impact At 339 fps

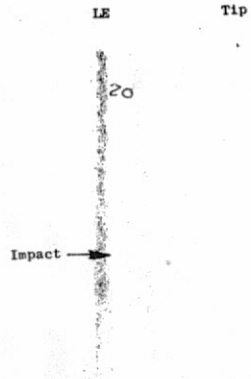

After Impact At 537 fps

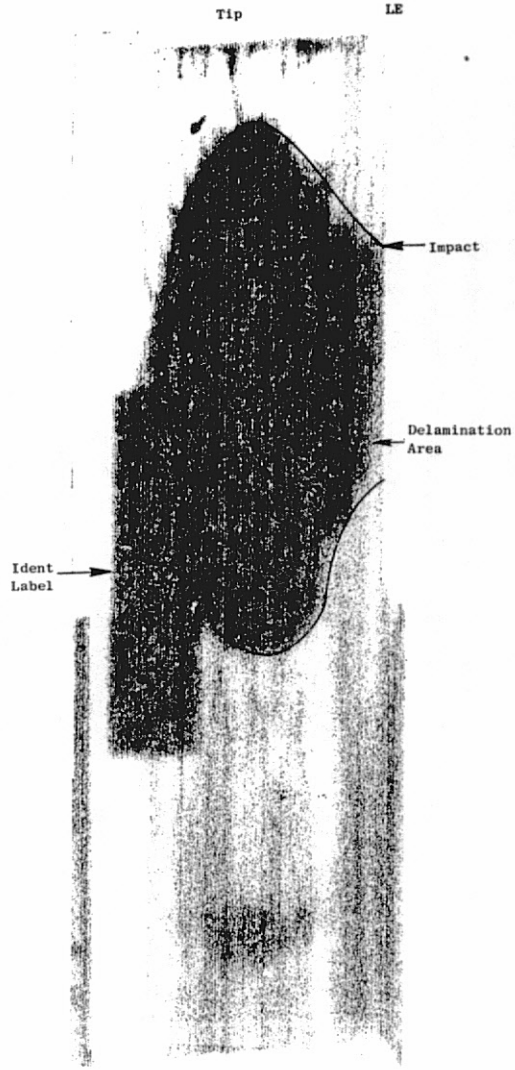

After Impact At 742 fps

Specimen S/N 25
8 mil Boron/1100 Aluminum
± 15° Fiber Orientation

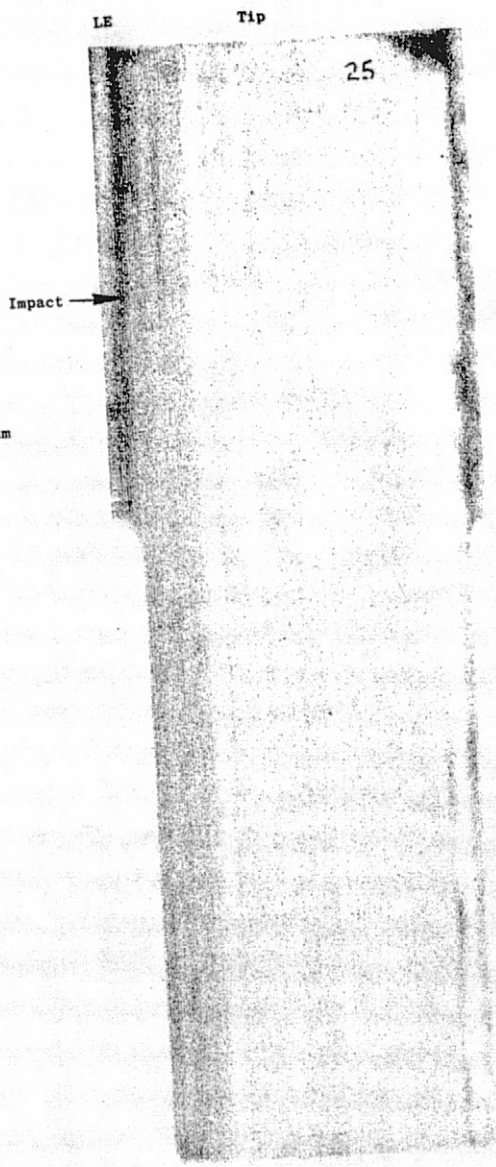

After Impact At 350 fps

After Impact At 512 fps

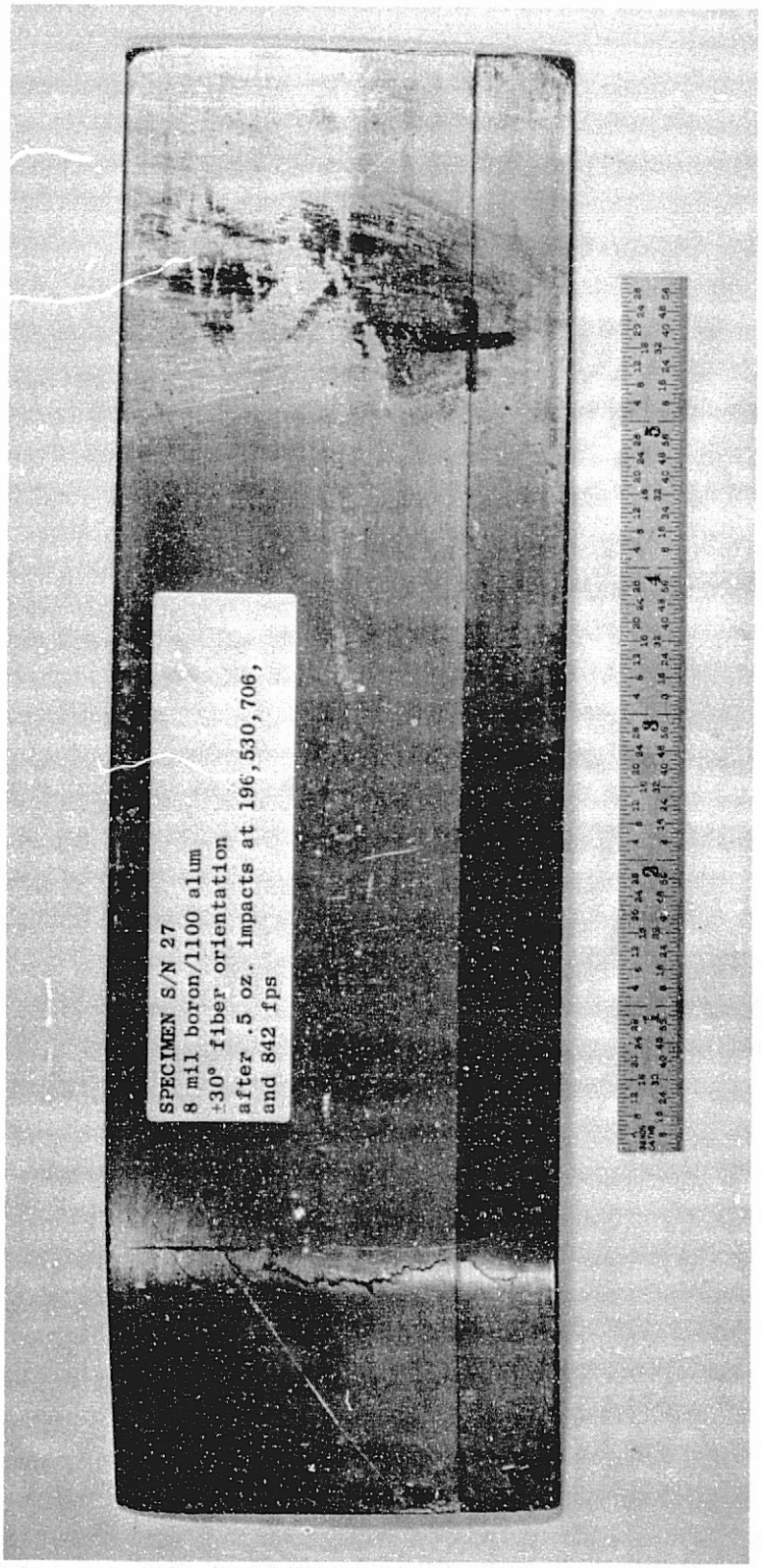

ORIGINAL PAGE IS
OF POOR QUALITY

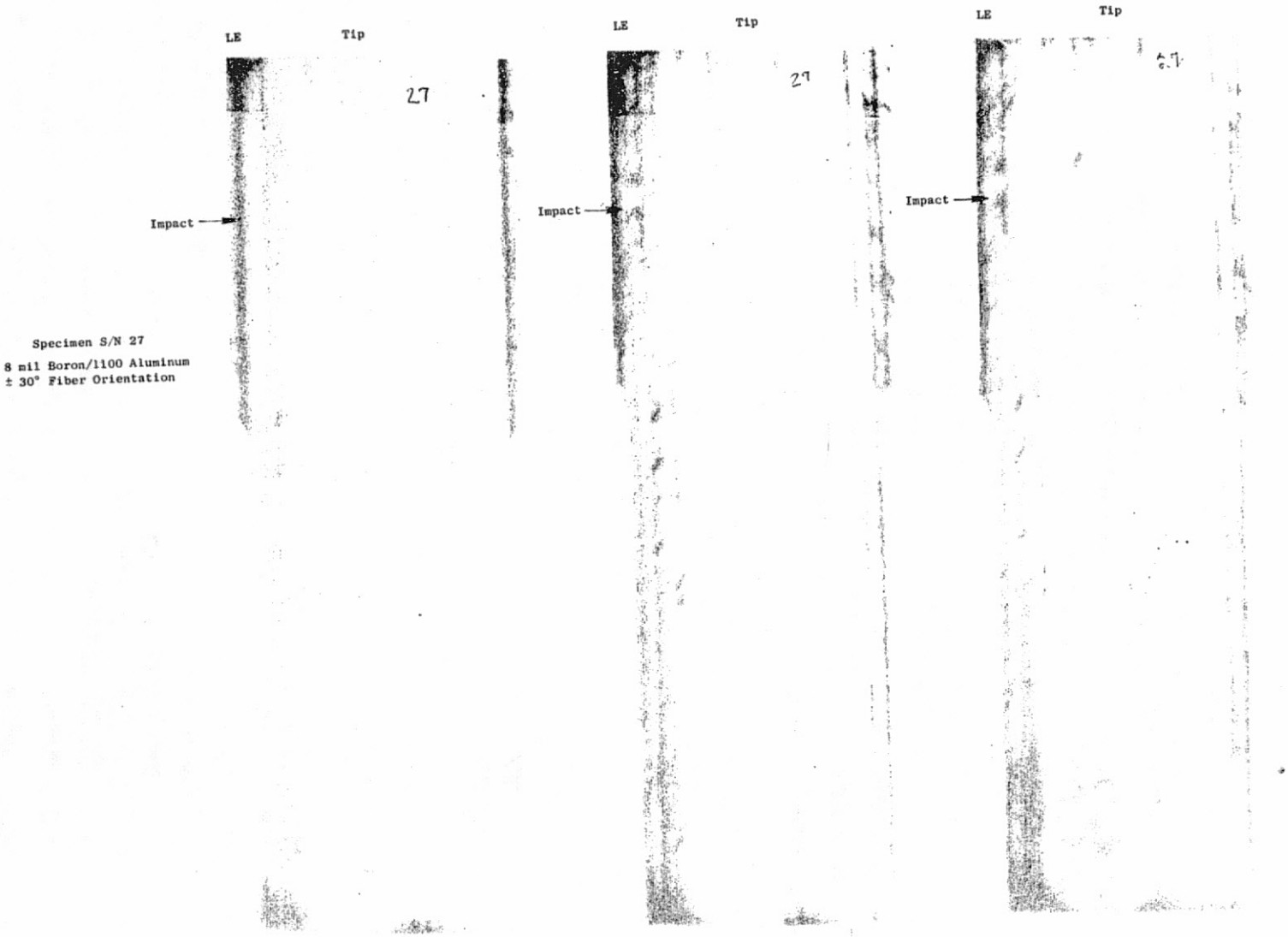

Specimen S/N 27

8 mil Boron/1100 Aluminum
± 30° Fiber Orientation

After Impact At 196 fps

After Impact At 530 fps

After Impact At 706 fps

Specimen S/N 34

8 mil Boron/1100 Aluminum
± 45° Fiber Orientation

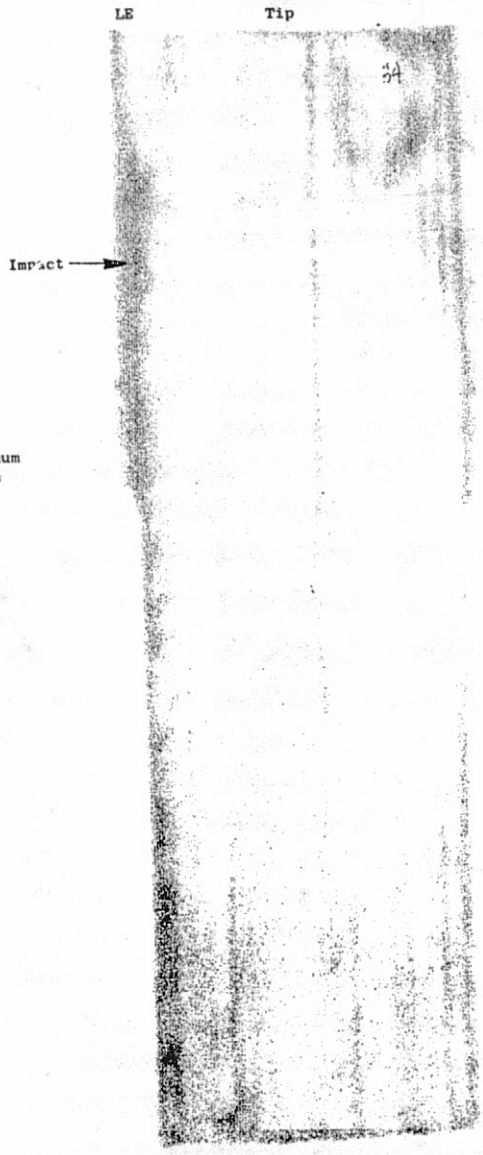

After Impact At 307 fps

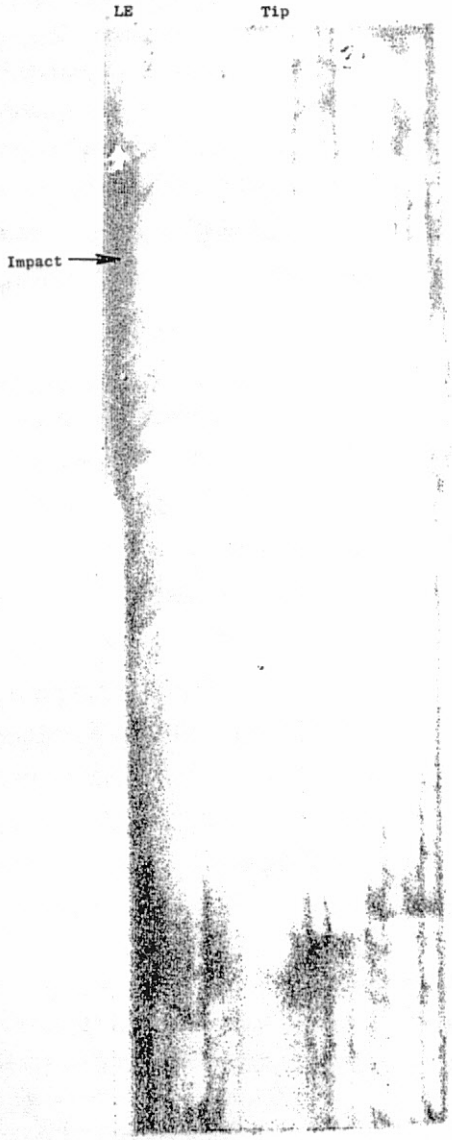

After Impact At 508 fps

SPECIMEN S/N 48
8 mil boron/1500 alum
Ti 6-4 core spar
+45° fiber orientation
after .5 oz. impacts at 324,534 & 727 fps

ORIGINAL PAGE IS
OF POOR QUALITY

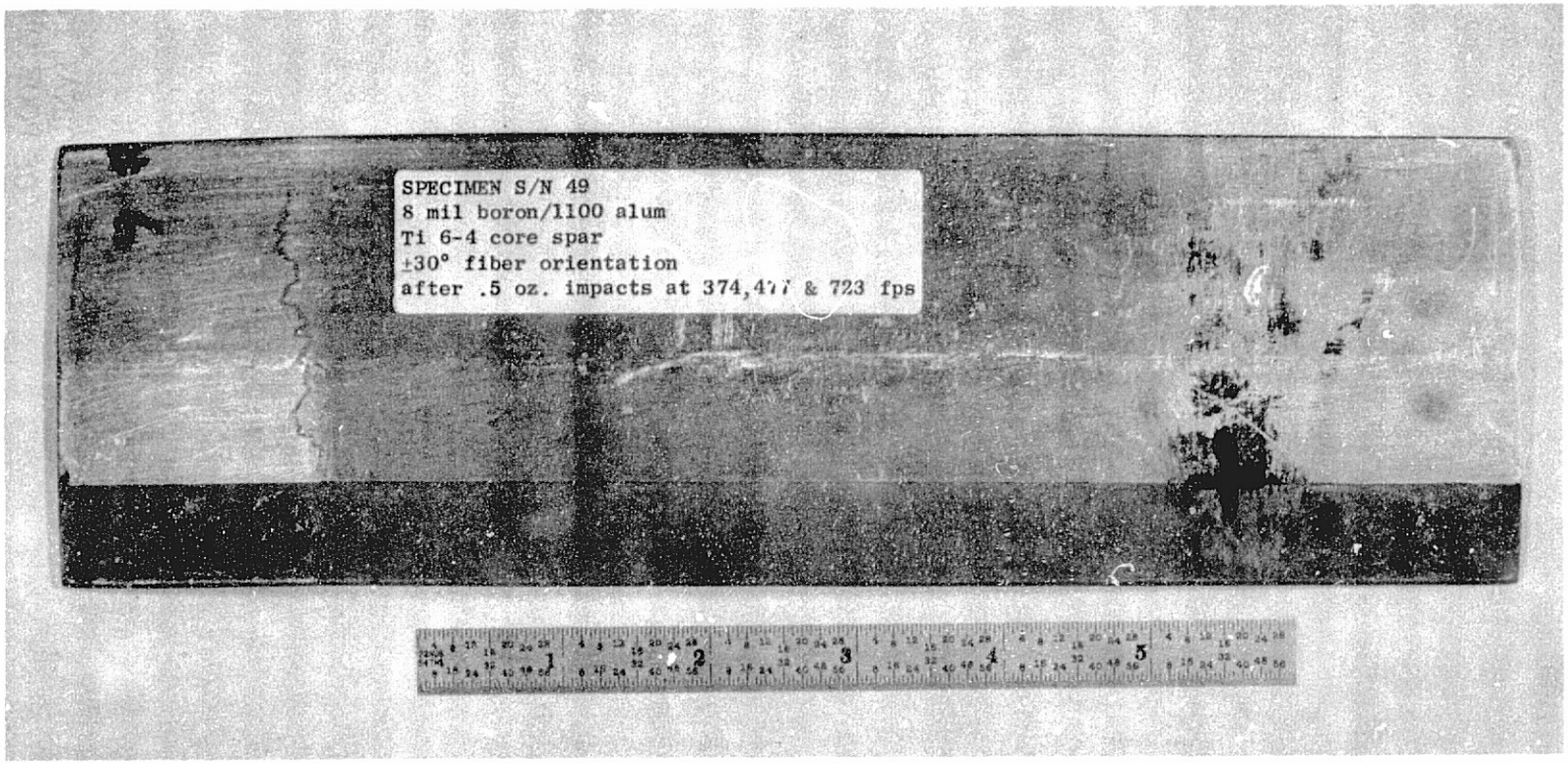
SPECIMEN S/N 49
8 mil boron/1100 alum
Ti 6-4 core spar
±30° fiber orientation
after .5 oz. impacts at 374,477 & 723 fps

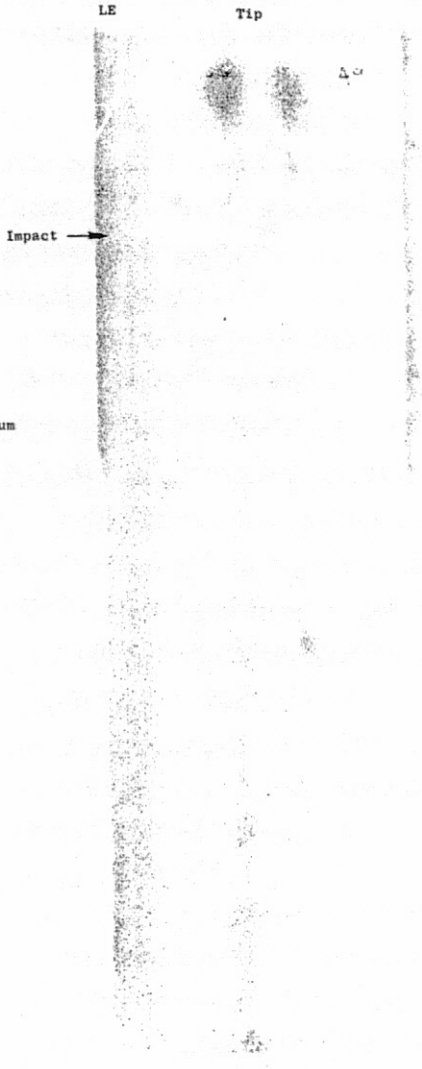

Specimen S/N 49

8 mil Boron/1100 Aluminum
±30° Fiber Orientation
Ti 6-4 Core Spar

After Impact At 374 fps

After Impact At 477 fps

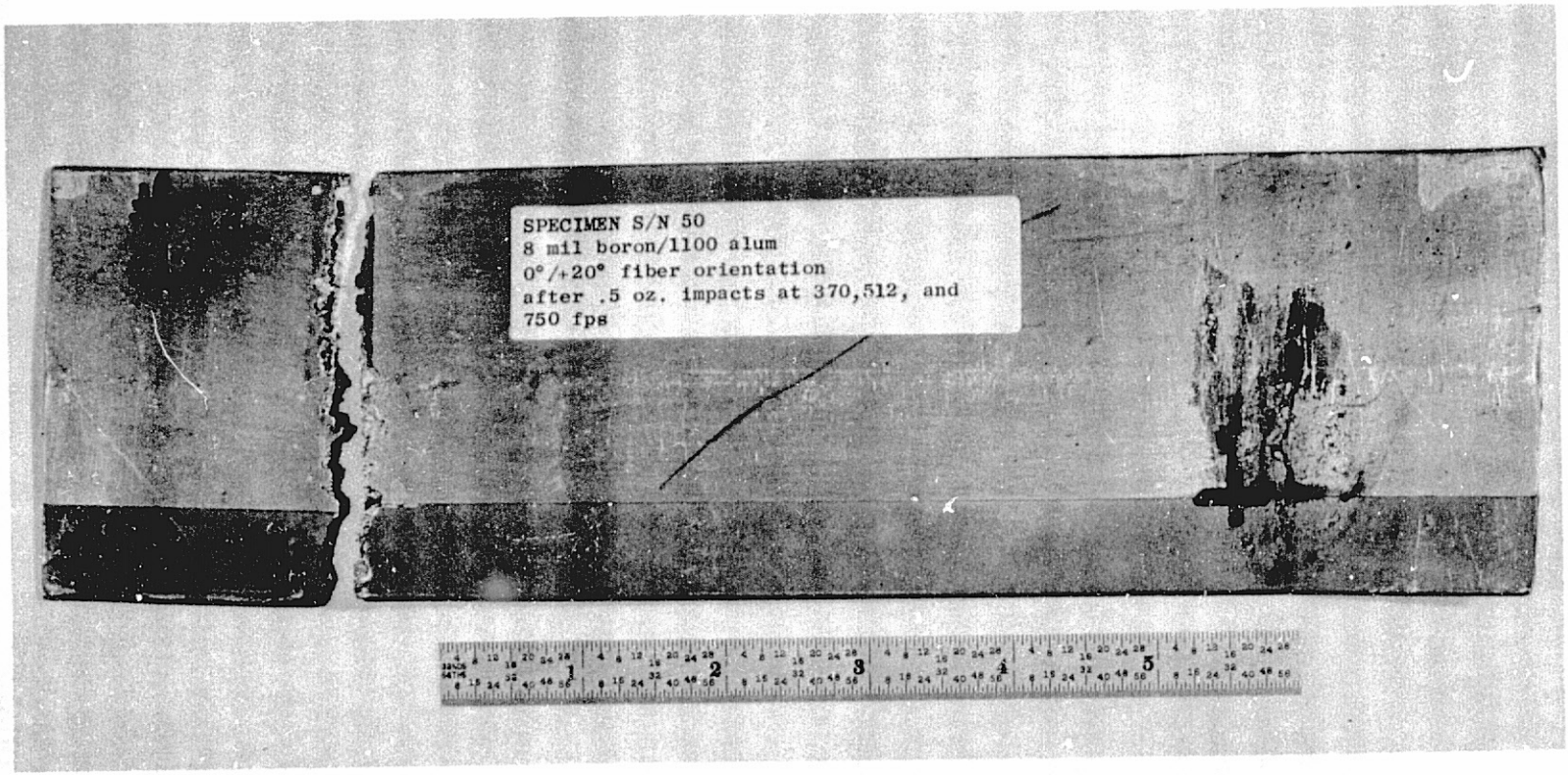
SPECIMEN S/N 50
8 mil boron/1100 alum
0°/+20° fiber orientation
after .5 oz. impacts at 370,512, and
750 fps

ORIGINAL PAGE IS
OF POOR QUALITY

APPENDIX C

- Test Specimens after Test Series Number Two and NDT Results Following Impacts

Specimen S/N 43
8 mil boron/1100 aluminum
±30° fiber orientation
Ti 6-4 Core Spar
After 32 gm. impacts at
649, 887, and 1110 ft/sec.

Specimen S/N 45
8 mil boron/1100 aluminum
±30° fiber orientation (Ti 6-4 L.E.)
After 32 gm. impacts at
656, 863, 1014, and 1090 ft/sec.

Specimen S/N 19
8 mil boron/1100 aluminum
±15° fiber orientation (no mesh or Ni)
after 32 gm. impacts at
654, 899, and 1100 ft/sec.

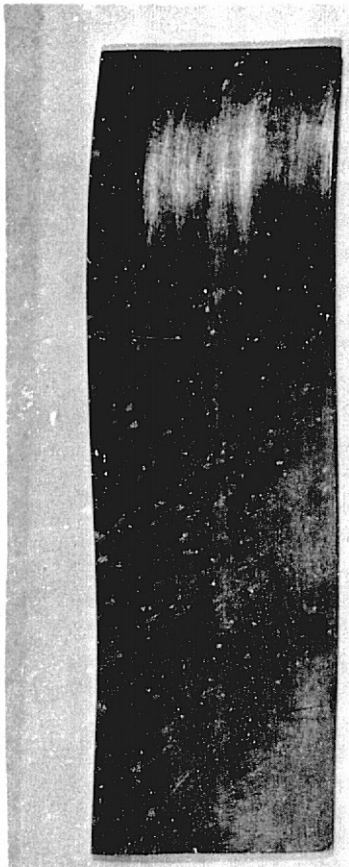

Specimen S/N 35
8 mil boron/1100 aluminum
±45° fiber orientation
After a 32 gm. impact
at 653 ft./sec.

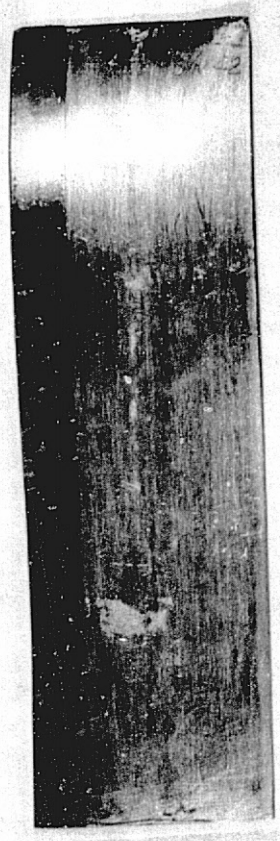

Specimen S/N 42
8 mil boron/1100 aluminum
±45° fiber orientation (Ti 6-4 core)
After a 32 gm impact at
671 ft/sec.

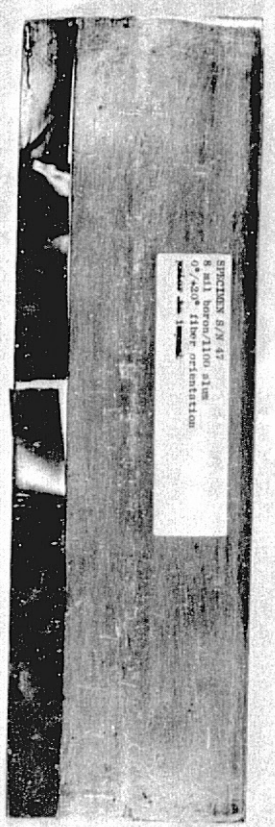

Specimen S/N 47
8 mil boron/1100 aluminum
0°/±20° fiber orientation
following 32 gm. impacts at
829 ft./sec

Specimen S/N 26
8 mil boron/1100 aluminum
± 15° fiber orientation
After 32 gm. impacts
at 651 and 921 ft/sec.

Specimen S/N 18
PR288/80% AS/20% S-GLASS
0°/±35° fiber orientation
after 32 gm. impacts at
660, 858, and 1060 ft/sec.

Specimen S/N 36
8 mil boron/1100 aluminum
± 30° fiber orientation
After 32gm. impacts at
454, 895, and 1028 ft/sec.

V (ft/sec) = 660 = 858 = 1060

Specimen S/N 18

Specimen S/N 19

V (ft/sec) = 654 = 899 = 1100

Specimen S/N 26

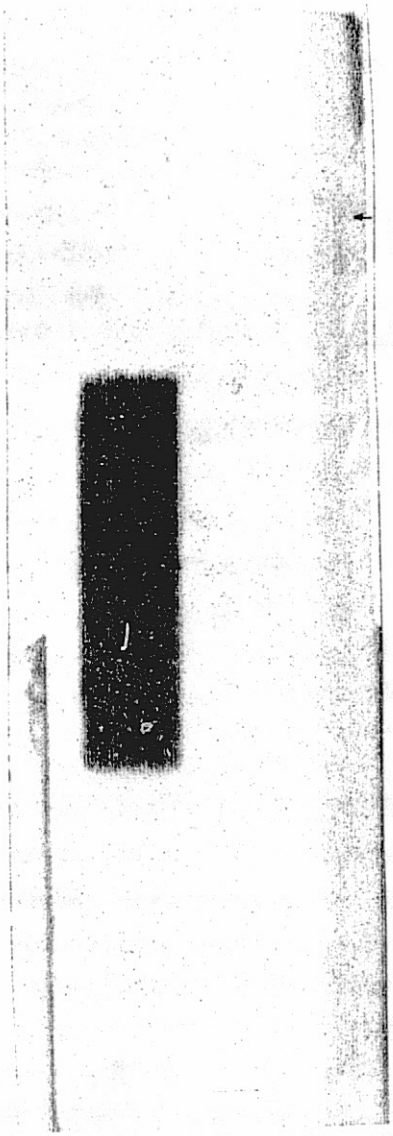

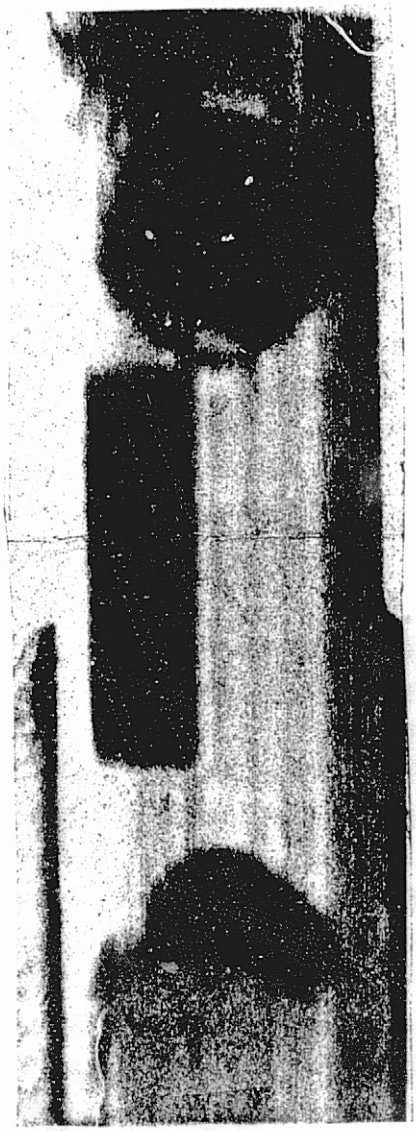

V (ft/sec) = 651 = 921